

MODELING EFFECTS OF MATERIAL PROPERTIES AND COMPOSITION ON  
ULTRASOUND PROPAGATION

A THESIS SUBMITTED TO  
THE GRADUATE SCHOOL OF NATURAL AND APPLIED SCIENCES  
OF  
MIDDLE EAST TECHNICAL UNIVERSITY

BY

OKAN ÖZKÖK

IN PARTIAL FULFILLMENT OF THE REQUIREMENTS  
FOR  
THE DEGREE OF DOCTOR OF PHILOSOPHY  
IN  
CHEMICAL ENGINEERING

JANUARY 2017



Approval of the thesis:

**MODELING EFFECTS OF MATERIAL PROPERTIES AND  
COMPOSITION ON ULTRASOUND PROPAGATION**

submitted by **OKAN ÖZKÖK** in partial fulfillment of the requirements for the degree of **Doctor of Philosophy in Chemical Engineering Department, Middle East Technical University** by,

Prof. Dr. Gülbin Dural Ünver  
Dean, Graduate School of **Natural and Applied Sciences** \_\_\_\_\_

Prof. Dr. Halil Kalıpçılar  
Head of Department, **Chemical Engineering** \_\_\_\_\_

Prof. Dr. Yusuf Uludağ  
Supervisor, **Chemical Engineering Dept., METU** \_\_\_\_\_

**Examining Committee Members:**

Prof. Dr. Bülent Karasözen  
Mathematics Dept & Inst. of Applied Mathematics., METU \_\_\_\_\_

Prof. Dr. Yusuf Uludağ  
Chemical Engineering Dept., METU \_\_\_\_\_

Prof. Dr. Halil Kalıpçılar  
Chemical Engineering Dept., METU \_\_\_\_\_

Prof. Dr. Nihal Aydoğan  
Chemical Engineering Dept., Hacettepe University \_\_\_\_\_

Assoc. Prof. Dr. Kerim Yapıcı  
Chemical Engineering Dept., Süleyman Demirel University \_\_\_\_\_

**Date:** 27.01.2017

**I hereby declare that all information in this document has been obtained and presented in accordance with academic rules and ethical conduct. I also declare that, as required by these rules and conduct, I have fully cited and referenced all material and results that are not original to this work.**

Name, Last name: Okan Özkök

Signature :

## **ABSTRACT**

Modeling Effects of Material Properties and Composition on Ultrasound Propagation

Özkök, Okan

Ph.D., Department of Chemical Engineering

Supervisor: Prof. Dr. Yusuf Uludağ

January 2017, 150 pages

Ultrasonic methods for material characterization have increasingly been used for the last decades thanks to advances in electronics and digital technologies since conventional methods accommodate several disadvantages like being time consuming. Advanced technology has brought highly accurate measurements with reasonable confidence level, and flexible ultrasonic testing parameters. The aim of this work is to carry out material characterization by combining modeling study and outputs of the ultrasonic device. This study, being both theoretical and experimental, is divided into three subsections; characterization of non-linear viscoelastic parameters, concentration measurement of solutions and particle size measurement by ultrasonic methods.

Viscoelastic parameters can be determined by the use of ultrasonic methods. In order to evaluate the output of the ultrasonic measurements properly, these outputs should be related to the material properties. Hence, a proper modeling of sound propagation in viscoelastic medium is necessary for adequate ultrasonic characterization of viscoelastic properties. The earlier studies on this subject essentially dealt with material characterization by the continuous wave propagation in viscoelastic mediums on the basis of base frequency of ultrasound. Nevertheless, material characterization by discrete wave propagation based on pulse repetition frequency has not been investigated apparently, so far. In our M.Sc. study, characterization of

linear viscoelastic properties based on pulse repetition frequency is done. Therefore, in this study a mathematical model is developed for investigating the discrete sound propagation in non-linear viscoelastic medium for determination of non-linear viscoelastic parameters. As the viscoelastic model, Oldroyd-B model is applied. Viscoelastic parameters of CMC/water solutions are determined by the evaluation of the ultrasonic outputs in the model developed.

Sound velocity is also a tool for the determination of concentration. However, compressibilities of liquid mixtures tend to show important deviations from the ideal behavior. It is strongly dependent on the interactions between molecules and provides valuable information on the structure of liquids. Hence, to interpret the concentration from the sound speed, a thermodynamical approach is followed. For this purpose, volume-translated Peng-Robinson equation of state is used to predict the concentrations of solutions from sound speed. In addition, experiments are done to verify the modeling outputs.

The particle size distribution of colloidal dispersions can be determined by measuring its ultrasonic velocity and/or sound attenuation coefficient as a function of frequency. Once they are measured a suitable mathematical model should be used to interpret the spectra. Ultrasonic spectroscopy can be used to analyze particle sizes between about 10 nm and 1000  $\mu\text{m}$ , and is suitable for application to concentrated systems (often up to 50 wt. %). This technique has considerable advantages over many alternative technologies because it can be applied to optically opaque systems without the need of any sample preparation. Nevertheless, modeling studies done so far use natural frequency of ultrasound, as in viscoelasticity. Hence, in this work mathematical model depending on pulse repetition frequency is developed for particle size measurement.

**Keywords:** Ultrasonic Characterization Techniques, Discrete Sound Signal Propagation, Non-linear Viscoelasticity, Concentration Measurement, Particle Size Characterization

## ÖZ

### Malzeme Özelliklerinin ve Kompozisyonunun Ultrason Yayılımı Üzerindeki Etkilerinin Modellemesi

Özkök, Okan

Doktora, Kimya Mühendisliği Bölümü

Tez Yöneticisi: Prof. Dr. Yusuf Uludağ

Ocak 2017, 150 sayfa

Elektronik ve dijital teknolojideki gelişmeler sayesinde ultrasonik metotlar malzeme karakterizasyonunda son on yıllardır yaygın olarak kullanılmaktadır çünkü geleneksel metotların zaman harcama gibi dezavantajları vardır. Gelişen teknoloji makul güven seviyesinde ve esnek test parametreleriyle yüksek doğrulukta ölçümleri mümkün kılmıştır. Bu çalışmanın amacı ultrasonik cihazın çıktılarıyla modelleme çalışmalarını birleştirip malzeme karakterizasyonu yapmaktır. Bu çalışma üç alt bölüme ayrılmıştır; doğrusal olmayan viskoelastik parametrelerin karakterizasyonu, çözeltilerin derişimlerinin ölçülmesi ve parçacık boyutu ölçümü.

Viskoelastik parametreler ultrasonic metotların kullanımıyla ölçülebilmektedir. Ultrasonik ölçümlerin çıktılarını uygun bir şekilde değerlendirebilmek için, bu çıktılar malzeme özellikleriyle ilişkilendirilmelidir. Bu sebeple, viskoelastik özelliklerin karakterizasyonu için sesin viskoelastik ortamda yayılımının modellenmesi uygun bir şekilde yapılmalıdır. Bu amaçla bugüne kadar yapılan çalışmalar temel olarak ultrasonun doğal frekansını baz alarak sürekli ses dalgasının viskoelastik ortamda yayılmasını esas almışlardır. Fakat, dalga tekrarlanma frekansını baz alan ve kesikli ses dalgalarının yayılımını inceleyerek malzeme karakterizasyonu bugüne kadar çalışılmamıştır. Yüksek lisans çalışmamızda linear

viskoelastik özelliklerin dalga tekrarlanma frekansına bağlı olarak tayini yapılmıştır. Bu çalışmada ise dalga tekrarlanma frekansını temel alan ve doğrusal olmayan viskoelastik parametrelerin tayini için kesikli ses dalgasının viskoelastik ortamlarda yayılmasını inceleyen matematiksel bir modelleme geliştirilmiştir. Viskoelastik model olarak Oldroyd-B modeli kullanılmıştır. Ultrasonik ölçümlerin sonuçları geliştirilen model içerisinde değerlendirilerek CMC/su çözeltilerinin viskoelastik özellikleri belirlenmiştir

Ses hızı da derişim tayini için bir araçtır. Fakat sıvı karışımların sıkıştırılabilirlikleri ideal davranıştan önemli ölçüde sapabilmektedir. Bu moleküllerin etkileşimlerine kuvvetli bir şekilde bağlıdır ve sıvı karışımların yapısıyla ilgili önemli bilgiler sağlamaktadır. Bu yüzden, ses hızından derişim ölçümü için termodinamik bir yöntem izlenmiştir. Bu amaçla, volume-translated Peng-Robinson denklemi ses hızından derişim ölçümü için kullanılmıştır. Ayrıca, modelleme çıktılarını doğrulamak için deneysel ölçümler yapılmıştır.

Kolloidal dispersiyonların parçacık boyut dağılımı ultrasonik ses ve/veya sönümlenmenin frekansa bağlı fonksiyonu olarak ölçümüyle belirlenebilir. Ölçümler yapıldıktan sonra elde edilen spectra uygun bir matematiksel modelle değerlendirilir. Ultrasonik spektroskopi 10 nm ile 1000 µm arasındaki parçacık boyutlarının ölçümü için ve derişik sistemler için (genellikle ağırlıkça %50'ye kadar) kullanılabilir. Bu teknik pek çok alternatif teknolojiye göre önemli avantajlara sahiptir çünkü opak sistemlerde ve herhangi bir numune hazırlama işlemine gerek kalmadan kullanılabilir. Fakat, viskoelastisite bölümünde olduğu gibi bugüne kadar yapılan çalışmalar ultrasonun doğal frekansını kullanmaktadır. Su sebebiyle bu çalışmada parçacık boyutu ölçümü için dalga tekrarlanma frekansına dayanan bir model geliştirilmiştir.

Anahtar Kelimeler: Ultrasonik Karakterizasyon Teknikleri, Kesikli Ses Sinyali Yayılımı, Doğrusal Olmayan Viskoelastisite, Konsantrasyon Ölçümü, Parçacık Boyutu Karakterizasyonu

To my family

## ACKNOWLEDGEMENTS

First of all, I am very grateful to my supervisor Prof. Dr. Yusuf Uludağ for his support and supervision during this study. Without his criticisms and guidance this study could not be completed.

I also would like to thank my thesis progress committee members Prof. Dr. Halil Kalıpcılar and Prof. Dr. Bülent Karasözen their helps and supports in my study.

I would like to express sincere thanks to my colleagues Bayram İstanbullu, Melek Ertunç Altınoklu, Melih Fındıkoğlu and Cennet Keskin for their tolerance and support to complete my study.

I owe a debt of gratitude to my friend and laboratory member Zeynep Karakaş and Güler Bengüsu Tezel Tanrısever for her support and invaluable assistance.

I would also like to thank my special friend Gökhan Çelik for his friendship and mentor.

Finally, I would like to express my gratitude my family for their endless support and help.

## TABLE OF CONTENTS

ABSTRACT.....	v
ÖZ .....	vii
ACKNOWLEDGEMENTS .....	x
TABLE OF CONTENTS.....	xi
LIST OF TABLES .....	xvi
LIST OF FIGURES .....	xv
CHAPTERS	
1. INTRODUCTION .....	1
1.1 Sound and Material Interactions .....	2
1.1.1 Nature of Sound .....	2
1.1.2 Mathematical Representation of Oscillation and Waves .....	3
1.2 Generation of Ultrasonic Wave.....	4
1.3 Ultrasonic Transducers .....	5
1.4 Detection of Ultrasonic Wave.....	7
1.5 Ultrasonic Velocity .....	8
1.5.1 Measurement of Ultrasound Velocity.....	9
1.5.2 Application of Ultrasound Velocity in Material Characterization.....	9
1.6 Ultrasound Attenuation.....	10
1.7 Natural Frequency and Pulse Repetition Frequency.....	10
1.8 Relation between Complex Modulus and Acoustic Parameters .....	11
1.9 Physical Interpretation of Sound Absorption.....	12
1.10 Ultrasonic Device Used in the Experimental Sections of the Thesis.....	14
2. ULTRASONIC CHARACTERIZATION OF POLYMERS AND VISCOELASTICITY OF MATERIALS .....	17
2.1 Ultrasonic Techniques for Polymer Characterization.....	17

2.2 Fluid Viscoelasticity .....	22
2.3 Relation between Stress and Strain .....	23
2.4 Non-Linear Viscoelastic Behavior .....	24
2.4.1 Dilute solution theories .....	25
2.4.2 Reptation theories .....	25
2.4.3 Network theories .....	26
2.5 Oldroyd-B Model .....	27
2.6 Relation between Fluid Viscoelasticity and Physical Acoustics .....	29
3. MATHEMATICAL MODELING OF ULTRASOUND PROPAGATION IN A NON-LINEAR VISCOELASTIC MATERIAL .....	31
3.1 Propagation of Sound Waves in a Medium .....	31
3.2 Oldroyd-B Model Simulations .....	39
3.3 Results of the Simulations .....	45
3.4 Experimental Procedure .....	45
3.5 Experimental Results .....	47
4. CONCENTRATION DETERMINATION OF MIXTURES FROM SOUND SPEED .....	51
4.1 Sound Speed as a Tool for Material Characterization .....	51
4.2 Molecular Theories for Sound Speed Estimations in Mixtures .....	53
4.2.1 Jacobson Free Length Theory .....	54
4.2.2 Schaaff Collision Factor Theory .....	54
4.3 Empirical Relations for Sound Speed Estimations in Mixtures .....	55
4.3.1 Nomato Equation .....	55
4.3.2 Van Deal Equation .....	55
4.3.3 Junjie Equation .....	56
4.3.4 Impedance Equation .....	56

4.4 Speed of Sound Estimation from Equation of States.....	56
4.4.1 Cubic Equations of States and Peng-Robinson Equation of State.....	56
4.4.2 Advantages and Drawbacks of Using Cubic Equations of States.....	58
4.4.3 Volume Translation Method for Cubic Equation of States .....	59
4.5 Experimental Procedure.....	60
4.6 Results and Discussions .....	61
5. ULTRASONIC PARTICLE SIZE DETERMINATION.....	75
5.1 Particle Wave Interaction.....	76
5.1.1 Intrinsic Absorption .....	76
5.1.2 Visco-inertial Dissipation Losses.....	76
5.1.3 Thermal Dissipation Losses .....	77
5.1.4 Scattering Losses .....	77
5.2 Overview of the Researches Done for Ultrasonic Particle Size Determination .....	78
5.3 Mathematical Modeling of Ultrasound Propagation in Particulate Dispersions .....	81
5.3.1 Obtaining the Governing Differential Equations for the Wave Propagations in Particulate Dispersions .....	82
5.3.2 Investigation of the Behavior of the Particles and Fluid when Wave is Stopped .....	87
5.4 Simulations of Ultrasound Propagating in Particulate Suspensions .....	89
5.5 Experimental Procedure.....	95
5.6 Ultrasonic Particle Size Measurements.....	96
6. CONCLUSIONS & RECOMMENDATIONS.....	99
REFERENCES .....	103
APPENDIX.....	113
A1. Linear Viscoelastic Models.....	113

A2. Derivation of Loss and Storage Modulus in Terms of Acoustic Parameters	117
A3. Obtaining the Governing Differential Equations Used in the Characterization of Viscoelasticity.....	119
A4. Interpretation of Experimental Measurements with the Model Developed ..	121
A5. CMC/water Solutions Rheological Data .....	125
A6. Review of Cubic Equation of States.....	128
A7. Polydispersed System Revision.....	132
A8. Algorithm for Particle Size Determination from the Model Developed .....	136
A9. Particle Size Measurements by Mastersizer 2000 .....	137
A10. Technical Specifications of DOP2000 .....	140
A11. Technical Specification of ARES Rheometer (TA Instruments, Spain) ....	144
A12. Technical Specification of Mastersizer2000 .....	146
A13. Colemanite Specification.....	147
CURRICULUM VITAE .....	147

## LIST OF TABLES

Table 3.1 Physical Properties of the Hypothetical Medium Used in Simulations.....	40
Table 3.2 Properties of CMC.....	46
Table 3.3 Ultrasonic Measurements .....	48
Table 3.4 Rheologic Measurements.....	48
Table 4.1 Binary Interaction Parameters for Mixtures .....	61
Table 4.2 Volume Translation Parameters.....	61
Table 4.3 Ethanol/Water Sound Speed Estimations .....	62
Table 4.4 Methanol/Methyl Acetate Sound Speed Estimations .....	63
Table 4.5 Ethanol/Methyl Acetate Sound Speed Estimations .....	64
Table 4.6 Ethyl Acetate/Ethanol Sound Speed Estimations .....	65
Table 4.7 Ethanol/Water Mixture Thermodynamic Properties.....	67
Table 4.8 Ethanol/Methyl Acetate Mixture Thermodynamic Properties.....	68
Table 4.9 Ethyl Acetate/Ethanol Mixture Thermodynamic Properties.....	70
Table 4.10 Methanol/Methyl Acetate Mixture Thermodynamic Properties.....	72
Table 5.1 Particle Size Measurements of Colemanite/Water Dispersions.....	97
Table A5.1 Cubic Equation of States.....	126
Table A5.2 Equations to Calculate “p”, “q” and “r” .....	127
Table A5.3 Cubic Equation of States for Mixtures.....	128

## LIST OF FIGURES

Figure 1.1 Schematic Representation of Longitudinal (top) and Transverse (bottom) Wave Propagation .....	3
Figure 1.2 Representation of a Transducer .....	6
Figure 1.3 Illustration of Pulse-echo Method.....	8
Figure 1.4 Illustration of Transmission Method .....	8
Figure 1.5 Representations of Natural Frequency and PRF .....	11
Figure 1.6 DOP2000 System.....	15
Figure 2.1 Investigation of Linear and Non-Linear Viscoelastic Regions.....	25
Figure 2.2 a) Dilute Solution Theory, b) Reptation Theory .....	26
Figure 2.3 Polymer Network and Junction Points.....	27
Figure 2.4 Illustration of Fixed and Convected Frames .....	27
Figure 3.1 Representation of Modulated Ultrasound Waves in the Medium.....	32
Figure 3.2 Representation of the Displacement of Particles with Time.....	33
Figure 3.3 Ultrasound Input Used in Simulations .....	40
Figure 3.4 Pressure Behavior in the Case of Oldroyd B Simulation 1 .....	41
Figure 3.5 Pressure Behavior in the Case of Oldroyd B Simulation 2.....	42
Figure 3.6 Pressure Behavior in the Case of Oldroyd B Simulation 3.....	42
Figure 3.7 Pressure Behavior in the Case of Oldroyd B Simulation 4.....	43
Figure 3.8 Pressure Behavior in the Case of Oldroyd B Simulation 5.....	44
Figure 3.9 Pressure Behavior in the Case of Oldroyd B Simulation 6.....	44
Figure 3.10 Repeating Unit of CMC .....	46
Figure 3.11 ARES Rheometer.....	47
Figure 4.1 Sound Speed Measurement Unit of DOP2000 .....	60
Figure 4.2 Ethanol/Water Mixture Excess Molar Volume.....	67

Figure 4.3 Ethanol/Water Mixture Sound Speed and Bulk Modulus Deviations.....	68
Figure 4.4 Ethanol/Methyl Acetate Mixture Excess Molar Volume .....	69
Figure 4.5 Ethanol/Methyl Acetate Mixture Sound Speed and Bulk Modulus Deviations .....	69
Figure 4.6 Ethyl Acetate/Ethanol Mixture Excess Molar Volume .....	70
Figure 4.7 Ethyl Acetate/Ethanol Mixture Sound Speed and Bulk Modulus Deviations .....	71
Figure 4.8 Methanol/Methyl Acetate Mixture Excess Molar Volume .....	72
Figure 4.9 Methanol/Methyl Acetate Mixture Sound Speed and Bulk Modulus Deviations .....	70
Figure 5.1 Illustration of Modulated Ultrasound Propagation in Particulate Dispersions.....	82
Figure 5.2 Modulated Ultrasound Propagation for Particle Size of 10 $\mu\text{m}$ .....	90
Figure 5.3 Modulated Ultrasound Propagation for Particle Size of 100 $\mu\text{m}$ .....	90
Figure 5.4 Modulated Ultrasound Propagation for Particle Size of 1000 $\mu\text{m}$ .....	91
Figure 5.5 Modulated Ultrasound Propagation for Particle Size of 50 $\mu\text{m}$ .....	92
Figure 5.6 Modulated Ultrasound Propagation for Particle Size of 25 $\mu\text{m}$ .....	92
Figure 5.7 Modulated Ultrasound Propagation for Particle Size of 150 $\mu\text{m}$ .....	93
Figure 5.8 Modulated Ultrasound Propagation for Particle Size of 300 $\mu\text{m}$ .....	93
Figure 5.9 Modulated Ultrasound Propagation for Volume Fraction of 0.2 .....	94
Figure 5.10 Modulated Ultrasound Propagation for Volume Fraction of 0.3 .....	94
Figure 5.11 Mastersizer 2000 equipment.....	96
Figure A1.1 Spring-dashpot Representation of Maxwell Model.....	111
Figure A1.2 Spring-dashpot Representation of Voigt-Kelvin Model.....	113
Figure A5.1 CMC/water Stress/strain Data (2 wt.%) .....	123
Figure A5.2 CMC/water Loss/Storage Modulus (2 wt.%) .....	123

Figure A5.3 CMC/water Stress/strain Data (3 wt.%).....	124
Figure A5.4 CMC/water Loss/Storage Modulus (3 wt.%).....	124
Figure A5.5 CMC/water Stress/strain Data (4 wt.%).....	125
Figure A5.6 CMC/water Loss/Storage Modulus (4 wt.%).....	125
Figure A9.1 Particle Size Measurement of 10 $\mu\text{m}$ Particle .....	135
Figure A9.2 Particle Size Measurement of 75 $\mu\text{m}$ Particle .....	135
Figure A9.3 Particle Size Measurement of 100 $\mu\text{m}$ Particle .....	136
Figure A9.4 Particle Size Measurement of 150 $\mu\text{m}$ Particle .....	136
Figure A9.4 Particle Size Measurement of 1000 $\mu\text{m}$ Particle .....	137

## NOMENCLATURE

A	: Ultrasound Amplitude, Helmholtz Free energy
a	: Time Between Two Consecutive Pulses, Attractive Forces
b	: Collision Factor, Volume of Molecules
c	: Speed of Sound
$C_v$	: Constant Volume Heat Capacity
E	: Modulus of Elasticity
$E^*$	: Complex Modulus of Elasticity
$E^l$	: Dynamic Modulus of Elasticity
$E^{ll}$	: Loss Modulus of Elasticity
e	: Base of Natural Logarithm
f	: Frequency of Ultrasound
g	: Gravitational Acceleration
G	: Shear Modulus
$G^*$	: Complex Shear Modulus
$G^l$	: Dynamic Shear Modulus
$G^{ll}$	: Loss Shear Modulus
i	: $(-1)^{1/2}$
J	: Compliance
$J^*$	: Complex Compliance
$J^l$	: Dynamic Compliance
$J^{ll}$	: Loss Compliance
k	: Thermal Conductivity
K	: Bulk Modulus, Jacobson Constant
$K_T$	: Isothermal Bulk Modulus
L	: Longitudinal Modulus of Elasticity

$L_f$  : Intermolecular Free Length  
 $L^*$  : Complex Longitudinal Modulus of Elasticity  
 $L^I$  : Dynamic Longitudinal Modulus of Elasticity  
 $L^{II}$  : Loss Longitudinal Modulus of Elasticity  
 $M$  : Any Type of Modulus of Elasticity  
 $m$  : Duration of a Pulse  
 $P$  : Ultrasonic Pressure  
 $P_{0k}$  : Complex Pressure Amplitude  
 $q$  : Heat Flux  
 $r$  : molecular radius, particle radius  
 $R$  : Gas Constant, Molar Sound Speed  
 $s$  : geometric volume  
 $S$  : Entropy  
 $T$  : Temperature  
 $T_{0k}$  : Complex Temperature Amplitude  
 $t$  : Continuous Time, Volume Translation Parameter  
 $u$  : Displacement of Particles  
 $u_{0k}$  : Complex Displacement Amplitude  
 $u_{ik}$  : Strain Tensor  
 $v$  : Particle Velocity  
 $V_a$  : Available Volume per Mole  
 $\tilde{V}$  : Molar Volume  
 $w$  : Angular Frequency, Weight Fraction  
 $x$  : Axial Direction  
 $Y$  : Available Surface Area per Mole  
 $Z$  : Acoustic Impedance

## **Abbreviations**

CFT : Collision Factor Theory

CMC : Carboxy Methyl Cellulose

EtAc : Ethyl Acetate

EtOH : Ethanol

FLT : Free Length Theory

MeAc : Methyl Acetate

MeOH : Methanol

PRF : Pulse Repetition Frequency

UDV : Ultrasound Doppler Velocimetry

## **Greek Letters**

$\alpha$  : Sound Attenuation

$\alpha_v$  : Thermal Expansion Coefficient

$\beta$  : Compressibility

$\gamma$  : Strain Tensor

$\dot{\gamma}$  : Rate of Strain

$\eta$  : Viscosity

$\eta_0$  : Zero Shear Viscosity

$\eta_p$  : Polymer Viscosity

$\eta_s$  : Solvent Viscosity

$\lambda$  : Wavelength of Ultrasound

$\lambda_1$  : Relaxation Time

$\lambda_2$  : Retardation Time

$\mu$  : Time Constants

$\phi$  : Volume Fraction of Particles

$\rho$  : Density

$\rho$  : Complex Density Amplitude  
 $\sigma$  : Wave Number  
 $\tau$  : Stress Tensor  
 $\tau_{xx}$  : Normal Stress  
 $\tau_{xy}$  : Shear Stress  
 $\omega$  : Vorticity Tensor, Acentric Factor

### **Subscripts**

f : Fluid Phase  
i : Summation Index  
j : Summation Index  
s : Solid Phase

### **Superscripts**

\* : Complex Conjugate  
ex : Excess Property on Mixing

### **Functions and Operators**

H : Heaviside Unit Step Function  
Im() : Imaginary Part  
Re() : Real Part  
tr : Trace of a Matrix

# CHAPTER 1

## INTRODUCTION

Characterization of engineering materials has become very important for identifying their performance. Material characterization techniques can be divided into two groups; non-destructive testing and destructive testing [1]. Once destructive testing is applied on a material it cannot be reused. This makes destructive testing costly. On the other hand, in non-destructive testing material is not damaged; hence, it can be used again.

Non-destructive testing of materials has been frequently applied over the last decades as they provide some predominance over the conventional techniques [2]. Ultrasonic methods are one of the most favorable among them, since they enable rapid analysis with reduced equipment and labor costs. In addition, advances in technology have brought high accuracy measurements with reasonable confidence level, and flexible ultrasonic testing parameters. There are many properties investigated by ultrasonic methods like the material structure [3], thermal properties [4, 5], mechanical properties [6] and rheological properties [7]. However, any ultrasonic equipment measures only two arguments related with sound propagation; speed of ultrasound and attenuation coefficient. Attenuation can be defined as the decrease of the sound pressure level through its propagation. The magnitudes of these parameters are strongly dependent on the material properties. Hence, by relating these parameters to the material properties by the use of a suitable mathematical model, material properties can be determined.

Ultrasonic methods can be applied by low intensity or high intensity ultrasound waves. Low intensity and high frequency waves are non-destructive methods and can

be used in fields such as medical diagnosis and acoustical holography. Low intensity testing is suitable for on-line and in-line measurements of material properties in industrial applications. On the other hand, by the use of high intensity and low frequency ultrasonic waves, destructive testing can be obtained. They are used in areas like medical treatments, surgical applications, atomization of liquids, cutting, cleaning of materials, perturbation of bio-cells and homogenization of materials [1].

## **1.1 Sound and Material Interactions**

### **1.1.1 Nature of Sound**

Sound is transmission of mechanical energy through an elastic media by means of pressure waves [8]. Sound is firstly handled by great scientist Isaac Newton in his book Principia and defined as transmission of pressure disturbance. Successor studies are done by Euler, Lagrange and d'Alembert [9]. Then, great improvements are accomplished in the science of acoustic in 19<sup>th</sup> century. Majority of the physical and mathematical basics of acoustic is investigated in this century. The book "The Theory of Sound" published by Rayleigh in 1886 is still applied as an important source by researchers.

To deal with physical acoustic, sound waves are usually described by means of partial differential equations and these equations are specifically named as wave equations. In these equations, position and time appear as independent variables while dependent variable usually arises as pressure or displacement. Sound wave travels sinusoidally thus it has a frequency. Sounds having frequencies greater than 20 kHz have specific name, ultrasound. Human ear is not able to hear ultrasound. Sound propagation can be in two different characters; longitudinal and transverse waves [10]. In longitudinal wave propagation, the displacements of the molecules are in the same direction with the wave (Figure 1.1.a). In this manner, the section where the sound is exactly passing through is compressed. After wave passed, the molecules are decompressed; finally they return to their equilibrium position [11]. This is the wave propagation mechanism in liquids and gases. In transverse wave

propagation, however, the directions of the displacements of the molecules are normal to the direction of the wave (Figure 1.1.b). Transverse wave propagation take place in solids since a rigid structure is needed for transverse waves. Nevertheless, there is no mechanism in fluids for driving motion perpendicular to the direction of wave propagation [10].

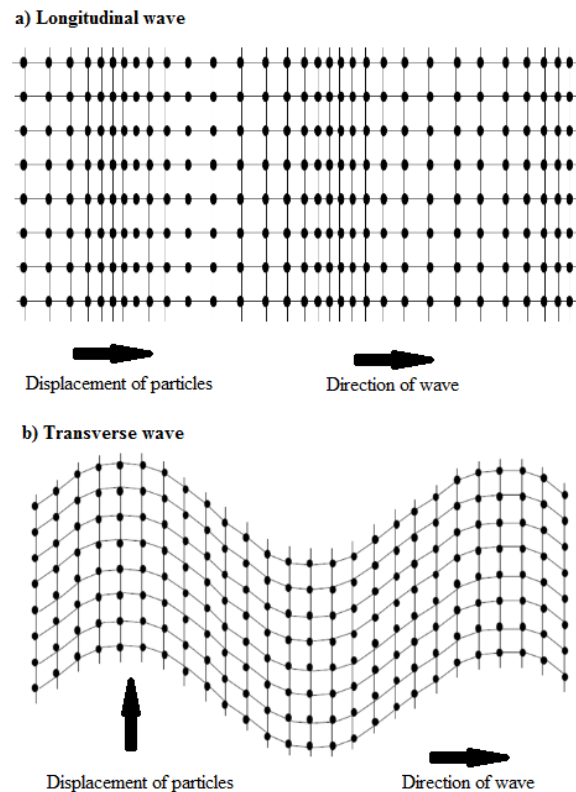


**Figure 1.1** Schematic Representation of Longitudinal (top) and Transverse (bottom) Wave Propagation

### 1.1.2 Mathematical Representation of Oscillation and Waves

Due that  $e^{i\theta} = \cos\theta + i\sin\theta$ , any sinusoidal oscillation of  $|A|\cos(\omega t + \varphi)$  can be defined as [12];

$$|A|\cos(\omega t + \varphi) = \text{Re}(Ae^{i\omega t}) \quad \text{eqn. 1.1}$$

A is the complex amplitude of oscillation and equals to;

$$A = |A|e^{i\phi} \quad \text{eqn. 1.2}$$

$|A|$  is constant for undamped traveling wave, but its phase “ $\phi$ ” gets behind by  $2\pi$  per wavelength through the direction of propagation. The phase shift per length is  $2\pi/\lambda$ . Thus, for undamped traveling wave;

$$A = Be^{-i\beta x} \quad \text{eqn. 1.3}$$

where

$$\beta = \frac{2\pi}{\lambda} = \frac{2\pi f}{\lambda f} = \frac{w}{c} \quad \text{eqn. 1.4}$$

For a damped wave, decay of amplitude can be expressed as  $|B|e^{-\alpha x}$ . The ratio of the amplitude of wave at position of “ $x+1$ ” to the position of “ $x$ ” is hold as  $e^{-\alpha}$ . Hence,  $\alpha$  defines the attenuation of wave per unit length. As a result;

- phase shift is “ $\beta$ ” radians,
- attenuation is “ $\alpha$ ”, per length.

Ultimately, the wave can be expressed as;

$$A = Be^{i\omega t - \alpha x} \quad \text{eqn. 1.5}$$

where “ $\sigma$ ” is the wave number and defined as;

$$\alpha = \frac{w}{c} \quad \text{eqn. 1.6}$$

## 1.2 Generation of Ultrasonic Wave

Ultrasonic waves can be produced by means of mechanical, electrostatic, electrodynamic, electromagnetic, magnetostrictive effect, piezoelectric effect and laser techniques. Mechanical technique or Galton Whistle technique is the pioneering method for the production of ultrasonic wave. In this method mechanical shock or friction is utilized to get ultrasonic wave with frequency between 100 kHz and 1

MHz. Ultrasonic waves with frequencies between 10 and 200 MHz can be obtained by electrostatic method. Magneto inductive effect is benefited in electrodynamic techniques for ultrasound generation. Mechanical deformation of ferromagnetic substances in the presence of magnetic field is magnetostriction. This is dominant in metals like nickel, iron, cobalt and their alloys. Magnetostriction can also be used in generation of ultrasonic wave. Most widely applied technique in ultrasound generation is piezoelectric effect. In this technique inverse piezoelectric effect is applied for ultrasound generation. Finally, when a laser light beam is shed on a surface of a material, some part of the energy is absorbed while remaining reflected back. Absorbed energy causes tangential stress and bulk strain; hence, ultrasound is generated [1].

### **1.3 Ultrasonic Transducers**

Transducer is a device that changes the form of energy. Ultrasonic transducers alter the electrical energy to mechanical energy (ultrasound). The fundamental components of a transducer are active element, backing and wear plate [1, 13]. Representation of a typical transducer is shown in Figure 1.2.

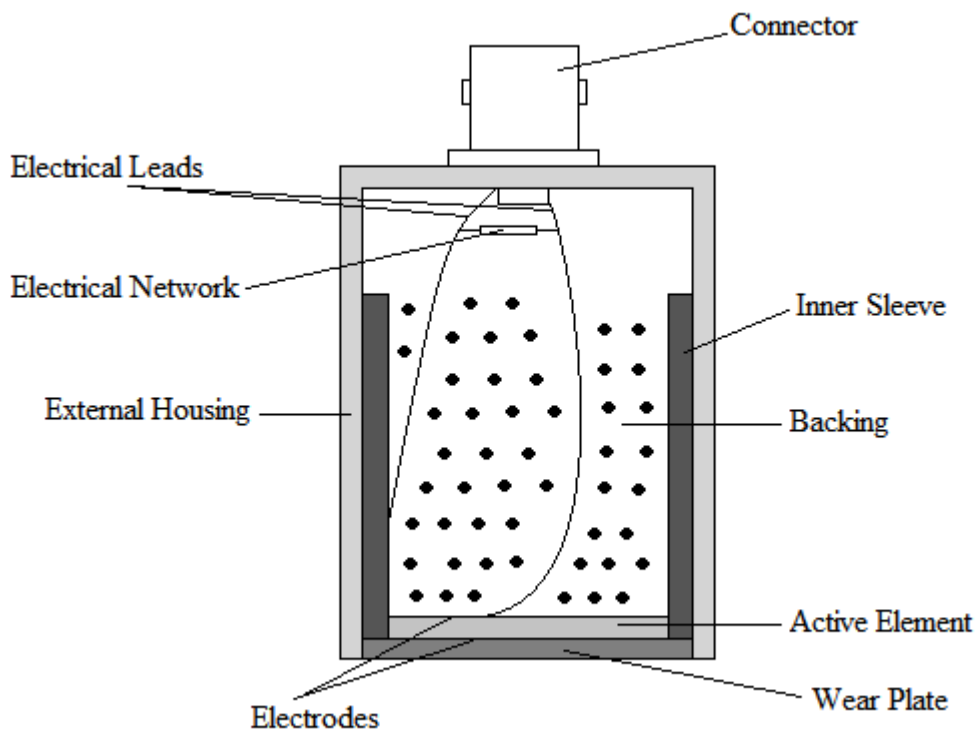


*Figure 1.2 Representation of a Transducer*

- Active Element

Active element is made of piezzo or ferroelectric material. It uses electrical energy to produce ultrasound energy. Most widely employed materials in the structure of the active element is polarized ceramics. They can bet cut in different modes that makes is possible to generate different wave types. In addition, to increase the performance of transducers alternative materials like piezzo polymers and composite materials can also be used.

- Backing

Backing is a high constituent of transducer material designed to obtain high attenuation. This is employed to govern the vibration of the transducer by absorbing the vibration coming from the back face. If the acoustic impedance of backing is similar to that of the active element, proper resolution is obtained. However,

amplitude of the ultrasound might be low. When their impedances are not similar, higher ultrasonic amplitudes obtained with lower resolution.

- Wear Plate

Wear plate is designed to shield the ultrasonic transducers from the surrounding. For contact transducers, wear plate has to be durable and corrosion resistant.

#### **1.4 Detection of Ultrasonic Wave**

Several techniques can be applied for the detection of ultrasound. They are dependent on piezoelectric, electrostatic and magnetostriction effects. Conventional techniques such as mechanical and optical techniques are also applicable for detection of ultrasound. Equipments based on piezoelectric effects are commonly used for detection of ultrasound. These equipments use electrical techniques for the detection of ultrasound [1, 12, 13, 14, 15].

Ultrasonic techniques are based on pulsed ultrasound and operate in two modes; pulse -echo and transmittance mode. In pulse-echo mode, first, ultrasonic wave ( $A_0$ ) is emitted by a transducer (Figure 1.8). Then, some part of it ( $A_{0r}$ ) is reflected between the interface of the transducer and the material. This gives the first echo. Meanwhile, the remaining part of the wave ( $A_{1r}$ ) propagates through the material. When it reaches to the interface between the material and its bordering, some part of it ( $A_{0r}$ ) is reflected. This gives the second echo. Hence, the sound speed and attenuation can be determined by measuring the time between two successive echoes and their amplitudes.

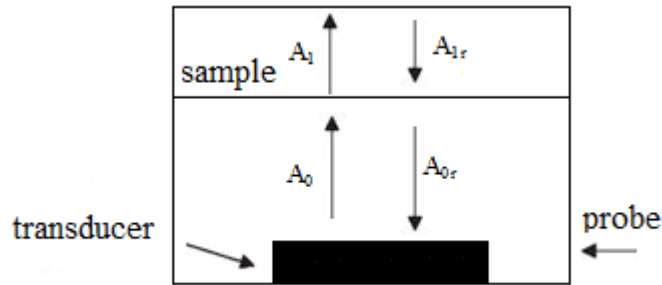


**Figure 1.3** Illustration of Pulse-echo Method [16]

In the transmission method, two probes are necessary, one is used as transmitter and the other is used as receiver. Sound emitted by the transducer with  $A_0$  amplitude eventually reaches to the receiver as  $A_2$  (Figure 1.9). The sound attenuation here can be determined by comparing the amplitudes of the echo received with and without material of interest between the transducers.

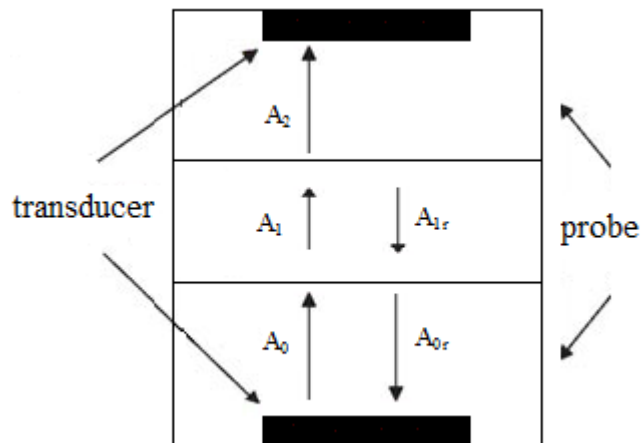


**Figure 1.4** Illustration of Transmission Method [16]

### 1.5 Ultrasonic Velocity

There are four classes of ultrasound speeds. They are longitudinal shear, surface and lamb sound speeds. Longitudinal and shear speeds have the major importance since they are strongly dependent on material elasticity and density. Mechanical properties of solids are different from liquids in two aspects. Firstly, greater intermolecular

forces present in solids hence they are able to sustain shear forces. Secondly, there may exist elastic-anisotropy in solid structures [1, 17].

### **1.5.1 Measurement of Ultrasound Velocity**

Elasticity of materials is dependent on important material properties like specific heat, Debye average velocity and Gruneisen constant. One of the methods of determining elasticity is determination of the longitudinal and shear ultrasound speeds. Elasticity of material is dependent on intermolecular forces and framework of the structure.

Both transmission and pulse-echo method can be applied for the measurement of ultrasound velocity.

### **1.5.2 Application of Ultrasound Velocity in Material Characterization**

Speed of ultrasound is used in variety of fields in material characterization. For example, determination of elasticity of the material by ultrasound velocity is common nowadays. Elastic parameters in a solid structure can be obtained by;

$$c_1 = \sqrt{\frac{L'}{\rho}} \quad \text{eqn. 1.9}$$

$$c_s = \sqrt{\frac{G'}{\rho}} \quad \text{eqn. 1.10}$$

where  $L'$  and  $G'$  are longitudinal and shear modulus of elasticity

In addition, stiffness constants or second and fourth order elastic constants can also be measured by the use of ultrasound velocity [21]. If ultrasound experiments are conducted in different conditions (i.e. temperature and pressure), the response of the material under different conditions are investigated.

## 1.6 Ultrasound Attenuation

Amplitude of ultrasound signal exponentially reduces through its traveling medium since its mechanical energy is lost as it travels [16]. Decrease of the energy of ultrasound is called attenuation. Diffraction, absorption and scattering of ultrasound are the mechanisms involved in the mechanical energy loss. While the physical properties of the medium govern the absorption losses, shape and the macroscopic structure of the material determine the diffraction and scattering losses. Attenuation of ultrasound can be formulized as;

$$A_x = A_0 e^{-\alpha x} \quad \text{eqn. 1.11}$$

where  $\alpha$ ,  $x$  and  $A$  refer to the sound attenuation, positions and the sound pressure amplitude, respectively.

Rearranging for the attenuation coefficient;

$$\alpha = \frac{1}{x_2 - x_1} \ln \left( \frac{A_1}{A_2} \right) \quad \text{eqn. 1.12}$$

In pulse-echo mode ( $x_2 - x_1$ ) is the twice of the distance since the wave travels the path twice due to reflection.

## 1.7 Natural Frequency and Pulse Repetition Frequency

In modulated wave propagation, besides the natural (or base) frequency of ultrasound a secondary frequency domain is obtained. This frequency has a specific name pulse repetition frequency (PRF). PRF defines how frequent ultrasound pulses are sent. PRF has great importance on rheological and particle size characterization sections in this thesis. Utilization of PRF in models is one of the main points discriminating this study from the similar works in the literature. Schematic representation of natural frequency and PRF is shown in Figure 1.5.

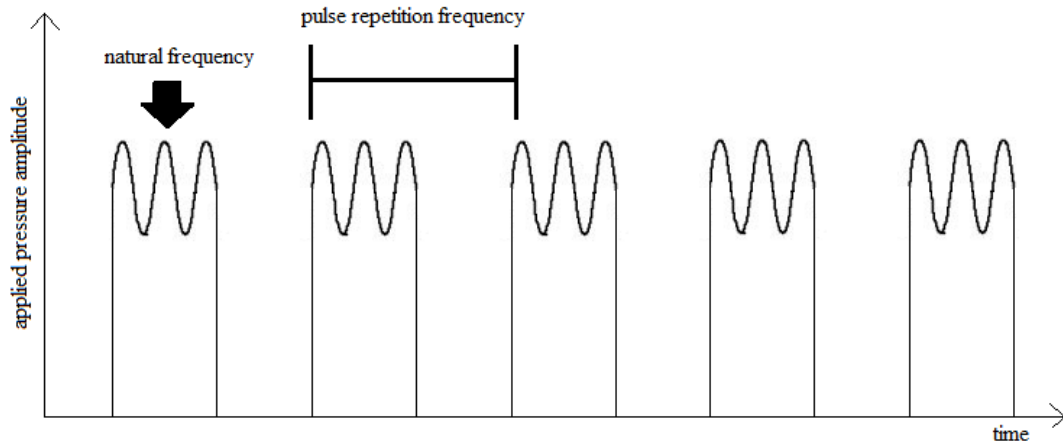


**Figure 1.5** Representations of Natural Frequency and PRF

### 1.8 Relation between Complex Modulus and Acoustic Parameters

Sound attenuation and sound speed are strongly affected by the physical and chemical character of the media [5]. For instance, complex modulus of elasticity can be related with these parameters by;

$$M' = \frac{\rho c^2 \left[ 1 - \left( \frac{\alpha \lambda}{2\pi} \right)^2 \right]}{\left[ 1 + \left( \frac{\alpha \lambda}{2\pi} \right)^2 \right]^2} \quad \text{eqn. 1.13}$$

$$M'' = \frac{2\rho c^2 \frac{\alpha \lambda}{2\pi}}{\left[ 1 + \left( \frac{\alpha \lambda}{2\pi} \right)^2 \right]^2} \quad \text{eqn. 1.14}$$

where  $M'$  and  $M''$  are the storage and loss modulus. Derivations of eqns. 1.13 and 1.14 are provided in Appendix A2 section. Then, the complex modulus of elasticity,  $M^*$ , is expressed by the following equation;

$$M^* = M' + iM'' \quad \text{eqn. 1.15}$$

Energy of bonds between the atoms constituting the main chain of the polymer and the intermolecular forces between the adjacent polymer chains governs the variation

of the complex modulus of elasticity as a function of frequency. In the acoustic measurements, each one of these forces can bring out itself separately. For instance, the speed of sound in a polymer fiber in the direction of the fiber placing is about  $(8-12)\times 10^5$  cm/s. Bonding energy is the principal factor determining this speed. Nevertheless, speed is found as about  $(1.2-1.5)\times 10^5$  cm/s when it is measured in other directions. For this case, intermolecular forces are dominant to determine sound speed [28, 29].

The dynamic modulus of elasticity contains major information about the physical features of the polymer. For instance, intermolecular interactions are higher in glassy polymers than rubbery ones. To illustrate, the order of dynamic modulus of elasticity is in  $10^9$  Pa for the glassy state polymers while its magnitude is around  $(10^5-10^6)$  Pa in the rubbery state polymers. Any alteration in the intermolecular structure of polymers changes the dynamic modulus of elasticity. Then acoustic parameters change, as well.

Hence, sound speed and attenuation carry important data about the mechanical properties, physical and chemical framework and the concentration of the materials. In addition, rheological properties can also be analyzed by evaluation of these acoustic parameters.

## **1.9 Physical Interpretation of Sound Absorption**

The relaxation theory clarifies the fundamental acoustic properties of polymers. Under the action of wave propagation, the system leaves the thermodynamic equilibrium state. When the wave propagation is interrupted the system starts to come back thermodynamic equilibrium by internal forces. This period of the system is called relaxation, and the time necessary for reaching equilibrium is the relaxation time. Various kinds of molecular motions have contribution on the system to come back thermodynamic equilibrium from the transition state. A proper relaxation process is defined by matching relaxation times to corresponding molecular motion. It is necessary to adjust the experimental duration with the relaxation time in the

same order of magnitude to determine the relaxation process with corresponding molecular motion.

Suppose that acoustic experiments are done with polymer by starting with a very low frequency of sound. Therefore, the period of wave is so large that  $T/\tau \gg 1$ . For this case, the period of wave is very high when compared with the relaxation time of the biggest kinetic element of the polymer. The vibration of sound is distributed to whole volume of the polymer due to the segmental mobility of macromolecules. In addition, mechanical energy loss is not high and the polymer quickly comes back to thermodynamic equilibrium upon the removal of stress. The dynamic modulus of elasticity and sound propagation velocity is very small for this case.

When the frequency of sound is increased (the period decreases), the time the energy dissipated due that segment diffusion constitutes longer portion of a period; hence, dispersion of sound energy is increased. Meanwhile, there are some very big arranged segments, which do not have enough time to transfer energy to adjacent during an oscillation period. Hence, they behave like rigid elements of chains. They causes the increase in the rigidity of polymer and increase in the dynamic modulus and sound propagation velocity. Loss tangent also increases.

By the further increase in the frequency of the sound, more part of the segments do not have enough time to transfer the energy of oscillations to their neighbor during an oscillation. Therefore, the amounts of segments behave as rigid body increases. The dynamic modulus of elasticity and sound propagation velocity continue to increase, as well. Although the energy dissipation increases further, the rate of energy dissipation starts to decrease. Since, some segments do not have enough time to convert the energy of oscillation to heat.

With the further increase in the frequency, which means more segments behave like rigid body. When the period of an oscillation becomes  $T/\tau = 1$ , the loss tangent makes maximum. By the further increase in the frequency mechanical loss starts to

decrease. Nevertheless, the dynamic modulus of elasticity and sound propagation velocity continue to increase.

The further growth in the frequency ( $T/\tau \ll 1$ ),  $T$  becomes much smaller than the relaxation time. In this case almost none of the segments transfer the sound energy to neighbor. The sound propagation in this case is in quasi-equilibrium. The dispersion of the energy becomes very small and dynamic modulus of elasticity reaches upper limit value. This can be illustrated by the fact that at very high frequencies, the polymer in rubbery state reacts as if it were in glassy state, which is called as mechanical glass transition.

Ultimately, as frequency is increased further, shorter relaxation times of smaller kinetic elements are started to be observed. Upon further increase nearly all the kinetic elements behave as rigid body. For this case no relaxation spectrum is obtained. Hence, the ratio  $T/\tau$  is critical to determine the loss tangent and sound propagation velocity. This ratio can be either changed by changing frequency or changing the relaxation time. Since decreasing  $T/\tau$ , the sound velocity increases and loss tangent makes maximum. This can be accomplished by increasing frequency or relaxation time, which can be achieved by decreasing temperature. Hence, effects of increase in the frequency and decrease in the temperature on acoustic properties are similar [5].

### **1.10 Ultrasonic Device Used in the Experimental Sections of the Thesis**

For the ultrasonic measurements, Ultrasound Doppler Velocimetry (UDV) system DOP2000 (Signal-Processing, Switzerland) is used. Ultrasound frequency, pulse repetition frequency and number of gates can be set by the operator. The base frequency of ultrasound can be adjusted to 0.5, 1.0, 2.0, 4.0 and 8.0 MHz . The maximum attainable value of pulse repetition frequency is 15625 Hz. Room temperature is held at 25°C during the experiments by the help of air conditioner. The piezzo ceramic transducer (SUHNER Switzerland RG 174/U 50 ohm) is used in measurements. The operating frequency of the transducer is 2.0 MHz. DOP2000

System is shown in Figure 1.11. Further specifications of DOP2000 are provided in Appendix A10.

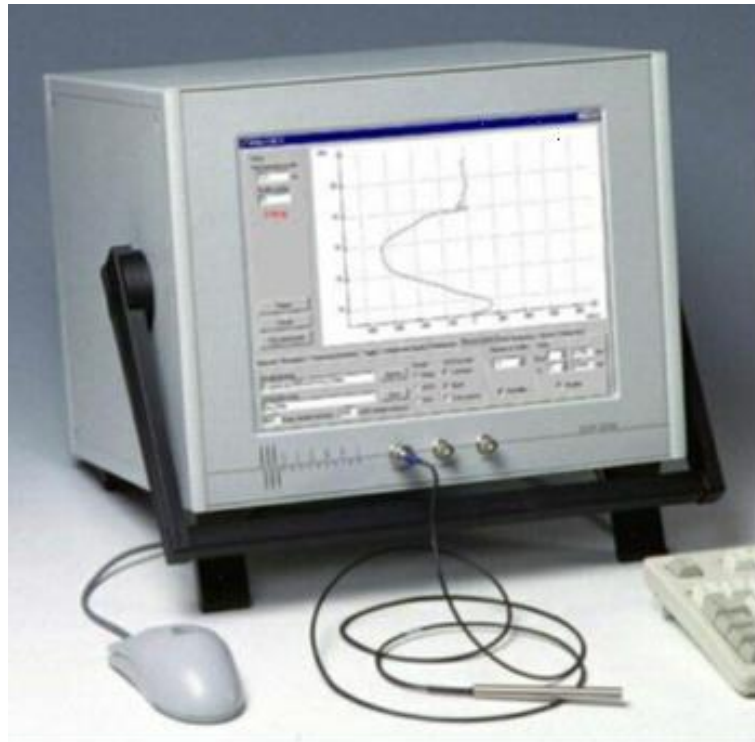


*Figure 1.6 DOP2000 System*

Ultrasound Doppler velocimetry has been used in medical diagnosis since 1970's. Applications of pulsed emissions widen the usage of the method in other disciplines like fluid dynamics measurements. The name "Ultrasound Doppler velocimetry" comes from that velocity is measured by the Doppler frequency. Velocity is calculated from the shifting of the positions between pulses [99].

Though DOP2000 is originally designed for characterization of fluid velocity profile in flow systems, ultrasonic measurements on stationary fluids can also be done. DOP2000 can provide significant ultrasonic data on stationary fluids.

Conducting ultrasonic field measurement feature of the device, the attenuation coefficient can be measured. Furthermore, amplitudes of the echoes belonging to

various times can be acquired by the DOP2000. By further utilization of these echoes, acoustic characterization of the material can be achieved. For this purpose, echo-history data with respect to position are acquired to utilize them in the mathematical models for rheological and particle size characterization sections of the thesis. In concentration determination part, sound speed measurements are done.

## CHAPTER 2

# ULTRASONIC CHARACTERIZATION OF POLYMERS AND VISCOELASTICITY OF MATERIALS

### 2.1 Ultrasonic Techniques for Polymer Characterization

Ultrasonic techniques are applicable for polymer processing as rapid audit of the process is necessary for the end product quality and economics of the production. For example, N. Zhou [30] worked on the product quality of poly (lactic acid) cellular matrix composites reinforced with three dimensional ramie fabrics woven with different types of co-wrapped yarns. Existence of voids in the structure was analyzed by measuring sound attenuation. The samples giving higher attenuation coefficients were concluded to have more voids than the others.

Applicability of in-line and on-line supervision of processes is one of the main advantages of ultrasound over conventional techniques. Hence, many researchers benefit from this superiority of ultrasound. P. Zhao et al. [3] applied ultrasonic techniques, depending on the measurement of attenuation, to investigate polymer viscoelasticity in injection molding. Any change in the attenuation with respect to time was considered as the implication of the change in the viscoelasticity of the polymer in the process.

Ultrasonic methods can also be utilized for kinetic studies on polymers. L. Zhao et al. [4] probed the relation between attenuation of sound and crystallization degree of poly(ethyleneterephthalate). By detecting the change of attenuation in polymer with respect to time and temperature, important insight about the crystallization degree

and kinetics was obtained. Similarly, W. Stark et al. [31] analyzed the crosslinking reaction of ethylene vinyl acetate online by ultrasonic technique. The ultrasonic evaluation of crosslinking behavior of ethylene vinyl acetate was achieved by means of ultrasound speed measurements. About 8 m/s increase in sound speed was obtained when the crosslinking process finished. Hence, by detecting the changes in the sound speed with respect to process time, the crosslinking kinetics could be obtained for ethylene vinyl acetate. In addition, crosslinking was also obtained by curemeter and results were in good agreement with each other. Use of ultrasound for identification of crystallization behavior was noted to be advantageous over curemeter, since online measurements were possible with ultrasound unlike curemeter.

Determination of complex modulus of elasticity by ultrasonic techniques is possible, as well. J. Pyrak-Nolte and co-workers [32] detected the complex modulus of elasticity of dough during fermentation process by measuring sound attenuation. As the fermentation proceeds, complex modulus changed due to the transformation of physical properties of the medium. As a result, on-line monitoring of the fermentation process became possible. Similarly, G. Álvarez and co-workers [33] measured the complex modulus of elasticity of silica aerogels dependent on the frequency of ultrasound. Storage modulus was found to increase with frequency. T. Miller et al. [34] studied on the ultrasonic imaging of in vivo tracheal elasticity. Pressure and volume relationship was obtained for static resting and dynamic loading periods since tracheal sizes could be detected online by ultrasonic methods. Instantaneous changes in bulk modulus and stress-strain relations were found. Hence, by evaluating the results of these types of experiments, improvements in respiratory therapies according to airway dynamics may be obtained.

Besides, several works were accomplished to probe viscoelastic properties of materials by investigating sound attenuation and speed. Numbers of mechanisms are responsible for the sound attenuation such as viscous effects, thermal conduction and chemical effects. Particularly, viscous or viscoelastic effects are the principal mechanisms determining the magnitude of the sound absorption in liquid systems

[7]. Complex modulus of elasticity is one of the important indicators of the viscoelastic character of the material [12, 35]. C. Schmitt et al. [36] determined the blood clot viscoelasticity in terms of complex modulus of blood clot samples. Frequency dependent results were fitted to Maxwell, Kelvin-Voigt, Jeffrey, Zener and third order generalized Maxwell models. Storage modulus was found to increase with frequency and stabilized to a plateau whereas loss modulus remained almost constant. Zener model was found to be the best fitting model to capture the rheological behavior of the blood clot. D. Manolis et al. [37] investigated wave propagation in a viscoelastic medium such that elastic modulus of the medium was fluctuating around a mean value. Owing to the complexity of the media, it was essential to determine the position dependent elastic modulus mathematically for analyzing such systems. For this purpose, wave equation was handled and solutions were acquired in the form of Green's function. Then elastic modulus of the material was obtained by the use of perturbation approach.

Applications of empirical correlations are another approach to interpret the acoustic parameters. B. Mert et al. [38] measured the rheological properties of liquid in cylindrical container by using acoustic techniques in audible range. Their technique based on measuring attenuation coefficient and relating attenuation coefficient to viscoelastic properties by the use of empirical correlations. The technique was originally considered for the food processing, hence, quality of the food could be supervised online. Presence of solid particles in the food might cause scattering of sound. However, use of audible frequency eliminated the presence of scattering of sound, which was one of the main points stressed in this study.

Deriving mathematical relations between sound attenuation and viscoelastic properties of the material is crucial for simulating the sound propagation in viscoelastic medium. One of the ways of obtaining such relations is to solve equation of continuity and motion with appropriate initial and boundary conditions, and acquiring the attenuation as a function of viscoelastic properties of the material.

To illustrate O. Assia et al. [6] handled the wave equation to simulate ultrasound propagation in Newtonian liquid by using Laplace transformation technique. Change of sound pressure amplitude with respect to frequency, length and relaxation time were simulated. P. Petrov et al. [39] solved the wave equation numerically to analyze the shallow sea acoustics. Viscoelastic behavior of the medium was assumed to obey Maxwell model. Promising results were obtained based on the model. This approach was expected to be useful in seismic surveying or anthropogenic noise monitoring in water areas. M. Ichihara et al. [40] analyzed the wave propagation in viscoelastic liquid in the presence of bubbles to identify the activities of magma. Motion of bubbles and wave propagation were modeled by Jeffrey's model. Equation of motion (including bubbles) was solved to obtain dispersion relation for wave propagation by the use of methodology derived by H. Fogler et al. [41]. Results of simulations reveal that both viscous and elastic characteristics were effecting the wave propagation and bubble motion. Provided that liquid was rigid enough, bubbles did not affect sound speed. Since magma had high rigidity, it was expected that sound speed is not affected by the bubbles in magma. A similar study was done by E. Marchetti et al. [42]. They also examined the wave propagation in viscoelastic medium including bubbles to simulate the occurrences in magma. Apart from the previous work effect of the depth on acoustic parameters was also analyzed by numerically solving equation of motion. Density of the liquid, bulk modulus, viscosity and sound speed changed according to depth since properties of the bubbles varied as a function of depth.

Nevertheless, dealing with mathematical modeling of sound propagation in viscoelastic medium includes many challenges [43]. Since, solving these types of equations requires complicated mathematical treatments. Simultaneous solutions of set of set of non-linear equations, especially when the thermal effects are included, are difficult to obtain. In most of the researches using such techniques, solutions are obtained with numerical calculations.

Alternatively, another method of solving these equations is to propose solution for the wave equation. By introducing the proposed solution into the conservation

equations acoustic parameters in terms of the physical properties are obtained. These types of approaches are more practical to use than the integral transformation techniques in wave propagation studies. By using this procedure, O. Sotolongo et al. modeled the propagation of small amplitude waves in viscoelastic media consisting of a polymer solution [44]. The model revealed that bulk modulus and viscoelasticity of the solution were effective for the determination of acoustic parameters. Compressible viscous fluid behavior was observed at low frequencies. In this case polymer addition increased the solution viscosity. For higher frequencies, on the other hand, change of polymer concentration did not alter the character of the solution. Solvent viscosity was controlling the sound propagation. At the intermediate frequencies both bulk modulus and solvent viscosity were important for the sound propagation.

A comprehensive study on the sound propagation in viscoelastic media including the heat effects by using similar method was done by I. Perepechko et al. [5]. They found that at low frequencies sound propagates adiabatically. However, as frequency gets higher, the sound propagation deviated from adiabatic condition and dissipation of sound energy became more observable. In addition, dynamic modulus of elasticity and sound speed increased with frequency, as well.

Aforementioned studies principally are based on the utilization of the base frequency of sound on propagation. Hence, the propagation of continuous sound wave has been fairly analyzed by the former researches. Nevertheless, the sound propagation with modulated ultrasound signal pattern or the influence of pulse repetition frequency was not apparently explored yet. The first study in literature developed based on the pulse repetition frequency was accomplished with our previous work [45]. In that study, a mathematical model simulating the modulated sound propagation was derived, for the characterization of viscoelastic liquids, depending on the pulse repetition frequency of ultrasound. For this purpose a linear model, Voigt-Kelvin model was employed. That study is extended in this thesis. Instead of linear viscoelastic behavior, modulated ultrasound propagation in non-linear viscoelastic medium is investigated in this study. In addition, it should be mentioned that base or

natural frequency of ultrasound can vary between kHz to MHz ranges. On the other hand, the pulse repetition frequency is in the order of Hz ranges. Therefore, it is possible to probe viscoelastic material properties or characteristic times of relaxation in the time scales from milliseconds to seconds as opposed to the previous studies. The confirmation of the proposed mathematical model is performed by comparing its predictions with those of experimental observations obtained during this work.

## 2.2 Fluid Viscoelasticity

Elastic materials have the ability of storing energy without experiencing dissipation of energy. However, Newtonian fluids are not able to store energy; they completely dissipate it due to their viscous characteristics [16]. Some materials can both exhibit viscous and elastic behavior simultaneously [46, 47]. Viscoelastic behavior is one of the most distinctive properties of polymeric materials [48, 49]. For them, stress is both dependent on strain ( $\gamma_{yx}$ ) and rate of strain ( $\dot{\gamma}_{yx}$ ) [50, 51].

It should be mentioned that majority of the liquids are perfectly Newtonian liquids such that they do not exhibit any elastic response. In addition, there is not a pure solid that entirely obey Hooke's law. It is the Maxwell J. who was one of the first people putting emphasis on this event [52].

There are two major tools for the characterization of mechanical properties of polymers; stress and strain. The force exerted on the surfaces of differential volume of a polymer is stress tensor. Strain tensor is the variation of the sizes of that volume under the influence of stress tensor.

Stress relaxation is the fundamental feature of the polymers defining time dependent response of them under stress. Suppose that a viscoelastic material is experienced constant strain  $\gamma_0$  instantaneously. Then, the stress required to endure this constant strain will start to reduce with time [50]. This constitutes the stress relaxation test.

Viscoelastic characteristics of polymers can also be probed by creep experiment. In creep experiment, suddenly a constant stress ( $\tau_0$ ) is imposed on the material. At the same time, the strain starts to increase for maintaining constant stress. If then the stress is eliminated, the strain will start to decline. This is the creep recovery experiment, another technique for analyzing viscoelastic properties of polymers.

There are some mathematical expressions manifested to indicate stress relaxation and creep behaviors of the viscoelastic materials under deformations. These expressions can be presented by spring and dashpot analogy (Appendix A1). In this analogy, springs and dashpots are representing elastic and viscous behaviors, respectively. Each model is developed from the different configurations of these elements joined with each other in series or parallel. In spring, elastic character of the material is described by Hooke's Law. In addition, viscous behavior is stated by the Newton's Law of viscosity in dashpot.

### 2.3 Relation between Stress and Strain

The relationship between stress and strain can be expressed by;

$$\tau = E^* \gamma \quad \text{eqn. 2.1}$$

Here,  $E^*$  denotes the complex modulus of elasticity. The real part of  $E^*$  defines dynamic modulus of elasticity while the imaginary part of  $E^*$  specifies the loss modulus. In other words;

$$E^*(\omega) = E'(\omega) + E''(\omega) \quad \text{eqn. 2.2}$$

The dynamic modulus of elasticity identifies the extent of energy stored while the loss modulus is associated with the energy dissipation properties of the material. Some commonly used linear viscoelastic models are presented in Appendix A1 part.

## 2.4 Non-Linear Viscoelastic Behavior

The theory of linear viscoelasticity provided very valuable information for the researches on rheology. Linear viscoelasticity restore the perception of two fundamental mechanical models, the Maxwell and Voigt models. It presents the idea of generalization of these models. The idea of the relaxation and retardation time spectra is one of its practical conclusions. Linear viscoelastic systems are usually handled by the use of this idea. However, usage of this theory is limited with the investigations of linear stress-strain relations and the case of small deformations (Figure 2.1).

On the other hand, important advancements are done on the experimental methods with large deformations. Hence, many respectable investigations are obtained about non-linear viscoelastic behaviors. Structural viscosity (non-Newtonian viscosity), tensile viscosity, non-Hookian elasticity are basic examples to non-linear character of materials. The normal stress effects (the Weissenberg effect for elasticoviscous liquids and the Poynting effect for viscoelastic solids) are the distinctive illustrations to non-linear effects. For non-linear viscoelasticity, classical linear theory is not valid anymore.

However, in evaluation of non-linear viscoelastic behavior, an important concern arises. The principle of superposition is no longer acceptable since the linear relation between stress and strain is not valid as opposed to linear behavior. Hence, unsophisticated mathematical models corresponding to the generalization of the mechanical models can not be used for non-linear behavior. Hence, in such models there are higher order differential equation comprising strain, stress, and their velocities, accelerations and higher order derivatives with respect to time [52].

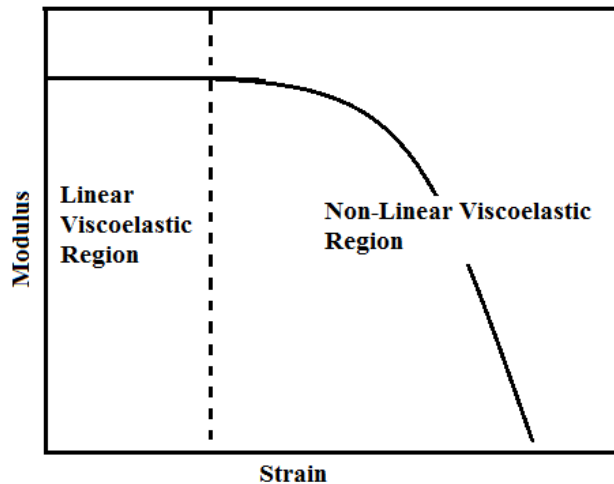


*Figure 2.1 Investigation of Linear and Non-linear Viscoelastic Regions*

The models introduced in this section are not obtained from the simple spring and dashpot analogy described in the previous section. Alternatively, a microstructural treatment is implemented [49]. There are three theoretical methods for developing the constitutive models from the behavior of polymer molecules:

#### **2.4.1 Dilute solution theories:**

Dilute solution theories handle the polymer molecules individually. Each molecule is described as a chain of beads and springs or beads and rods. The interaction with the flow is due to the hydrodynamic drag applied from the fluid on the beads. The Upper Convected Maxwell model is developed from this theory.

#### **2.4.2 Reptation theories:**

In reptation theories, polymer molecules are handled individually as in dilute solution theories. However, reptation theory is valid for undiluted solutions. In this type, molecular motion is restricted by the neighboring molecules. Hence, molecules exhibit snakelike motion. Figure 2.2 schematically illustrates the dilute solution and reptation theories.

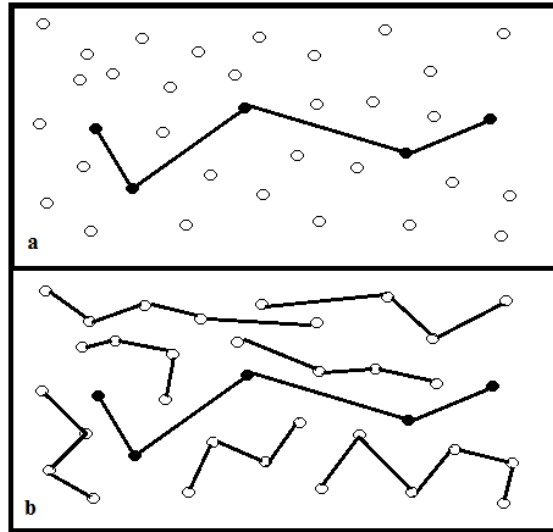


**Figure 2.2** a) Dilute Solution Theory (polymer can move freely in the solvent), b) Reptation Theory (movement of the polymer is restricted by the other polymer chains)

### 2.4.3 Network theories:

The rheological behavior of polymer is modelled as a network of springs joined at junction points. The primitive methods are developed for solid rubber and junctions are modelled as fixed (Figure 2.3). Then, models are modified to allow the junctions to form and decay following established statistical laws. The interaction between the polymer chains and the flow take place thanks to the movement of these junctions. The origin of the PTT model, developed by Phan-Thien and Tanner, is network theory.

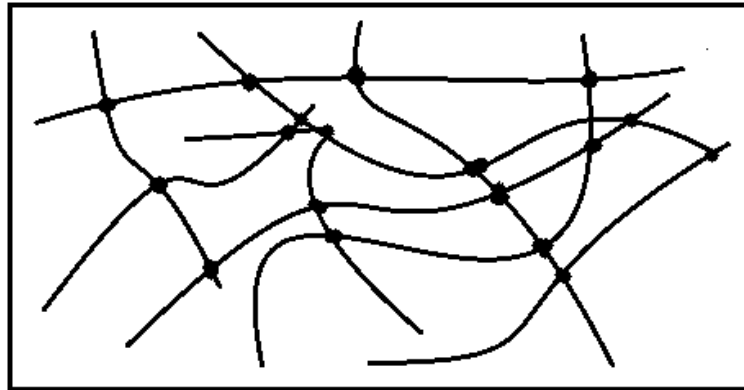


*Figure 2.3 Polymer Network and Junction Points*

## 2.5 Oldroyd-B Model

General linear viscoelastic models may fail to identify fluid motions properly especially upon large deformations from its initial position take place as discussed in pervious section. This drawback of linear models may be overcome by reformulating them into convected reference frame. Visualization of convected coordinate system is shown in the Figure 2.4. In convected frame the observer displaced with the motion of fluid while in fixed system position of the observer is fixed. By this approach non-linear convected models are obtained.

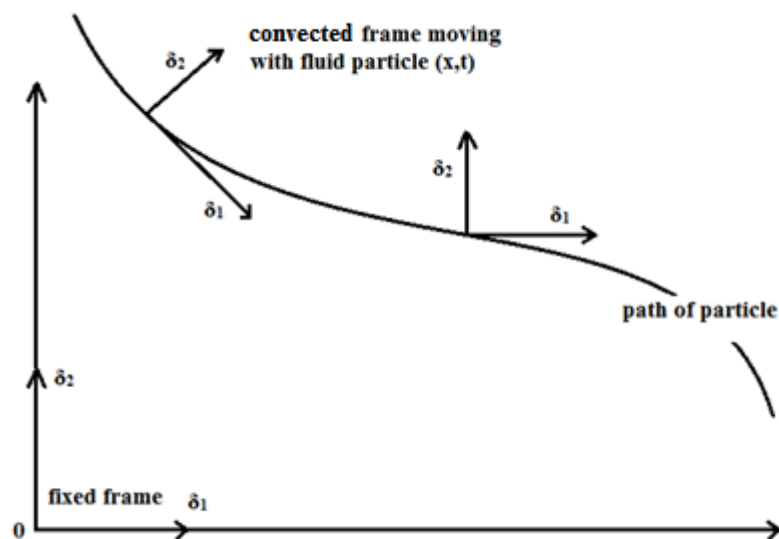


*Figure 2.4 Illustration of Fixed and Convected Frames*

Jeffreys model can be extended by the addition of some non-linear terms as [52];

$$\bar{\tau} + \lambda_1 \frac{\partial}{\partial t} \bar{\tau} + \frac{1}{2} \mu_0 (\text{tr} \bar{\tau}) \dot{\bar{\gamma}} - \frac{1}{2} \mu_1 |\dot{\bar{\gamma}} \cdot \bar{\tau} + \bar{\tau} \cdot \dot{\bar{\gamma}}| = -\eta_0 \left( \dot{\bar{\gamma}} + \lambda_2 \frac{\partial}{\partial t} \dot{\bar{\gamma}} - \mu_2 |\dot{\bar{\gamma}} \cdot \dot{\bar{\gamma}}| \right) \quad \text{eqn. 2.3}$$

The marks on the stress and rate of strain tensors indicate that their components are defined according to convected reference frame.  $\lambda_1$ ,  $\lambda_2$ ,  $\mu_0$ ,  $\mu_1$  and  $\mu_2$  are time constants. Since the equation of continuity and motion are written for xyz frame (fixed position), the equation should be turned from convected reference frame into ordinary xyz frame. For this purpose partial time derivatives should be replaced by convected time derivatives. Convected time derivative is given as;

$$\frac{\tilde{D}}{\tilde{D}t} \psi = \frac{D}{Dt} \psi + \frac{1}{2} |\omega \cdot \psi - \psi \cdot \omega| \quad \text{eqn. 2.4}$$

Where “ $\omega$ ” is vorticity tensor defined as;

$$\omega = \nabla \mathbf{v} - (\nabla \mathbf{v})^\dagger \quad \text{eqn. 2.5}$$

In addition, D/Dt is substantial time derivative given as;

$$\frac{D}{Dt} = \frac{\partial}{\partial t} + (\mathbf{v} \cdot \nabla) \quad \text{eqn. 2.6}$$

The dot products in the equation are given for convected frame hence they should also be transformed into dot products in xyz frame. By making these substitutions;

$$\tau + \lambda_1 \frac{\tilde{D}}{\tilde{D}t} \tau + \frac{1}{2} \mu_0 (\text{tr} \tau) \dot{\gamma} - \frac{1}{2} \mu_1 |\dot{\gamma} \cdot \tau + \tau \cdot \dot{\gamma}| = -\eta_0 \left( \dot{\gamma} + \lambda_2 \frac{\tilde{D}}{\tilde{D}t} \dot{\gamma} - \mu_2 |\dot{\gamma} \cdot \dot{\gamma}| \right) \quad \text{eqn. 2.7}$$

This equation is known as Oldroyd 6-constant model. When the constants in the model are appropriately determined, rheological behavior of the fluids can be successfully identified. This is the reason why Oldroyd models are extensively applied in calculations. A further simplification of the model by taking  $\mu_1 = \lambda_1$ ,  $\mu_2 = \lambda_2$  and  $\mu_0 = 0$  gives the Oldroyd-B model. Hence, Oldroyd-B model is obtained as;

$$\tau + \lambda_1 \frac{\tilde{D}}{\tilde{D}t} \tau - \frac{1}{2} \lambda_1 |\dot{\gamma} \cdot \tau + \tau \cdot \dot{\gamma}| = -\eta_0 \left( \dot{\gamma} + \lambda_2 \frac{\tilde{D}}{\tilde{D}t} \dot{\gamma} - \lambda_2 |\dot{\gamma} \cdot \dot{\gamma}| \right) \quad \text{eqn. 2.8}$$

## **2.6 Relation between Fluid Viscoelasticity and Physical Acoustics**

The concepts of physical acoustics state that sound propagate such that the region in the material, where the sound is propagating on it, is compressed. This fact is also defined as the displacement of particles. When the wave propagation is terminated, then the region starts to decompress (or particles settle their initial equilibrium positions). Thus, there is a characteristic time for particles to recover their equilibrium position. This time is called as relaxation time in physical acoustics. A similar physical phenomenon is also handled by rheology. Some characteristic times for describing the recovery of the shape of the material are applied by rheology, as well. In this perspective, the ideas of physical acoustics and rheology are coinciding. Physical acoustics perceives relaxation behavior in micro scale while rheology detects it in macro scale. Viscous and elastic effects in rheology are corresponding to sound attenuation coefficient and sound speed, respectively, in acoustics. Therefore, constructing a relationship between acoustic parameters and viscoelastic parameters is strongly important for ultrasonic characterization of viscoelasticity.



## CHAPTER 3

# MATHEMATICAL MODELING OF ULTRASOUND PROPAGATION IN A NON-LINEAR VISCOELASTIC MATERIAL

### 3.1 Propagation of Sound Waves in a Medium

In this part, modulated ultrasound propagation in non-linear viscoelastic media is modeled. A similar approach with our previous work [45] is followed. Ultimately, a model relating acoustic parameters with the viscoelastic parameters is obtained.

Displacement of particles under the action of a continuous wave can be defined as;

$$\mathbf{u} = \mathbf{u}_{0k} e^{i\omega t - \sigma x} \quad \text{eqn. 3.1}$$

where  $\sigma$  is complex wave number and described as;

$$\sigma = \alpha + i \frac{\omega}{c} \quad \text{eqn. 3.2}$$

It should be noted that wave number “ $\sigma$ ” includes both attenuation coefficient and sound speed. This is the fundamental parameter characterizing the propagation of wave as it implicitly contains information about the material properties. For this reason, all the operations in the rest of the model is simply for obtaining a relation between wave number “ $\sigma$ ” and material properties.

Nevertheless, eqn. 3.1 is not able to describe the propagation of modulated wave propagation. This expression should be modified to explain modulated sound propagation. The representation of the modulation procedure is shown in Figure 3.1.

In this figure, pulses are delivered to system. Duration of each pulse is designated as “n”. In addition, the time between the end of a pulse and the beginning of the next one is specified as “a”.

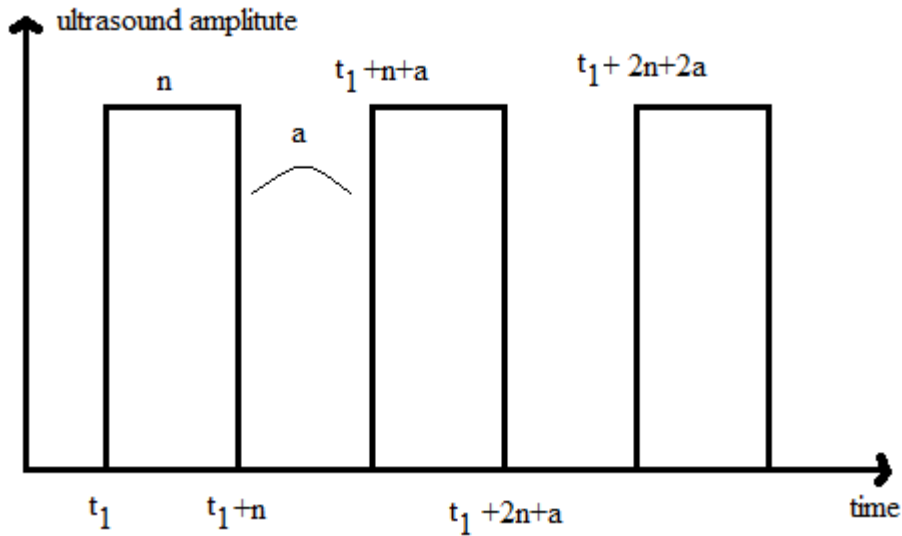


**Figure 3.1** Representation of Modulated Ultrasound Waves in the Medium

At time,  $t_1$  the first sound signal is sent to material. Hence, eqn. 3.1 can simulate the displacement of particles between the time  $t_1$  and  $t_1+n$ . After the time,  $t_1+n$ , the sound propagation is stopped until the time,  $t_1+n+a$ .

In order to express the pulsatile form of the ultrasound, the following modification can be done on eqn. 3.1;

$$u = H(t - t_1)u_{0k}e^{i\omega t - \sigma x} - H(t - (t_1 + n))u_{0k}e^{i\omega t - \sigma x} \quad \text{eqn. 3.3}$$

where H is the Heaviside unit step function, defined as;

$$H(t - a) = \begin{cases} 1 & \text{if } t > a \\ 1/2 & \text{if } t = a \\ 0 & \text{if } t < a \end{cases}$$

The first term in eqn. 3.3 becomes  $u_{0k}e^{i\omega t - \sigma x}$  after the time,  $t_1$ ; however, the second term is still equal to zero until the time,  $t_1+n$ . After time,  $t_1+n$  the second term is

equalized to  $-u_{0k}e^{i\omega t - \sigma x}$ ; thus, these terms cancel each other, and eqn. 3.3 becomes zero. Nevertheless, this is not enough to simulate the process yet. Eqn. 3.3 defines the behavior of the system only in the time between  $t_1$  and  $t_1+n$ . When times passes  $t_1+n$ , particles start to recover their equilibrium positions. Hence, a term expressing the particles' recovery to their equilibrium positions is needed to complete the model. At time,  $t_1+n$  the displacement of the particles is  $u_{0k}e^{i\omega(t_1+n) - \sigma x}$  and this value should be adjusted as the initial condition of the recovery term. Furthermore, mathematical formulation of that recovery behavior can be identified by the use of viscoelastic constitutive equations. The displacement of particles under the action of modulated sound propagation is represented in Figure 3.2.

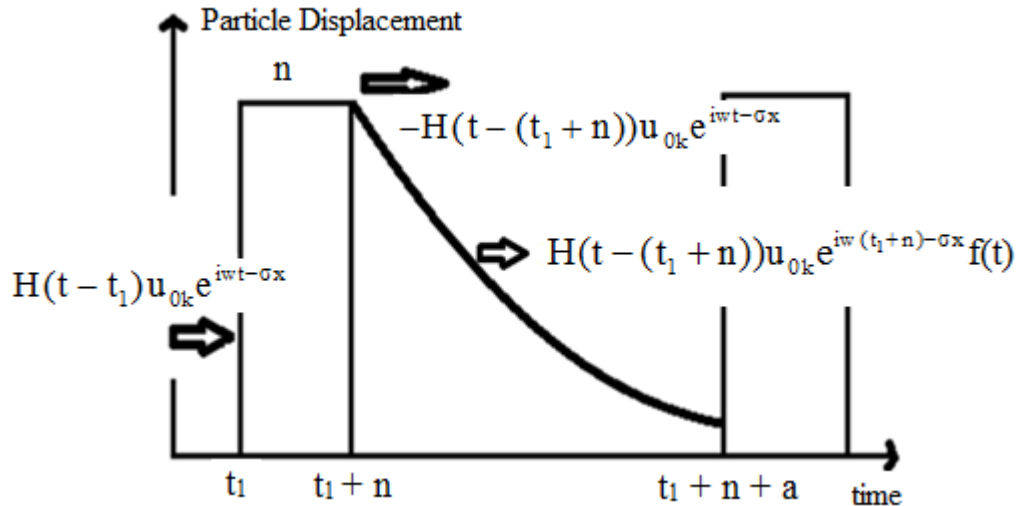


**Figure 3.2** Representation of the Displacement of Particles with Time

To express the behavior of molecules Oldroyd-B model is applied. Though the wave propagates in sinusoidal manner, the mean amplitude of the wave pressure remains constant. Thus, during this time interval (“n”) the molecules can be regarded to be under the action of constant loading. As the wave stops, the molecules start to settle their equilibrium position. This behavior can be expresses by the model provided that the term defining the recovery of molecules with respect to Oldroyd-B model is involved in the main model. To simplify Oldroyd-B model according to our case, first define the stress and rate of strain tensors in open form.

$$\tau = \begin{vmatrix} \tau_{xx} & \tau_{xy} & \tau_{xz} \\ \tau_{yx} & \tau_{yy} & \tau_{yz} \\ \tau_{zx} & \tau_{zy} & \tau_{zz} \end{vmatrix} \text{ and } \dot{\gamma} = \begin{vmatrix} \gamma_{xx} & \gamma_{xy} & \gamma_{xz} \\ \gamma_{yx} & \gamma_{yy} & \gamma_{yz} \\ \gamma_{zx} & \gamma_{zy} & \gamma_{zz} \end{vmatrix} \quad \text{eqn. 3.4}$$

In these tensors only  $\tau_{xx}$  and  $\gamma_{xx}$  components survive for the physics of this problem. In this system longitudinal wave propagation takes place. Therefore, movements of the particles are parallel to the direction of wave propagation. Therefore, only  $\gamma_{xx}$  term has a value other than zero. In addition, shear waves are not able to be sustained by liquid systems. Hence, shear stresses in the stress tensor can be omitted. By substituting  $\tau_{xx}$  and  $\gamma_{xx}$  into Oldroyd-B equation, it is finally obtained;

$$\tau_0 - \lambda_1 \tau_0 \dot{\gamma} = -\eta_0 \left( \dot{\gamma} + \lambda_2 \left( \frac{\partial \dot{\gamma}}{\partial t} - \dot{\gamma}^2 \right) \right) \quad \text{eqn. 3.5}$$

It should be noted that  $\tau_0$  is the pressure of ultrasound. When wave stops, applied pressure  $\tau_0$  becomes zero. Hence, during recovery period the following equation should be used;

$$0 = \left( \dot{\gamma} + \lambda_2 \left( \frac{\partial \dot{\gamma}}{\partial t} - \dot{\gamma}^2 \right) \right) \quad \text{eqn. 3.6}$$

Solving the differential equation for recovery period;

$$\gamma_{xx} = \frac{\exp\left(\frac{-1}{\lambda_2}(t-t_0)\right) \frac{\gamma_0}{(-\lambda_2 \gamma_0 + 1)}}{1 + \exp\left(\frac{-1}{\lambda_2}(t-t_0)\right) \frac{\gamma_0}{(-\lambda_2 \gamma_0 + 1)} \lambda_2} \quad \text{eqn. 3.7}$$

Using this equation in terms of  $u$  is more practical for sound propagation simulations.

Hence, it can be written that;

$$u = \frac{\exp\left(\frac{-1}{\lambda_2} t\right) \frac{u_{0k}}{(-\lambda_2 u_{0k} + 1)}}{1 + \exp\left(\frac{-1}{\lambda_2} t\right) \frac{u_{0k}}{(-\lambda_2 u_{0k} + 1)} \lambda_2} \quad \text{eqn. 3.8}$$

Here,  $u_0$  refers to displacement of particles just before the wave stops. Hence, this constitutes the initial condition of the model in recovery period.

By adding this term into eqn. 3.3, and making the similar calculation for the second wave, it is obtained that;

$$\begin{aligned}
u &= H(t-t_1)u_{0k}e^{i\omega t-\sigma x} - H(t-(t_1+n))u_{0k}e^{i\omega t-\sigma x} \\
&+ H(t-(t_1+n))u_{0k}e^{i\omega(t_1+n)-\sigma x} \frac{\exp\left(\frac{-1}{\lambda_2}t\right)\frac{1}{(-\lambda_2 u_{0k}+1)}}{1+\exp\left(\frac{-1}{\lambda_2}t\right)\frac{u_{0k}}{(-\lambda_2 u_{0k}+1)}\lambda_2} \\
&+ H(t-(t_1+n+a))u_{0k}e^{i\omega t-\sigma x} - H(t-(t_1+2n+a))u_{0k}e^{i\omega t-\sigma x} \\
&+ H(t-(t_1+2n+a))u_{0k}e^{i\omega(t_1+2n+a)-\sigma x} \frac{\exp\left(\frac{-(t-(t_1+2n+a))}{\lambda_2}\right)\frac{1}{(-\lambda_2 u_{0k}+1)}}{1+\exp\left(\frac{-1}{\lambda_2}t\right)\frac{u_{0k}}{(-\lambda_2 u_{0k}+1)}\lambda_2}
\end{aligned}$$

eqn. 3.9

Eqn. 3.9 can be generalized for “m” number waves as;

$$\begin{aligned}
u &= \sum_{j=0}^m u_{0k} e^{-\sigma x} [e^{i\omega t} H(t-(t_1+j(n+a))) - e^{i\omega t} H(t-(t_1+(j+1)n+ja))] \\
&+ e^{i\omega(t_1+(j+1)n+ja)} H(t-(t_1+(j+1)n+ja)) \frac{\exp\left(\frac{-(t-(t_1+(j+1)n+ja))}{\lambda_2}\right)\frac{1}{(-\lambda_2 u_{0k}+1)}}{1+\exp\left(\frac{-(t-(t_1+(j+1)n+ja))}{\lambda_2}\right)\frac{u_{0k}}{(-\lambda_2 u_{0k}+1)}\lambda_2}
\end{aligned}$$

eqn. 3.10

Temperature and density variations can also be expressed similar to the displacement;

$$\begin{aligned}
T &= \sum_{j=0}^m T_{0k} e^{-\sigma x} [e^{i\omega t} H(t-(t_1+j(n+a))) - e^{i\omega t} H(t-(t_1+(j+1)n+ja))] \\
&+ e^{i\omega(t_1+(j+1)n+ja)} H(t-(t_1+(j+1)n+ja)) \frac{\exp\left(\frac{-(t-(t_1+(j+1)n+ja))}{\lambda_2}\right)\frac{1}{(-\lambda_2 T_{0k}+1)}}{1+\exp\left(\frac{-(t-(t_1+(j+1)n+ja))}{\lambda_2}\right)\frac{T_{0k}}{(-\lambda_2 T_{0k}+1)}\lambda_2}
\end{aligned}$$

eqn.3.11

$$\rho = \sum_{j=0}^m \rho_{0k} e^{-\sigma x} [e^{i\omega t} \mathbf{H}(t - (t_1 + j(n+a))) - e^{i\omega t} \mathbf{H}(t - (t_1 + (j+1)n + ja))] + e^{i\omega(t_1 + (j+1)n + ja)} \mathbf{H}(t - (t_1 + (j+1)n + ja)) \frac{\exp\left(-\frac{(t - (t_1 + (j+1)n + ja))}{\lambda_2}\right) \frac{1}{(-\lambda_2 \rho_{0k} + 1)}}{1 + \exp\left(-\frac{(t - (t_1 + (j+1)n + ja))}{\lambda_2}\right) \frac{\rho_{0k}}{(-\lambda_2 \rho_{0k} + 1)} \lambda_2}$$

eqn. 3.12

Furthermore, the pressure variation can also be defined as;

$$P = \sum_{j=0}^m P_{0k} e^{-\sigma x} [e^{i\omega t} \mathbf{H}(t - (t_1 + j(n+a))) - e^{i\omega t} \mathbf{H}(t - (t_1 + (j+1)n + ja))] + e^{i\omega(t_1 + (j+1)n + ja)} \mathbf{H}(t - (t_1 + (j+1)n + ja)) \frac{\exp\left(-\frac{(t - (t_1 + (j+1)n + ja))}{\lambda_2}\right) \frac{1}{(-\lambda_2 P_{0k} + 1)}}{1 + \exp\left(-\frac{(t - (t_1 + (j+1)n + ja))}{\lambda_2}\right) \frac{P_{0k}}{(-\lambda_2 P_{0k} + 1)} \lambda_2}$$

eqn. 3.13

For the sake of simplicity, let's define A, B and C as;

$$A = \mathbf{H}(t - (t_1 + j(n+a))) - \mathbf{H}(t - (t_1 + (j+1)n + ja))$$

eqn. 3.14

$$B = e^{i\omega(t_1 + (j+1)n + ja)} \mathbf{H}(t - (t_1 + (j+1)n + ja))$$

eqn. 3.15

$$C = e^{i\omega(t_1 + (j+1)n + ja)}$$

eqn. 3.16

Now, proposed solutions for u, ρ and T are obtained. Here, the main quantity characterizing the u, ρ and T variations is “σ”. Hence, in order to identify the u, ρ and T variations through “σ”, these suggested solutions for u, ρ and T, should be inserted into the governing differential equations. Dependent variables in the governing differential equations should be written in terms of u, ρ and T. Hence, some simplifications and modifications are done in the equation of continuity, motion and energy. Ultimately, the governing differential equations take the form of;

$$\frac{\partial \rho}{\partial t} + \rho_0 \frac{\partial^2 u}{\partial x \partial t} = 0$$

eqn. 3.17

$$\rho_0 \frac{\partial^2 \mathbf{u}}{\partial t^2} + \mathbf{K}_T \alpha_v \frac{\partial T}{\partial x} - \mathbf{L} \frac{\partial^2 \mathbf{u}}{\partial x^2} = 0 \quad \text{eqn. 3.18}$$

$$C_v \frac{\partial T}{\partial t} - \frac{T \alpha_v \mathbf{K}_T}{\rho_0^2} \frac{\partial \rho}{\partial t} - \frac{k}{\rho_0} \frac{\partial^2 T}{\partial x^2} = 0 \quad \text{eqn. 3.19}$$

Detailed calculations about obtaining the governing differential equations are shown in the Appendix A3 part.

Differentiating  $u$ ,  $\rho$  and  $T$ ;

$$\frac{\partial \rho}{\partial t} = \sum_{j=1}^m \left[ \rho_{0k} e^{i\omega t - \sigma x} (i\omega) + \rho_{0k} e^{-\sigma x} \mathbf{B} \exp \left( -\frac{1}{\lambda_2} (t - (t_1 + (j+1)n + ja)) \right) \right] \frac{1}{(-\lambda_2 \rho_{0k} \mathbf{C} e^{-\sigma x} + 1)} \left( -\frac{1}{\lambda_2} \right)$$

$$\frac{\partial T}{\partial t} = \sum_{j=1}^m \left[ T_{0k} e^{i\omega t - \sigma x} (i\omega) + T_{0k} e^{-\sigma x} \mathbf{B} \exp \left( -\frac{1}{\lambda_2} (t - (t_1 + (j+1)n + ja)) \right) \right] \frac{1}{(-\lambda_2 T_{0k} \mathbf{C} e^{-\sigma x} + 1)} \left( -\frac{1}{\lambda_2} \right)$$

$$\begin{aligned} \frac{\partial T}{\partial x} &= \sum_{j=1}^m T_{0k} e^{i\omega t - \sigma x} (-\sigma) + T_{0k} e^{-\sigma x} \mathbf{B} (-\sigma) \exp \left( -\frac{1}{\lambda_2} (t - (t_1 + (j+1)n + ja)) \right) \frac{1}{(-\lambda_2 T_{0k} \mathbf{C} e^{-\sigma x} + 1)} \\ &+ T_{0k} e^{-\sigma x} \mathbf{B} \exp \left( -\frac{1}{\lambda_2} (t - (t_1 + (j+1)n + ja)) \right) \frac{-\lambda_2 T_{0k} \mathbf{C} \sigma e^{-\sigma x}}{(-\lambda_2 T_{0k} \mathbf{C} e^{-\sigma x} + 1)^2} \end{aligned}$$

$$\begin{aligned} \frac{\partial^2 T}{\partial x^2} &= \sum_{j=1}^m T_{0k} e^{i\omega t - \sigma x} \sigma^2 + T_{0k} e^{-\sigma x} \mathbf{B} \sigma^2 \exp \left( -\frac{1}{\lambda_2} (t - (t_1 + (j+1)n + ja)) \right) \frac{1}{(-\lambda_2 T_{0k} \mathbf{C} e^{-\sigma x} + 1)} \\ &+ 2T_{0k} e^{-\sigma x} \mathbf{B} (-\sigma) \exp \left( -\frac{1}{\lambda_2} (t - (t_1 + (j+1)n + ja)) \right) \frac{-\lambda_2 T_{0k} \mathbf{C} \sigma e^{-\sigma x}}{(-\lambda_2 T_{0k} \mathbf{C} e^{-\sigma x} + 1)^2} \\ &+ T_{0k} e^{-\sigma x} \mathbf{B} \exp \left( -\frac{1}{\lambda_2} (t - (t_1 + (j+1)n + ja)) \right) \left( \frac{2(-\lambda_2 T_{0k} \mathbf{C})^2 \sigma^2 e^{-2\sigma x}}{(-\lambda_2 T_{0k} \mathbf{C} e^{-\sigma x} + 1)^3} - \frac{(-\lambda_2 T_{0k} \mathbf{C}) \sigma^2 e^{-\sigma x}}{(-\lambda_2 T_{0k} \mathbf{C} e^{-\sigma x} + 1)^2} \right) \end{aligned}$$

$$\begin{aligned}
\frac{\partial^2 \mathbf{u}}{\partial X^2} &= \sum_{j=1}^m \mathbf{u}_{0k} e^{i\omega t - \sigma x} \sigma^2 + \mathbf{u}_{0k} e^{-\sigma x} \mathbf{B} \sigma^2 \exp\left(-\frac{1}{\lambda_2} (t - (t_1 + (j+1)n + ja))\right) \frac{1}{(-\lambda_2 \mathbf{u}_{0k} \mathbf{C} e^{-\sigma x} + 1)} \\
&+ 2\mathbf{u}_{0k} e^{-\sigma x} \mathbf{B} (-\sigma) \exp\left(-\frac{1}{\lambda_2} (t - (t_1 + (j+1)n + ja))\right) \frac{-\lambda_2 \mathbf{u}_{0k} \mathbf{C} \sigma e^{-\sigma x}}{(-\lambda_2 \mathbf{u}_{0k} \mathbf{C} e^{-\sigma x} + 1)^2} \\
&+ \mathbf{u}_{0k} e^{-\sigma x} \mathbf{B} \exp\left(-\frac{1}{\lambda_2} (t - (t_1 + (j+1)n + ja))\right) \left( \frac{2(-\lambda_2 \mathbf{u}_{0k} \mathbf{C})^2 \sigma^2 e^{-2\sigma x}}{(-\lambda_2 \mathbf{u}_{0k} \mathbf{C} e^{-\sigma x} + 1)^3} - \frac{(-\lambda_2 \mathbf{u}_{0k} \mathbf{C}) \sigma^2 e^{-\sigma x}}{(-\lambda_2 \mathbf{u}_{0k} \mathbf{C} e^{-\sigma x} + 1)^2} \right) \\
\frac{\partial^2 \mathbf{u}}{\partial t^2} &= \sum_{j=1}^m \mathbf{u}_{0k} e^{i\omega t - \sigma x} (-\omega^2) + \mathbf{u}_{0k} e^{-\sigma x} \mathbf{B} \exp\left(-\frac{1}{\lambda_2} (t - (t_1 + (j+1)n + ja))\right) \frac{1}{(-\lambda_2 \mathbf{u}_{0k} \mathbf{C} e^{-\sigma x} + 1)} \\
\frac{\partial^2 \mathbf{u}}{\partial x \partial t} &= \sum_{j=1}^m \mathbf{u}_{0k} e^{i\omega t - \sigma x} (i\omega) (-\sigma) + \mathbf{u}_{0k} e^{-\sigma x} \mathbf{B} (-\sigma) \exp\left(-\frac{1}{\lambda_2} (t - (t_1 + (j+1)n + ja))\right) \frac{1}{(-\lambda_2 \mathbf{u}_{0k} \mathbf{C} e^{-\sigma x} + 1)} \left(-\frac{1}{\lambda_2}\right) \\
&+ \mathbf{u}_{0k} e^{-\sigma x} \mathbf{B} \exp\left(-\frac{1}{\lambda_2} (t - (t_1 + (j+1)n + ja))\right) \left( \frac{-\lambda_2 \mathbf{u}_{0k} \mathbf{C} \sigma e^{-\sigma x}}{(-\lambda_2 \mathbf{u}_{0k} \mathbf{C} e^{-\sigma x} + 1)^2} \right) \left(-\frac{1}{\lambda_2}\right)
\end{aligned}$$

Inserting them into our governing differential equations and solving for  $\sigma$ , it is obtained after order of magnitude analysis simplifications that;

$$\sigma = \sqrt{\frac{\rho_0}{L} \frac{\sum_{j=0}^m \left[ -\left( \mathbf{H}(t - (t_1 + j(n+a))) - \mathbf{H}(t - (t_1 + (j+1)n + ja)) \right) e^{i\omega t} \omega^2 + e^{i\omega(t_1 + (j+1)n + ja)} \mathbf{H}(t - (t_1 + (j+1)n + ja)) \left( -\frac{1}{\lambda_2} \right) e^{\left( -\frac{t - (t_1 + (j+1)n + ja)}{\lambda_2} \right)} \right]}{\sum_{j=0}^m \left[ \left( \mathbf{H}(t - (t_1 + j(n+a))) - \mathbf{H}(t - (t_1 + (j+1)n + ja)) \right) e^{i\omega t} i\omega + \mathbf{H}(t - (t_1 + (j+1)n + ja)) e^{\left( -\frac{t - (t_1 + (j+1)n + ja)}{\lambda_2} \right)} \right]}}$$

eqn. 3.20

where

$$L = \frac{\eta_p \lambda_1 \omega^2}{1 + (\lambda_1 \omega)^2} + \left( \eta_s \omega + \frac{\eta_p \omega}{1 + (\lambda_1 \omega)^2} \right) i \quad \text{eqn. 3.21}$$

and

$$\frac{\lambda_2}{\lambda_1} = \frac{\eta_s}{\eta_s + \eta_p} \quad \text{eqn. 3.22}$$

Eqn. 3.20 is the dispersion equation relating the viscoelastic properties of the media with the acoustic parameters.

Hence, density and longitudinal modulus is much more dominant for the determination of  $\sigma$ . Heat effects and thermal expansion is negligibly small. On the basis of this model set of simulations are done with Matlab to see the effects of viscoelastic parameters on sound propagation.

### **3.2 Oldroyd-B Model Simulations**

In order to investigate the behavior of the sound pressure according to material properties a Matlab program is written based on the model. The figures are obtained as a result of the program representing modulated ultrasound propagation in a medium at a fixed position. The vertical axis shows the normalized sound pressure and  $(P/P_0)$  the horizontal axis represents the time. During the discrete sound propagation the medium is periodically compressed and then relaxed like a spring. The compression zone (or loading period) corresponds to the continuous propagation of wave. Then, the ultrasound pulse is stopped and material starts to unload the stress in itself. The duration of the loading and unloading periods are determined by the pulse length and PRF (“n” and “a”) of the sound. In the simulations, “n” and “a” are kept as 0.5 s. In the figures, material is compressed from the time 0.0 s to 0.5 s. Then, wave stops and material relaxes until the time 1.0 s. At this time new compression period starts. This trend continues during the application of the sound pulses.

Simulations are done for different material properties while the pulse repetition frequency is kept constant. The input of ultrasound used in the simulations is shown in the Figure 3.3.

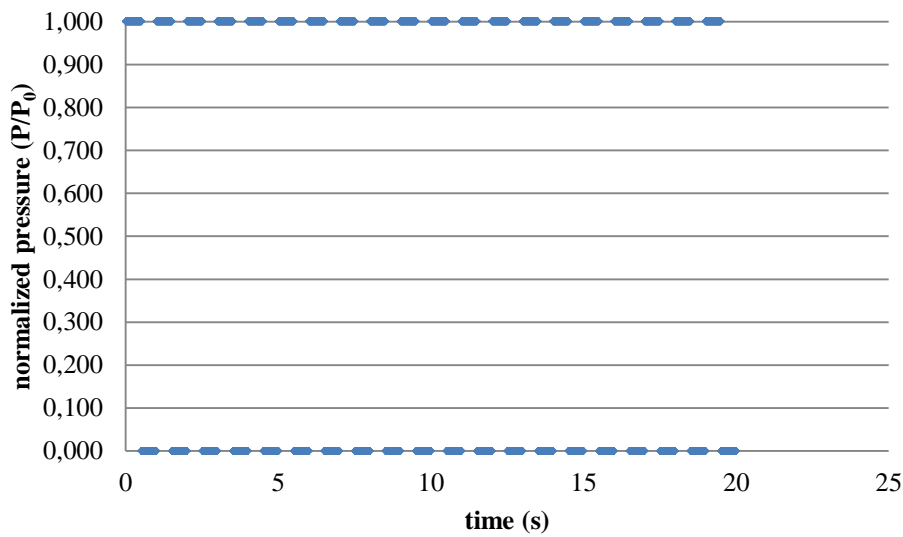


**Figure 3.1** *Ultrasound Input Used in Simulations*

In addition, in the simulations average fluid properties are used. Physical properties of the hypothetical medium are shown in Table 3.1.

**Table 3.1** *Physical Properties of the Hypothetical Medium Used in Simulations*

<b>Physical Property</b>	<b>Value</b>
Density ( $\rho_0$ )	1000 kg/m <sup>3</sup>
Temperature ( $T_0$ )	300 K
Thermal Conductivity ( $k$ )	0.5 W/mK
Constant Volume Heat Capacity ( $C_v$ )	5000 J/kgK
Thermal Expansion Coefficient ( $\alpha_v$ )	$2.5 \times 10^{-4}$

Effects of Oldroyd-B model parameters ( $\lambda_1$ ,  $\lambda_2$  and  $\eta_s$ ) on sound propagation are investigated in the simulations. For this purpose, one of these parameters is changed in each simulation to analyze the materials response. Behavior of the mediums against applied modulated ultrasound are presented and discussed in the simulations below.

**Simulation 1** ( $\lambda_1 = 20, \lambda_2 = 2, \eta_s = 1$ )

In the first simulation (Figure 3.4), retardation time is 2 s. This is greater than  $a$ . The fluid does not have enough time to release all the stress during unloading period. Hence, pressure is not reaching to zero in this period. It is also seen that pressure on the fluid is also increasing in loading periods.

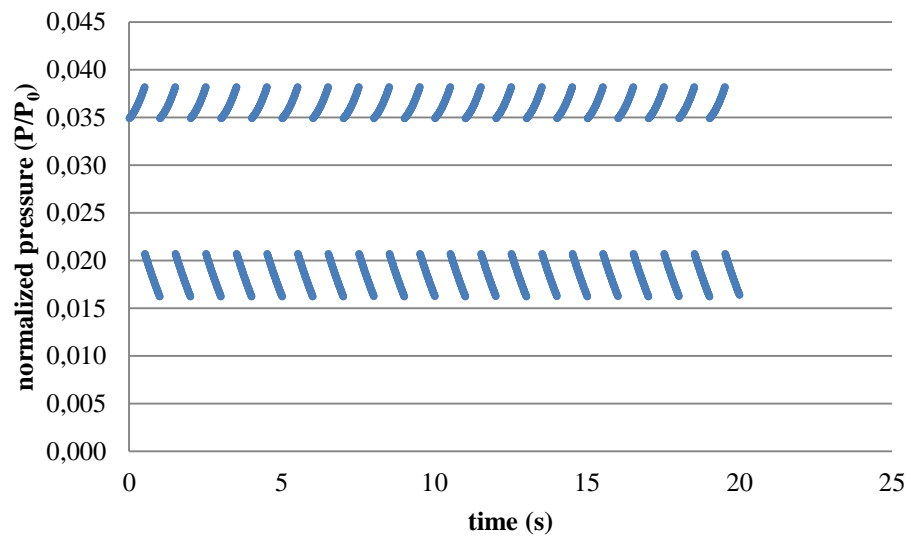


*Figure 3.2 Pressure Behavior in the Case of Oldroyd B Simulation 1*

**Simulation 2** ( $\lambda_1 = 5, \lambda_2 = 2, \eta_s = 1$ )

In the second simulation (Figure 3.5) relaxation time is lowered to 5 s. The pressures in the loading period are relatively higher with respect to first simulation. Behaviors of the unloading periods are similar.

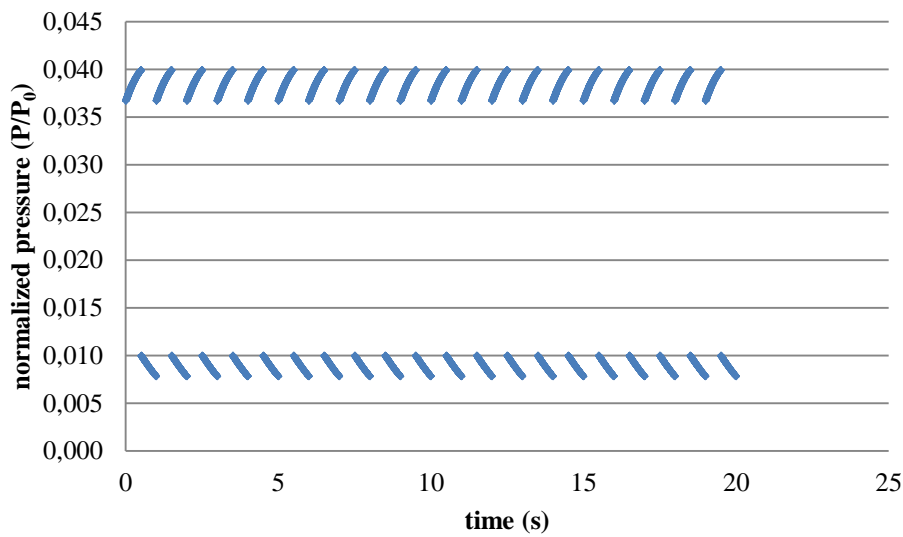


**Figure 3.3** Pressure Behavior in the Case of Oldroyd B Simulation 2

**Simulation 3** ( $\lambda_1=5, \lambda_2=0.2, \eta_s=1$ )

In the third simulation (Figure 3.6), retardation time is further lowered to 0.2 s. In this mode, the pressure is nearly reaching to zero during unloading period. Pressures in the loading periods are lower than the second one. The rises in pressures in loading periods are less distinctive. This is due to increase in polymer viscosity.

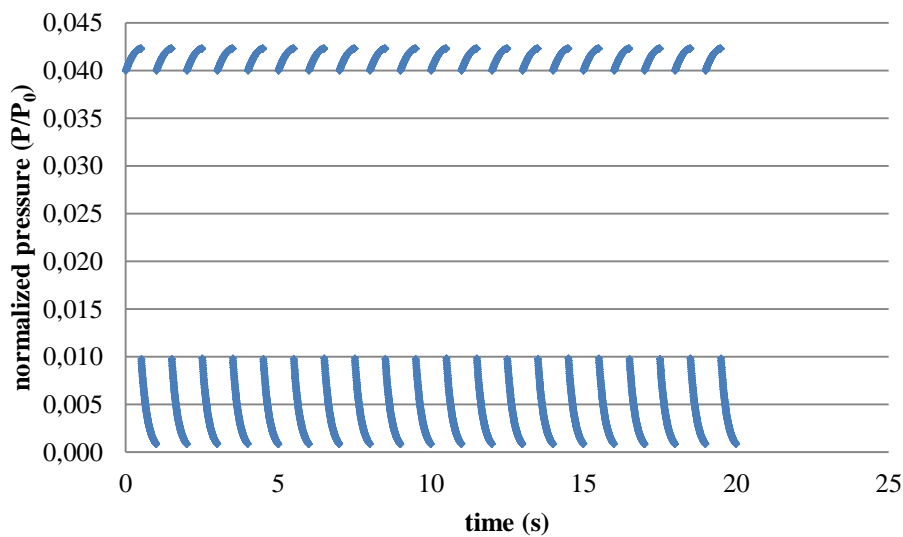


**Figure 3.4** Pressure Behavior in the Case of Oldroyd B Simulation 3

**Simulation 4** ( $\lambda_1=5, \lambda_2=0.02, \eta_s =1$ )

In the fourth simulation (Figure 3.7), retardation time decreased to 0.02 s. In this one, pressure reaches to zero immediately in unloading period. In addition, pressures in loading period immediately reach their equilibrium values as the polymer viscosity becomes higher.

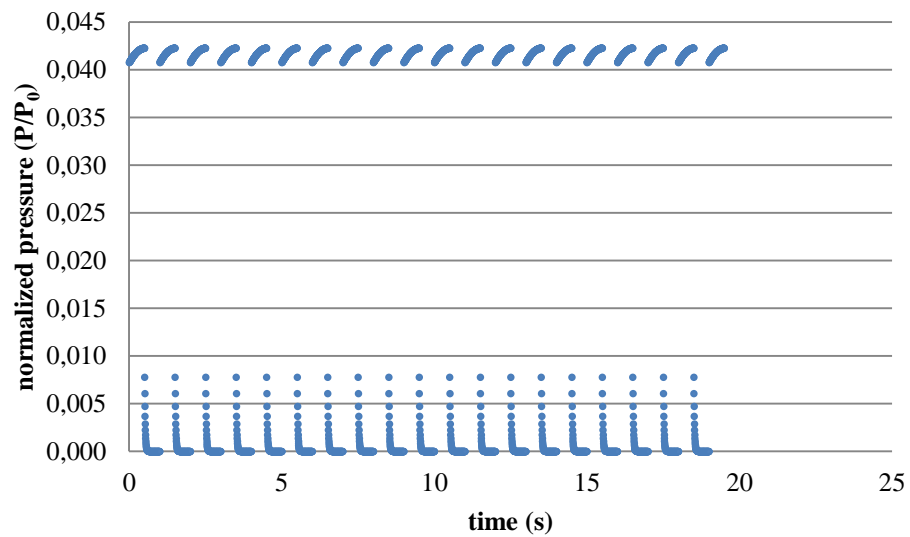


*Figure 3.5 Pressure Behavior in the Case of Oldroyd B Simulation 4*

**Simulation 5** ( $\lambda_1=0.5, \lambda_2=0.02, \eta_s =1$ )

In the fifth simulation (Figure 3.8), relaxation time is decreased to 0.5 s. As in the previous case, the pressure immediately goes to zero during unloading period. The pressures more sharply reach equilibrium values in loading period. This can be attributed to the decrease in relaxation time.

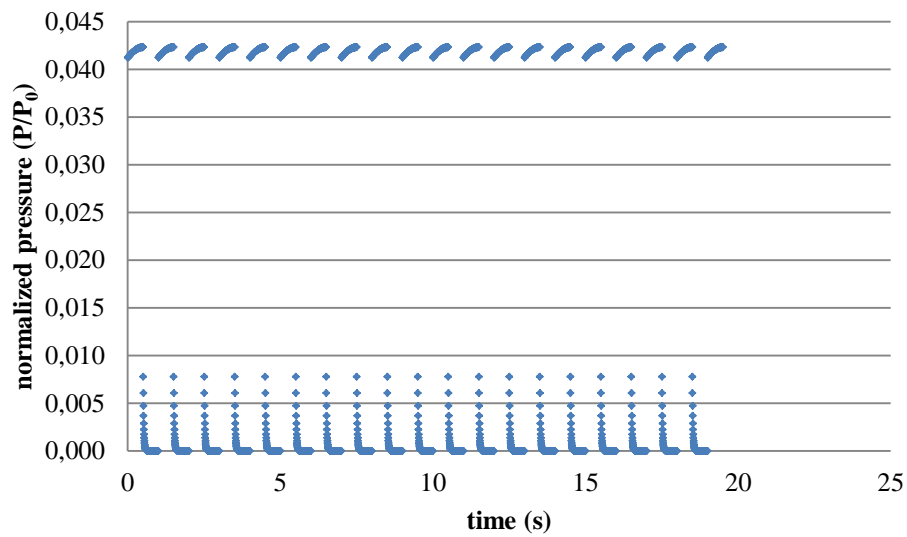


*Figure 3.6 Pressure Behavior in the Case of Oldroyd B Simulation 5*

**Simulation 6** ( $\lambda_1=5, \lambda_2=0.2, \eta_s =10$ )

In this mode (Figure 3.9), recovery behavior is apparent. In addition, sound pressure sharply increased due to higher solvent viscosity.

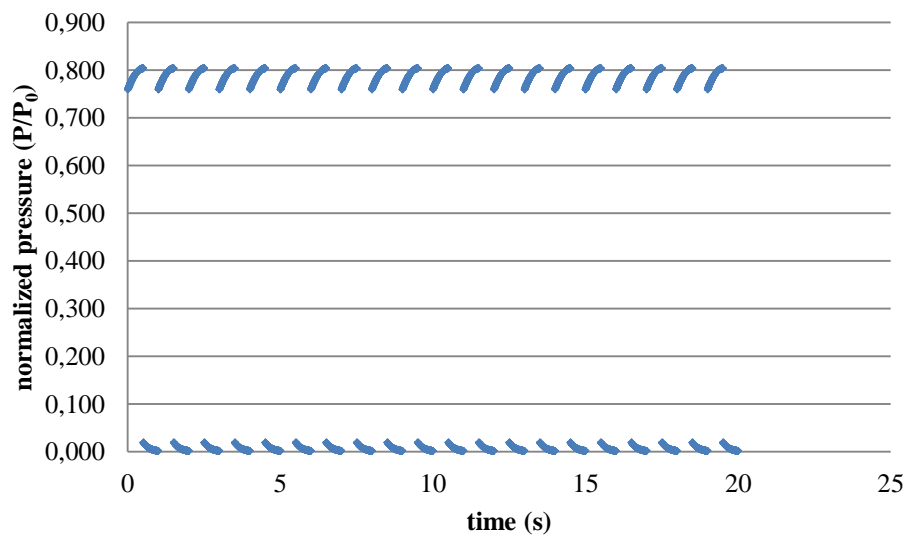


*Figure 3.7 Pressure Behavior in the Case of Oldroyd B Simulation 6*

### 3.3 Results of the Simulations

In the simulations, as relaxation time increases, the increments in loading periods get more apparent. At low relaxation times the pressures reaches their equilibrium values immediately. Solvent viscosity is mainly responsible for the magnitude of the sound pressure level. Higher solvent viscosities give higher pressures. The effects of retardation times are observed in recovery periods. If it is small, the pressure immediately becomes zero during recovery period. When it gets higher, the recovery period is observed clearer. As a result, the order of magnitude of duration time in loading periods and recovery periods (“n” and “a” ) should be the same with those of relaxation and retardation times. Otherwise, they cannot be characterized. Therefore parameters n and a act as a filter for the material characteristic times.

Hence, the model equation and results of simulations show that by using this technique, Oldroyd-B parameters of a material can be determined experimentally. By using the sound pressure data in the recovery period  $\lambda_2$  can be determined. In addition, by analyzing the sound pressure data in loading period,  $\lambda_1$ ,  $\eta_s$  and  $\eta_p$  can also be found. The procedure to obtain them from ultrasonic data is shown in Appendix A4.

### 3.4 Experimental Procedure

In rheological measurements, carboxy methyl cellulose (CMC) / water solutions (2 wt %, 3 wt % and 4 wt %) are used. CMC is bought from Sigma-Aldrich. Deionized water obtained from Innovation Pure Water System is used to prepare CMC solutions.

Methodology of preparing CMC solutions is critical as solving CMC in water is a difficult process. Dissolution CMC is added to water in pieces for well mixing. When added CMC is completely dissolved, the next piece of CMC is added. In addition, solution is kept at 30°C during the preparation period to speed up the rate of

dissolution. It takes 48 hours for preparation of CMC/water solution. Furthermore, qualities of CMC obtained from Sigma-Aldrich are presented in Table 3.2.

**Table 3.2** *Properties of CMC*

<b>Property</b>	<b>Value</b>
Molecular Weight	90 kDa
Degree of Polymerization	400
Degree of Substitution	0.65-0.90 (6.5-9.0 carboxymethyl groups per 10 anhydroglucose units)
Purity	99.5 % by weight

CMC is a derivative of cellulose made up of carboxymethyl groups and its structure is represented in Figure 3.10.

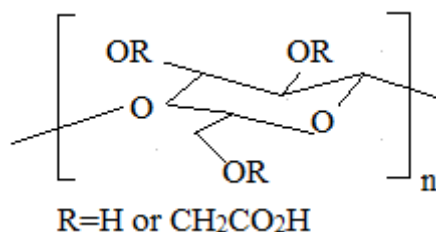


**Figure 3.8** *Repeating Unit of CMC*

In ultrasonic experiments, room temperature is held at 25°C by the help of air conditioner. The piezzo ceramic transducer (SUHNER Switzerland RG 174/U 50 ohm) is immersed into 1 liter CMC/water solutions. The transducer tip is positioned 2 cm from the surface of the sample solution. Base frequency of ultrasound is kept as 2.0 MHz. In addition, for pulse repetition frequency a=6500-9000 μs is used. Echo-history data with respect to position are acquired to utilize them in the mathematical models.

In order to evaluate the results obtained by the UDV measurements, the samples are also characterized by a well-established rheological measurement technique. These

rheological measurements are done in METU Central Laboratory by ARES Rheometer (TA Instruments, Spain) (Figure 3.11) . During the measurements, the device is operated in parallel plate mode at 25<sup>0</sup>C. The diameters of the plates are 25 mm. Technical specifications of the rheometer are provided in Appendix A11.

By the rheometer creep experiments are done on the CMC/water solutions. In these experiments, constant stress is applied on the samples. Thus, strain data with respect to time are collected.



*Figure 3.11 ARES Rheometer*

### **3.5 Experimental Results**

For the evaluation of the mathematical model developed, two different set of experiments are done. In first one, ultrasonic measurements are done with Ultrasound Doppler Velocimeter (DOP 2015). The output of the velocimeter is fitted to the model to determine the viscoelastic parameters. The method to evaluate the ultrasonic parameters is given in Appendix A4. Viscoelastic parameters obtained from the ultrasonic measurements are listed in Table 3.3.

**Table 3.3 Ultrasonic Measurements**

<b>Solution</b>	$\lambda_1$ (s)	$\lambda_2$ (s)	$\eta_0$ Pas
2.0 wt. % CMC	0.049	0.002	6.891
3.0 wt. % CMC	0.117	0.003	27.984
4.0 wt. % CMC	0.204	0.005	41.724

In the second part, viscoelastic properties of the solutions are determined by the conventional rheometer to verify the results of the model developed. The obtained data are fitted to Oldroyd-B model. Results of the experimental measurements are given in Table 3.4.

**Table 3.4 Rheometer Measurements**

<b>Solution</b>	$\lambda_1$ (s)	$\lambda_2$ (s)	$\eta_0$ Pas
2.0 wt. % CMC	0.044	0.002	7.114
3.0 wt. % CMC	0.113	0.003	26.852
4.0 wt. % CMC	0.196	0.005	40.872

For each datum in the table, arithmetic mean of the multiple measurements is taken. The typical standard deviation for the measurements is 0.1. Results of the ultrasonic experiments show that as concentration of CMC in the solution increases the value of relaxation time and retardation time increases. This shows that elastic character of the solutions increases with CMC addition. In other words, as the concentration of CMC decreases, the behavior of the solution approaches to water. In addition, solution viscosities also increase with CMC addition. The relaxation times for 2.0, 3.0 and 4.0 wt. % CMC solutions are calculated as 0.049s, 0.117s and 0.204s, respectively. The corresponding retardation time values are 0.006s, 0.020s and 0.058s. Viscoelastic parameters are calculated by the evaluation of the model shown in A.4 (eqn. A4.1, eqn. A4.2 and eqn. A4.3). In the calculation of retardation time, linear relation between  $\ln(P/P_0)$  and “a” is hold, as the model implied. The results of

the rheometer experiments are consistent with the output of ultrasonic measurements. Deviation of the ultrasonic results is not more than 5%. In addition, further rheological properties of CMC/water solutions are provided in Appendix A5.



## CHAPTER 4

### CONCENTRATION DETERMINATION OF MIXTURES FROM SOUND SPEED

#### 4.1 Sound Speed as a Tool for Material Characterization

As well as sound attenuation, sound speed measurement is also commonly applied for material characterization [53]. Test methods based on sound speed are utilized in variety of fields like medicine, astronomy, geology, automotive and defense industry and thermodynamics. For example, use of sound speed for a sensitive measurement of thickness of any material like metals, plastics or layer of coatings has become very common practice [54]. In sound speed measurements, the time required for the sound pass through material is determined. By multiplying sound speed in material with that time, thickness is easily found. Similarly, morphological defects in materials can be detected by means of sound speed measurements [55]. For this purpose, sound speed is measured for any material. If measured value differs from the real value, that it must be, it is a sign of any morphological defects in materials. This method is extensively used especially in the nondestructive tests of concretes and steels. In addition, evaluation of phase morphology is possible by sound speed measurements. S. Wang et al. probed the effects of phase morphology on sound speed [56]. They worked with high density polyethylene/ polyamide 6 blend melts. They detected that sound speed was directly proportional with polyamide 6 blend concentration.

Sound speed contains important data about the features of liquids [57]. Determination of sound speed in liquids offers a way of acquiring equilibrium thermodynamic information that are not obtained by conventional methods.

Intermolecular forces in the liquids are mainly responsible for the determination of sound speed. T. Langeman et al. [58] evaluated sound speed in liquids as the summation of the bond speeds. R. Rendall et al. [59] estimated sound speeds theoretically by the use of adiabatic compressibility, which were close to experimental values. H. Eyring et al. [60] suggested that molecules are broadly packed in liquids; hence there is some free space in the volume. They defined the sound speed in liquid as framed by both the sound speed in the liquid molecules and the sound speed in the gas molecules in free spaces. Excess thermodynamic properties of liquid mixtures provide the understanding of the intermolecular forces, phase stability and structural influences based on concentration [53]. It also stimulates the derivation of empirical models to predict the mixture properties.

The studies on the sonic determination of concentration are mostly dependent on the estimation of compressibility of mixtures or, use of molecular theories or empirical models. In addition, values of excess compressibility (positive or negative) provide important information about the intermolecular interactions. P. Resa et al. [61] developed a model to estimate sound speed and compressibility in liquid mixtures. Their model separated the volume into two parts; compressible and incompressible volumes. It was proposed that attractive forces (hydrogen bonds and Wan der Waals forces) were responsible from compressible volume. In addition, covalent bonds accounted incompressible volume. Effective compressibility was found by excluding incompressible volume from the total volume. Incompressible volumes were calculated by experimental data. Compressibility and sound speed were estimated once incompressible volumes were obtained.

R. Mahajan et al. [62] measured the sound speed and density of binary mixtures of n-octane, n-decane, n-dodecane, and n-tetradecane with heptan-2-ol. Excess molar volumes and excess compressibilities were calculated based on these measurements. The results were fitted to Redlick-Kister polynomial expansion. Positive values of excess molar volumes and excess compressibilities were obtained. It was concluded that there was a rupture of hydrogen-bonded chain of the dipolar interaction between

solute and heptan-2-ol. This surpassed the intermolecular interaction through dipole-dipole and hydrogen bonding between n-alkanes and heptan-2-ol molecules.

For theoretical estimation of sound speed in mixtures, mostly Jacobson Free Length Theory, Schaff's Collision Factor Theory, Nomoto's relation, Van Dael's relation, Junjie's relation and impedance relation were applied in the researches. H. Kumar et al. measured the and sound speed in water and dimethyl sulfoxide mixtures. Positive excess sound speeds were obtained [63]. This was contributed to the fact that dipole-dipole dispersive interactions between unlike molecules were dominant. In addition, density, excess molar volumes and excess compressibilities was calculated. Negative values of excess compressibilities and excess molar volumes were also grasped. This also supported the idea of strong dispersive forces between unlike molecules. In addition, sound speeds were also theoretically estimated by of Jacobson Free Length Theory, Schaff's Collision Factor Theory, Nomoto's relation, and Van Dael's relation. Fair agreements between experimental and theoretical results were obtained. Similar studies [64, 65, 66, 67] were conducted by researchers by using these relations. In this study, these relations were also applied for comparison purposes.

Even though, sound speed provides important data about the thermodynamic properties of material, there is no equation of state based work to predict sound speed in the literature. Hence, main purpose of this work is to estimate concentration of solutions from sound speed by using Peng-Robinson equation of state. For this reason, speed of sounds in ethanol/water, methanol/methyl acetate, ethanol/methyl acetate and ethyl acetate/ethanol mixtures are measured and calculated by previously mentioned molecular theories and empirical models, and Peng-Robinson equation of state.

#### **4.2 Molecular Theories for Sound Speed Estimations in Mixtures**

Some theories are also developed for estimating the sound speed in mixtures. The most commonly used ones are Jacobson Free Length Theory and Schaaff Collision Factor Theory.

### 4.2.1 Jacobson Free Length Theory

According to Jacobson Free Length Theory [68], sound speed in mixtures can be expressed by the following relation;

$$u_{\text{mix}} = \frac{K}{L_{f,\text{mix}} \rho_{\text{mix}}^{0.5}} \quad \text{eqn. 4.1}$$

In the theory “K” is the Jacobson constant and depends only on temperature.  $L_f$  represents the intermolecular free length. Here,  $L_f$  can be calculated by  $L_f = 2V_a / Y$ . “ $V_a$ ” and “ $Y$ ” denote available volume per mole and surface area per mole, respectively. They are calculated by;

$$V_a = V_T - V_0 \quad \text{eqn. 4.2}$$

$$Y = (36\pi N_A V_0^2)^{1/3} \quad \text{eqn. 4.3}$$

$N_A$  is Avogadro number,  $V_T$  and  $V_0$  are the molar volumes at operating temperature and zero Kelvin, respectively.  $V_0$  can also be found by the help of the following relation;

$$V_0 = V_T \left(1 - \frac{T}{T_c}\right)^{0.3} \quad \text{eqn. 4.4}$$

$T_c$  is the critical temperature. Free length for binary mixtures can be found by;

$$L_{f,\text{mix}} = 2 \frac{\left[ V_T - (x_1 V_{0(1)} + x_2 V_{0(2)}) \right]}{(x_1 V_1 + x_2 V_2)} \quad \text{eqn. 4.5}$$

### 4.2.2 Schaaff Collision Factor Theory

Speed of sound in mixtures can also be calculated by the Schaaff’s Theory [69], it is given as;

$$u_{\text{mix}} = u_{\infty} (x_1 s_1 + x_2 s_2) \left( \frac{x_1 b_1 + x_2 b_2}{x_1 V_1 + x_2 V_2} \right) \quad \text{eqn. 4.6}$$

$u_\infty$  is 1600 m/s, in addition, “s” and “b” represents geometric volume and collision factor, respectively. Following equation is used to find “b”;

$$b = \frac{4}{3} \pi r^3 N \quad \text{eqn. 4.7}$$

Here “r” is molecular radius and calculated by;

$$r = \left( \frac{3b'}{16\pi N} \right)^{1/3} \quad \text{eqn. 4.8}$$

Where

$$b' = \left[ \frac{M}{\rho} - \frac{\gamma RT}{\rho u^2} \left( \left( 1 + \frac{Mu^2}{3\gamma RT} \right)^{1/2} - 1 \right) \right] \quad \text{eqn. 4.9}$$

### 4.3 Empirical Relations for Sound Speed Estimations in Mixtures

Several researchers develop relations for estimating the sound speed in mixtures. Some of them are given below;

#### 4.3.1 Nomato Equation

O. Nomato et al. [70] proposed the following relation for sound speed calculation. Here, “R” denotes molar sound speed.

$$u_{\text{mix}} = \left( \frac{x_1 R_1 + x_2 R_2}{x_1 V_1 + x_2 V_2} \right)^3 \quad \text{eqn. 4.10}$$

#### 4.3.2 Van Deal Equation

W. Val Deal relates [71] sound speed with the following equation;

$$\frac{1}{x_1 M_1 + x_2 M_2} \frac{1}{u_{\text{mix}}} = \frac{x_1}{M_1 u_1^2} + \frac{x_2}{M_2 u_2^2} \quad \text{eqn. 4.11}$$

### 4.3.3 Junjie Equation

Another relation for sound speed is developed by Z. Junjie [66];

$$u_{\text{mix}} = \frac{(x_1 V_1 + x_2 V_2)}{(x_1 M_1 + x_2 M_2)^{0.5} \left( \frac{x_1 M_1}{\rho_1 u_1^2} + \frac{x_2 M_2}{\rho_2 u_2^2} \right)^{0.5}} \quad \text{eqn. 4.12}$$

### 4.3.4 Impedance Equation

Acoustic Impedance is also applied to estimate sound speed in mixtures [72];

$$u_{\text{mix}} = \frac{x_1 Z_1 + x_2 Z_2}{x_1 \rho_1 + x_2 \rho_2} \quad \text{eqn. 4.13}$$

Results of the calculations for ethyl acetate/methyl acetate, ethyl acetate/ethanol and methyl acetate/ethanol systems are tabulated in the results and discussion part below. In addition, since experimental measurements are done for ethyl acetate/ethanol and methyl acetate/ethanol systems they can be compared with calculated values. For this purpose, figures are prepared. Results state that Junjie equation estimates the sound speed most closely to the experimentally found values.

## 4.4 Speed of Sound Estimation from Equation of States

### 4.4.1 Cubic Equations of States and Peng-Robinson Equation of State

Cubic equations of states are commonly applied in thermodynamics [73]. They can be applied to identify the  $P\tilde{V}T$  relations of single and multicomponent mixtures. This makes it possible to estimate the sound speed in mixtures by the use of cubic equations of states.

The name cubic comes from that they are in the third degree in molar volume such that;

$$\tilde{V}^3 + c_1 \tilde{V}^2 + c_2 \tilde{V} + c_3 = 0 \quad \text{eqn. 4.14}$$

and Peng-Robinson equation of state can be written as;

$$P = \frac{RT}{\tilde{V} - b} - \frac{a}{\tilde{V}(\tilde{V} + b) + b(\tilde{V} - b)} \quad \text{eqn. 4.15}$$

where

$$a = 0.45724 \left( \frac{R^2 T_c^2}{P_c} \right) \alpha \quad \text{eqn. 4.16}$$

and

$$b = 0.07780 \left( \frac{RT_c}{P_c} \right) \quad \text{eqn. 4.17}$$

In Peng-Robinson equation of state first term “ $RT/(\tilde{V} - b)$ ” describes the repulsive forces between molecules. Second term is defining the attractive forces between molecules. “ $a$ ” and “ $b$ ” represent the attractive forces and volume of the molecules, respectively [74]. Parameter “ $\alpha$ ” is temperature dependent equation of state variable and defines as

$$\alpha = \left[ 1 + (0.37464 + 1.54226\omega - 0.26992\omega^2)(1 - \sqrt{T_r}) \right]^2 \quad \text{eqn. 4.18}$$

In addition, to estimate mixture properties, mixture form of the parameters “ $a$ ” and “ $b$ ” should be used in eqn. 4.15. They can be calculated by van der Waals mixing rule such that

$$a_{\text{mix}} = \sum_{i=1}^k \sum_{j=1}^k x_i x_j a_{ij} \quad \text{eqn. 4.19}$$

$$b_{\text{mix}} = \sum_{i=1}^k \sum_{j=1}^k x_i x_j b_{ij} \quad \text{eqn. 4.20}$$

“ $a_{ii}$ ” and “ $b_{ii}$ ” are the parameters for individual components. Parameters “ $a_{ij}$ ” and “ $b_{ij}$ ” can also be calculated by;

$$a_{ij} = (1 - k_{ij}) \sqrt{a_{ii} a_{jj}} \quad \text{eqn. 4.21}$$

$$k_{ij} = k_{ji} \quad \text{eqn. 4.22}$$

$$b_{ij} = \frac{b_i + b_j}{2} \quad \text{eqn. 4.23}$$

Other commonly applied cubic equations of states models are given in Appendix A6.

#### 4.4.2 Advantages and Drawbacks of Using Cubic Equations of States

Cubic equations of states are advantageous in that [73, 74];

- They are straightforward models, and rapid results are obtained.
- They can operate in extensive pressure and temperature intervals.
- They can identify the component properties in both liquid and vapor states; thus, they are applicable for equilibrium calculations.
- Usually, use of only one interaction parameter is enough for estimating the properties of gas and hydrocarbon mixtures.
- Adequate outcomes are acquired low/high pressure vapor/liquid equilibrium.
- Satisfactory predictions of mixtures of hydrocarbons, gases and apolar component are obtained by utilizing binary interaction parameters.
- There is a well established database for binary interaction parameters.
- For ordinary systems van der Waals and other straightforward mixing rules gives accurate predictions for vapor/liquid equilibrium.

Despite these listed advantages of the usage of cubic equation of states, there are some drawbacks of cubic equation of states:

- Particularly for gas and hydrocarbon mixtures, results are strictly dependent on binary interaction parameter.
- Interaction parameters changes with temperature.
- Saturated liquid volumes are predicted incorrectly.
- Vapor pressures are closely dependent on critical properties.
- Usually, taking binary interaction parameters zero give incorrect results. Therefore, experimental data is required for interaction parameters.

- Most of the time, insufficient results are obtained for equilibrium properties of polar mixtures.
- Cubic equation of states can not be smoothly expanded for complex molecules such as electrolytes and bio-molecules.

Based on the listed advantages and drawbacks we decided to use cubic equation of states. Since, there is well-established database for cubic equation of states and hydrocarbon mixture properties are predicted precisely. In addition, they have analytical P $\tilde{V}$ T relations; hence, they can be easily integrated to ultrasonic relations.

#### 4.4.3 Volume Translation Method for Cubic Equation of States

Cubic equations of states are essentially developed from van der Waals equation of state and are commonly applied in many engineering practices. However, major drawback of cubic equation of states is the poor estimation of saturated liquid densities. To overcome this, A. Peneloux et al. [75] proposed volume translation method for Peng Robinson equation of state by including a constant volume correction term into the equation. Volume translated Peng Robinson equation of state is obtained by substituting “ $\tilde{V}$ ” with “ $\tilde{V} + t$ ” in the Peng Robinson equation of state. Hence, the resulting equation is;

$$P = \frac{RT}{\tilde{V} + t - b} - \frac{a}{(\tilde{V} + t)(\tilde{V} + t + b) + b(\tilde{V} + t - b)} \quad \text{eqn. 4.24}$$

Where “ $t$ ” is the volume translation parameter and found by the use of experimental value of “ $\tilde{V}$ ” such that;

$$t = \tilde{V}_{PR} - \tilde{V}_{exp} \quad \text{eqn. 4.25}$$

In addition, for mixture properties, like “ $a_{mix}$ ” and “ $b_{mix}$ ”, “ $t_{mix}$ ” can also be calculated by;

$$t_{mix} = \sum_i x_i t_i \quad \text{eqn. 4.26}$$

Finally, to relate the P $\tilde{V}$ T relation with sound speed, adiabatic sound speed equation can be used;

$$u = \sqrt{\left(\frac{\partial P}{\partial \rho}\right)_s} \quad \text{eqn. 4.27}$$

Since, for non-viscoelastic liquid systems with ultrasound frequencies of several MHz's  $\omega\tau \rightarrow 0$ ; hence, sound propagation takes place in adiabatic conditions.

#### 4.5 Experimental Procedure

For sound speed measurements, DOP2000 device has a specific sound speed measurement unit. The distance between the end of transducer and the micrometric screw is specified. By dividing the distance to time of travel of ultrasound, the sound speed is calculated by DOP200. This unit is applied for concentration measurements experiments (Figure 4.1). During the experiments, room temperature is held at 25°C by the help of air conditioner. The piezzo ceramic transducer (SUHNER Switzerland RG 174/U 50 ohm) is used. Base frequency of ultrasound is kept as 2.0 MHz.



*Figure 4.1 Sound Speed Measurement Unit of DOP2000*

Deionized water obtained from Innovation Pure Water System is used to prepare ethanol/water solutions. Ethanol, methanol, methyl acetate and ethyl acetate used in measurements are bought from Sigma-Aldrich. The quarantined purity of chemicals given from the company is minimum %99.5 by weight.

## 4.6 Results and Discussions

Results of the calculations for ethanol/water, methanol/methyl acetate, ethanol/methyl acetate and ethyl acetate/ethanol systems are tabulated below.

For Translated Peng Robinson Equation of State, used interaction parameters and translation parameters are shown in Tables 4.1 and 4.2 below;

*Table 4.1 Binary Interaction Parameters for Mixtures*

<b>Mixture</b>	<b><math>k_{ij}</math></b>
EtOH-Water	-0.4711
MeOH- MeAc	0.0048
EtOH- MeAc	0.0394
EtAc-EtOH	0.0098

*Table 4.2 Volume Translation Parameters*

<b>Component</b>	<b><math>t</math> (<math>\text{m}^3/\text{mol}</math>)</b>
EtOH	$-2.285 \times 10^{-6}$
Water	$-1.815 \times 10^{-6}$
MeOH	$-2.923 \times 10^{-6}$
MeAc	$1.866 \times 10^{-6}$
EtAc	$1.759 \times 10^{-6}$

The values of  $t$ 's are obtained by the experimental molar volumes from the molar volume found from the Peng Robinson Equation of State. Interaction parameters are determined by trial-error procedure to ensure that most close results with experimental values are obtained.

In Tables 4.3, 4.4, 4.5 and 4.6, experimental sound speed measurements and sound speed estimations obtained from the models according to various compositions are tabulated for corresponding mixtures.

In Tables 4.3, 4.4, 4.5 and 4.6; exp., T-PR, PR, NR, VD, FLT and CFT refer to experimental measurements, Volume Translated Peng Robinson Equation of State, Peng Robinson Equation of State, Nomato Equation, Van Deal Equation, Jacobson Free Length Theory and Schaaff Collision Factor Theory results, respectively.

*Table 4.3 Ethanol/Water Sound Speed Estimations*

$W_{EtOH}$	Exp	T-PR	PR	NR	VD	Junjie	Impedance	FLT	CFT
0.0	1478	1480	3185	1482	1482	1482	1482	1632	1482
0.1	1533	1519	3179	1434	1447	1407	1471	1632	1531
0.2	1572	1549	3146	1390	1411	1350	1458	1631	1585
0.3	1590	1571	3084	1350	1374	1304	1442	1630	1643
0.4	1582	1583	2993	1313	1337	1267	1424	1628	1707
0.5	1546	1581	2867	1279	1300	1236	1402	1623	1773
0.6	1482	1499	2705	1248	1264	1211	1375	1616	1839
0.7	1394	1416	2499	1219	1228	1190	1340	1601	1893
0.8	1297	1327	2246	1192	1194	1172	1295	1574	1908
0.9	1216	1229	1934	1167	1164	1157	1233	1517	1792
1.0	1143	1143	1549	1144	1144	1144	1144	1372	1144

In ethanol/water mixture (Table 4.3), Peng Robinson Equation of State results give too much deviation from experimental measurements. However, Volume Translated Peng Robinson Equation of State results are close experimental values. In addition, results of other models are not as accurate as Volume Translated Peng Robinson Equation of State. Best estimation is obtained by Impedance Equation between those models.

*Table 4.4 Methanol/Methyl Acetate Sound Speed Estimations*

$w_{\text{MeOH}}$	Exp	T-PR	PR	NR	VD	Junjie	Impedance	FLT	CFT
0.0	1151	1150	966	1150	1150	1150	1150	1227	1150
0.1	1146	1141	1043	1144	1069	1142	1141	1229	1153
0.2	1139	1135	1122	1139	1036	1134	1134	1232	1155
0.3	1132	1132	1200	1133	1025	1128	1128	1235	1156
0.4	1126	1128	1280	1128	1025	1123	1123	1237	1156
0.5	1121	1125	1360	1124	1031	1118	1118	1240	1155
0.6	1117	1122	1439	1119	1042	1114	1114	1242	1153
0.7	1113	1118	1518	1114	1055	1110	1111	1243	1147
0.8	1110	1113	1597	1110	1070	1107	1107	1245	1139
0.9	1106	1108	1674	1106	1085	1104	1105	1247	1124
1.0	1103	1102	1751	1102	1102	1102	1102	1248	1102

In methanol/methyl acetate mixture (Table 4.4) closest results to experimental measurements are obtained with Volume Translated Peng Robinson Equation of State. Nomato, Van Deal, Junjie, Impedance and Schaaff Collision Factor Theory estimations are better compared ethanol/water mixture since sound speeds in pure components are close. Performances of those relations are more accurate when sound speed difference between pure components is small.

**Table 4.5** Ethanol/Methyl Acetate Sound Speed Estimations

<b>w<sub>EtOH</sub></b>	<b>Exp</b>	<b>T-PR</b>	<b>PR</b>	<b>NR</b>	<b>VD</b>	<b>Junjie</b>	<b>Impedance</b>	<b>FLT</b>	<b>CFT</b>
0.0	1151	1150	966	1150	1150	1150	1150	1227	1150
0.1	1146	1141	1012	1149	1134	1148	1149	1277	1175
0.2	1141	1137	1062	1148	1124	1146	1148	1291	1188
0.3	1137	1136	1115	1147	1119	1144	1148	1304	1193
0.4	1135	1137	1172	1146	1117	1143	1147	1316	1192
0.5	1135	1138	1230	1146	1118	1143	1147	1327	1188
0.6	1135	1138	1291	1145	1121	1142	1146	1337	1181
0.7	1136	1139	1354	1145	1125	1142	1145	1347	1173
0.8	1138	1140	1417	1145	1131	1143	1145	1356	1164
0.9	1140	1142	1483	1144	1137	1143	1144	1364	1154
1.0	1143	1143	1549	1144	1144	1144	1144	1372	1144

Volume Translated Peng Robinson Equation of State performs best in ethanol/methyl acetate mixture (Table 4.5), as well. Peng Robinson Equation of State results are far away from the experimental measurements. Sound speeds in ethanol and methyl acetate are closer compared to methanol and methyl acetate. Thus, other relations respond better according to methanol/ methyl acetate mixture.

**Table 4.6** Ethyl Acetate/Ethanol Sound Speed Estimations

$w_{\text{EtAc}}$	Exp	T-PR	PR	NR	VD	Junjie	Impedance	FLT	CFT
0.0	1143	1143	1549	1144	1144	1144	1144	1372	1144
0.1	1141	1142	1490	1144	1132	1142	1144	1363	1170
0.2	1139	1141	1430	1144	1121	1140	1143	1353	1197
0.3	1138	1140	1372	1144	1110	1138	1143	1342	1224
0.4	1136	1139	1315	1143	1101	1136	1143	1330	1250
0.5	1135	1137	1258	1143	1094	1135	1142	1317	1273
0.6	1134	1136	1202	1143	1090	1135	1142	1302	1292
0.7	1134	1137	1146	1142	1089	1135	1142	1286	1301
0.8	1136	1138	1093	1142	1094	1136	1141	1269	1292
0.9	1138	1138	1040	1141	1109	1137	1141	1249	1249
1.0	1140	1140	990	1140	1140	1140	1140	1227	1140

Ethyl acetate/ethanol mixture (Table 4.6), Volume Translated Peng Robinson Equation of State gives best prediction as in the previous cases. Sound speeds in pure components are much closer with respect to other mixtures. Hence, estimations of other mixtures are better according to previous mixtures. In addition, as the sound speeds in pure components get close to each other, performance of Volume Translated Peng Robinson Equation of State rises.

To summarize the experimental measurements and predictions of the models, for each mixture, results of Peng Robinson Equation of State are far away from the experimental measurements. Main reason of this can be contributed to be poor estimation of saturated liquid density as discussed in section 4.5.1. Since, sound speed is directly dependent on variation of pressure with respect to density. Use of translated Peng Robinson Equation of State overcomes wrong estimation of liquid density. As a result, fair agreement with experimental measurements is obtained. Performances of Nomato, Van Deal, Junjie and Impedance relations are straightforward but not enough for industrial applications. Results of Jacobson Free Length Theory and Schaff Collision Factor Theory are different from their experimental counterparts.

In addition, in ethyl acetate/ethanol and methyl acetate/ethanol mixtures, sound speed values of pure components are close to each other. This causes that sound speeds in some concentration ranges is similar. Hence, in those ranges concentration measurement by ultrasound is not applicable. Those ranges are corresponding to maximums or minimums in the sound speed vs. concentration curves.

To explain the deviations of sound speed values from ideality, thermodynamic analysis of the mixtures should be done. For this purpose, excess sound speeds, molar volumes and bulk modulus of corresponding solutions are tabulated in Tables 4.7, 4.8, 4.9 and 4.10. In addition, excess molar volumes of the mixtures according to composition are figurized in Figures 4.2, 4.4, 4.6 and 4.8. Excess sound speeds and bulk modulus of the mixtures are also shown in Figures 4.3, 4.5, 4.7 and 4.9. From the left axis excess sound speed data and from the right axis excess bulk modulus data can be obtained.

Variation of excess molar volumes arise from three contributions; chemical, physical and structural. The magnitude and sign of excess molar volumes the mixtures can be interpreted by the evaluations of these effects together. Physical interactions contain dispersion forces causing volume increase and attractive forces like hydrogen bonds, charge transfer complexes and dipole interactions resulting in volume decrease [76, 77]. Break up of associative equilibrium of alcohol molecules by the addition of secondary component may lead all these contributions.

Deviation of bulk modulus and sound speed values are also related with chemical, physical and structural changes by the addition of secondary component [76, 78]. Strong interaction between molecules via charge-transfer, dipole induced dipole and dipole-dipole yield positive value of bulk modulus deviation as more rigid structures are obtained. Formation of more compacted structures also results in positive deviations. On the other hand, dispersive forces have negative contribution on bulk modulus and sound speed. Deviation of bulk modulus and sound speed values are calculated by;

$$\Delta c = c_{\text{mix}} - (x_1 c_1 + x_2 c_2) \quad \text{eqn. 4.28}$$

$$\Delta K = K_{\text{mix}} - (x_1 K_1 + x_2 K_2) \quad \text{eqn. 4.29}$$

**Table 4.7** Ethanol/Water Mixture Thermodynamic Properties

$w_{\text{EtOH}}$	$c$ (m/s)	$\Delta c$ (m/s)	$\tilde{V}^{\text{ex}}$ (cm <sup>3</sup> /mol)	$\Delta K$ (GPa)
0.0	1478	0	0.000	0.000
0.1	1533	89	-0.078	0.239
0.2	1572	161	-0.308	0.442
0.3	1590	213	-0.491	0.571
0.4	1582	238	-0.725	0.621
0.5	1546	236	-0.967	0.589
0.6	1482	205	-1.039	0.477
0.7	1394	151	-0.883	0.313
0.8	1297	87	-0.718	0.158
0.9	1216	40	-0.435	0.062
1.0	1143	0	0.000	0.000

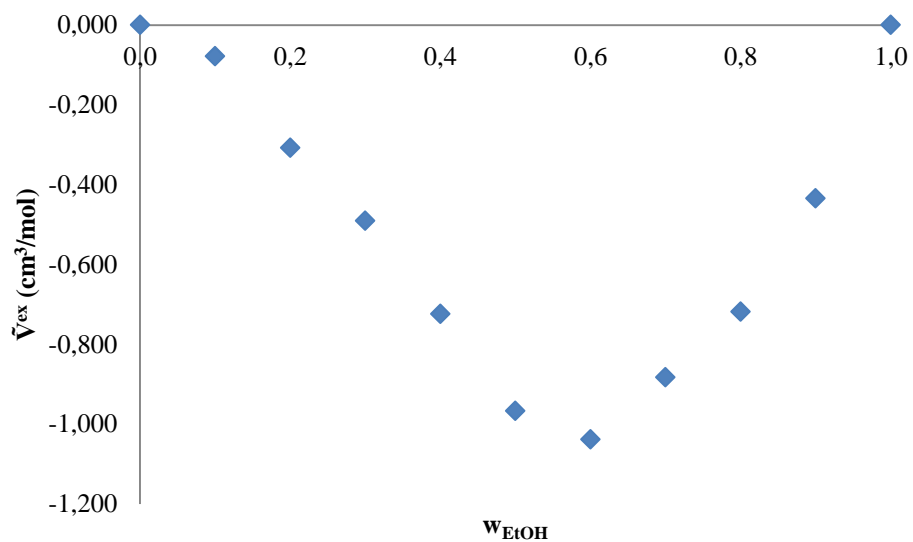


**Figure 4.2** Ethanol/Water Mixture Excess Molar Volume

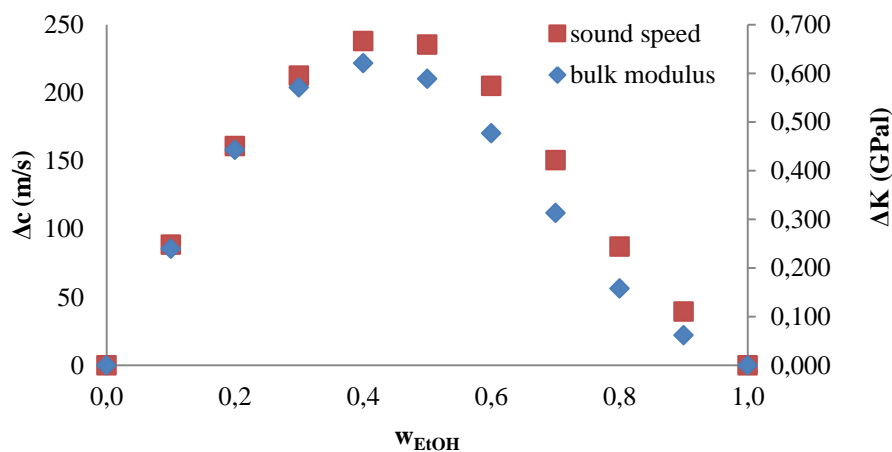


**Figure 4.3** Ethanol/Water Mixture Sound Speed and Bulk Modulus Deviations

In ethanol/water mixture, excess molar volumes have negative values. This is due to construction of strong hydrogen bonding between unlike molecules (Figure 4.2). Strong interaction between unlike molecules makes bulk modulus deviation positive. This also makes sound speed deviation in ethanol/water mixture positive (Figure 4.3).

**Table 4.8** Ethanol/Methyl Acetate Mixture Thermodynamic Properties

$w_{\text{EtOH}}$	$c$ (m/s)	$\Delta c$ (m/s)	$\tilde{V}^{\text{ex}}$ (cm <sup>3</sup> /mol)	$\Delta K$ (GPa)
0.0	1151	0	0.000	0.000
0.1	1146	-4	0.087	-0.017
0.2	1141	-8	0.133	-0.035
0.3	1137	-12	0.163	-0.052
0.4	1135	-13	0.187	-0.064
0.5	1135	-12	0.198	-0.070
0.6	1135	-11	0.195	-0.075
0.7	1136	-9	0.171	-0.080
0.8	1138	-7	0.137	-0.085
0.9	1140	-4	0.100	-0.094
1.0	1143	0	0.000	0.000

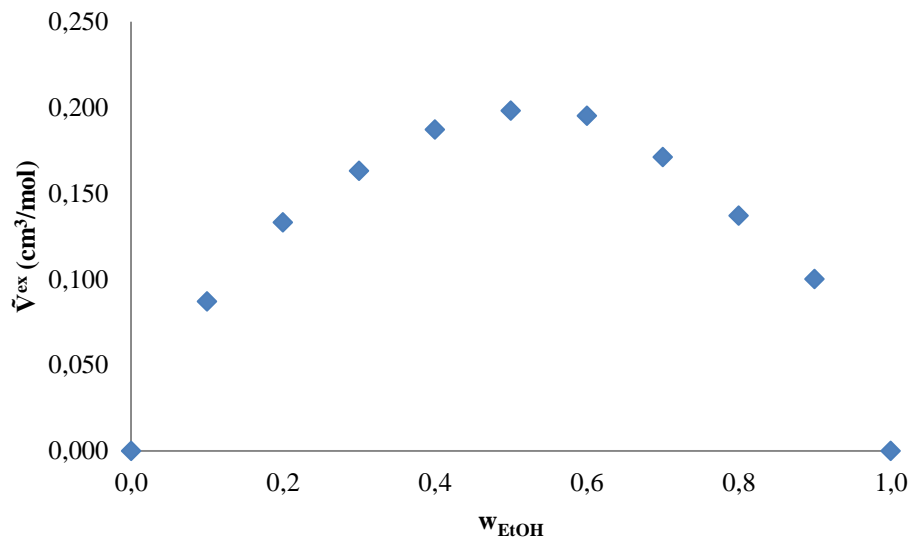


**Figure 4.4** Ethanol/Methyl Acetate Mixture Excess Molar Volume

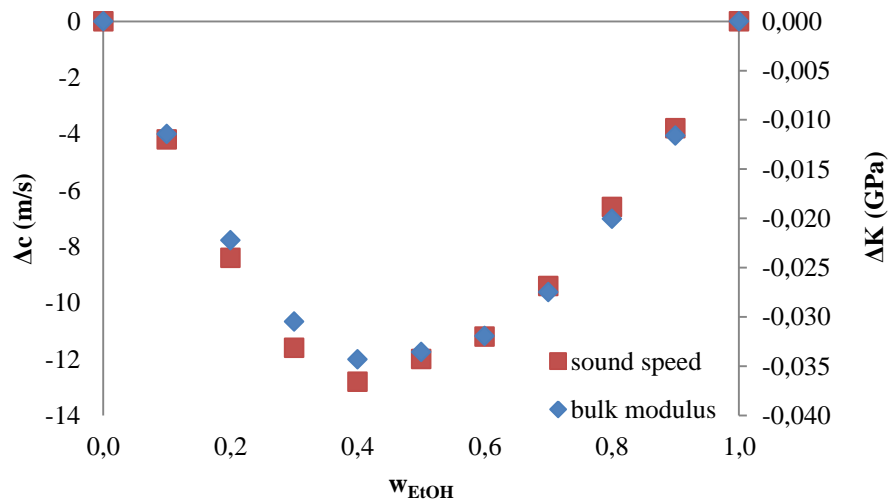


**Figure 4.5** Ethanol/Methyl Acetate Mixture Sound Speed and Bulk Modulus Deviations

In ethanol/methyl acetate mixture weak intermolecular interactions are established between unlike molecules. Unlike ethanol/water, excess molar volume values are positive (Figure 4.4 and 4.5). Addition of methyl acetate to ethanol breakdown the hydrogen bonds giving positive contribution. These effects are stronger than the interactions between unlike molecules; hence, net volume changes become positive.

In addition, deviation of sound speed and bulk modulus values are negative. This is due to the disturbance of alcohol structures by the addition of acetate molecules creating causing the less ordered structures.

**Table 4.9** Ethyl Acetate/Ethanol Mixture Thermodynamic Properties

$w_{\text{EtAc}}$	$c$ (m/s)	$\Delta c$ (m/s)	$\tilde{V}^{\text{ex}}$ (cm <sup>3</sup> /mol)	$\Delta K$ (GPa)
0.0	1143	0	0.000	0.000
0.1	1141	-2	0.021	-0.004
0.2	1139	-3	0.043	-0.008
0.3	1138	-4	0.097	-0.009
0.4	1136	-6	0.105	-0.012
0.5	1135	-7	0.131	-0.014
0.6	1134	-7	0.133	-0.015
0.7	1134	-7	0.132	-0.014
0.8	1136	-5	0.116	-0.009
0.9	1138	-2	0.047	-0.004
1.0	1140	0	0.000	0.000

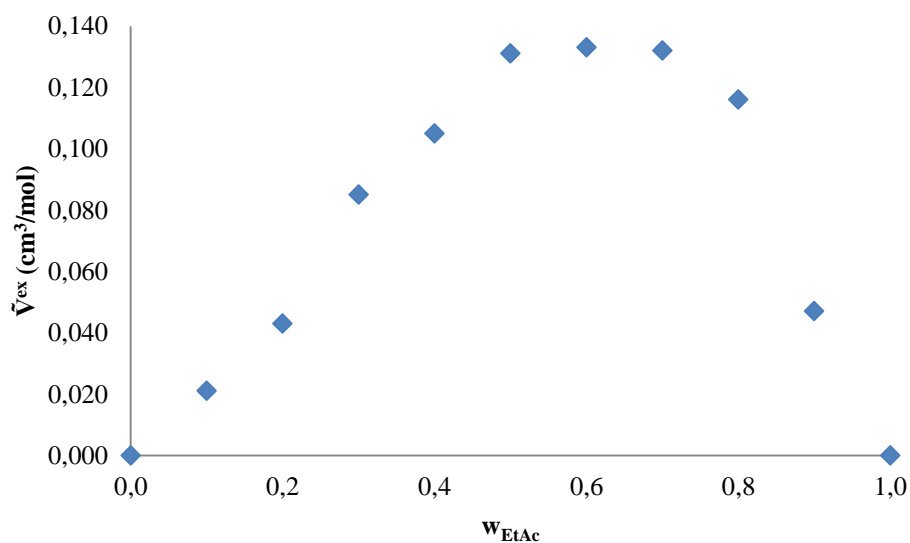


**Figure 4.6** Ethyl Acetate/Ethanol Mixture Excess Molar Volumes

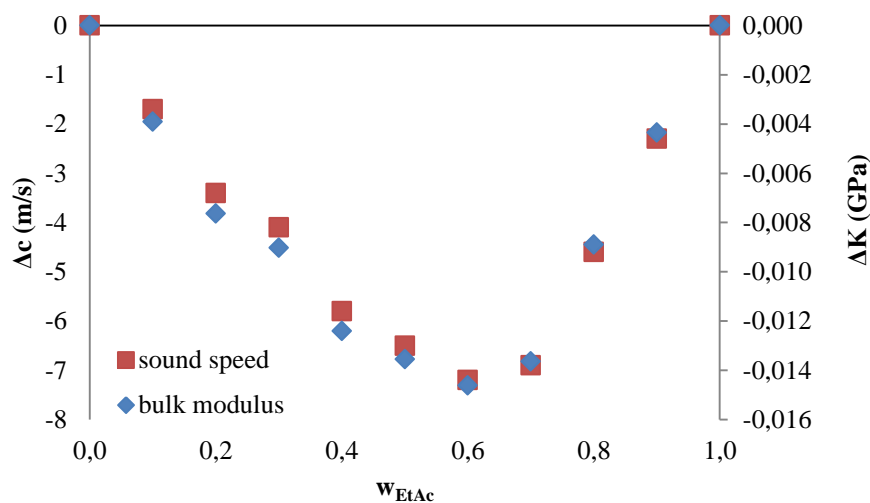


**Figure 4.7** Ethyl Acetate/Ethanol Mixture Sound Speed and Bulk Modulus Deviations

The situation of ethyl acetate/ethanol mixture is similar to that of ethanol/methyl acetate mixture. Weak intermolecular interactions are constructed between unlike molecules. In addition, excess molar volume values are positive (Figure 4.6). This is due that increasing the concentration of ethyl acetate in the mixture weakens hydrogen bonding. In addition, interactions between unlike molecules are not as high as repulsive force; hence, this results positive net volume change. Deviation from ideality is larger in ethanol/methyl acetate mixture since packing is worsened. Magnitude of the deviation of sound speed and bulk modulus values also indicate that orientational order is worse in ethanol/methyl acetate mixture (Figure 4.7).

**Table 4.10** Methanol/ Methyl Acetate Mixture Thermodynamic Properties

$w_{\text{MeOH}}$	$c$ (m/s)	$\Delta c$ (m/s)	$\tilde{V}^{\text{ex}}$ (cm <sup>3</sup> /mol)	$\Delta K$ (GPa)
0.0	1151	0	0.000	0.000
0.1	1146	0	-0.020	-0.002
0.2	1139	-2	-0.040	-0.008
0.3	1132	-5	-0.057	-0.013
0.4	1126	-6	-0.067	-0.016
0.5	1121	-6	-0.072	-0.016
0.6	1117	-5	-0.072	-0.014
0.7	1113	-4	-0.066	-0.012
0.8	1110	-3	-0.053	-0.007
0.9	1106	-2	-0.037	-0.005
1.0	1103	0	0.000	0.000

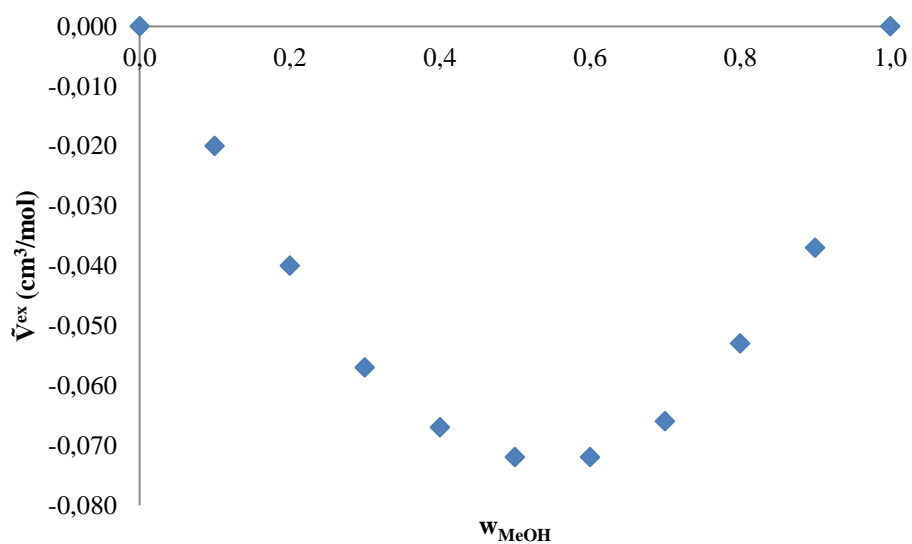


**Figure 4.8** Methanol/Methyl Acetate Mixture Excess Molar Volume

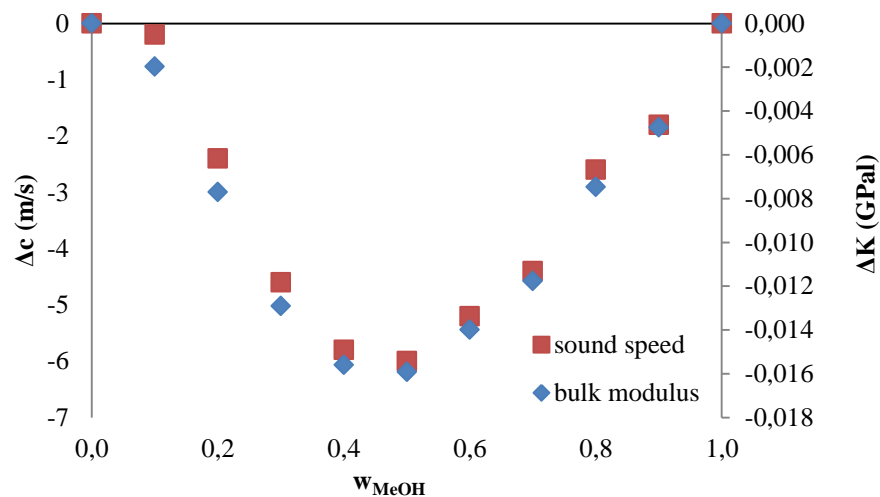


**Figure 4.9** *Methanol/Methyl Acetate Mixture Sound Speed and Bulk Modulus Deviations*

In methanol/methyl acetate mixture, dispersion forces are not as strong as in ethyl acetate/ethanol and ethanol/methyl acetate mixtures. Hence, dipole-dipole interactions are more dominant than dispersion forces resulting in negative excess molar volumes (Figure 4.8). However, interactions between unlike molecules are not as strong as in ethanol/water mixture. Negative values of deviation of bulk modulus and sound speed are obtained as packing of the structure is worsened (Figure 4.9).



## CHAPTER 5

### ULTRASONIC PARTICLE SIZE DETERMINATION

Ultrasonic techniques for characterizing concentration and particle size distributions of colloidal particles are dependent on acquiring attenuation or sound velocity as a function of frequency (velocity or attenuation spectrum). Sound velocity and attenuation in suspensions are mainly determined by the particle-wave interactions. As a result of these interactions, transmission, reflection, absorption and scattering of the wave may occur. Either one of those mechanisms or combinations of those mechanisms may arise depending on the nature of the suspension and ultrasonic parameters. Hence, particle wave interactions should be clearly understood and modelled for proper determination of particle size distribution by ultrasonic techniques.

Use of attenuation spectroscopy is more common than velocity spectroscopy though each method presents similar information and depends on identical models. Utilization of ultrasonic spectroscopy in particle size characterization has superiority on existing alternatives methods. In addition to being non-destructive and non-invasive and rapid, concentrated and optically opaque systems can also be analyzed unlike optical methods.

Particle systems whose radius varies between 10 nm and 1000  $\mu\text{m}$  can be analyzed by ultrasonic spectroscopy. The maximum particle concentration which can be analyzed changes between about 10 and 50 wt% depending on the system characteristics [79]. Nevertheless, ultrasonic spectroscopy fails to characterize dilute suspensions (below about 1 wt%) . Presence of air bubbles are one of the main obstacles in obtaining the spectrum.

There are two stages involved in the measurement of particle size distribution by ultrasonic spectroscopy:

- (1) to obtain ultrasonic velocity or attenuation spectra of the colloidal dispersion
- (2) to interpret of the spectra by a model

## **5.1 Particle Wave Interaction**

Understanding the physical essences of mechanisms of particle-wave interaction is essential for obtaining models to interpret spectrum for particle size analysis. There are four fundamental types of wave and particle interactions, and listed below [79, 80, 81];

### **5.1.1 Intrinsic Absorption**

This is governed by ordinary viscous loss mechanism. Each of the phases absorbs ultrasound separately. Concentrations of the suspensions are regulating the losses, instead of the microstructure of phases. Hence, extent of the loss can be determined by measuring absorption coefficient in each phase.

### **5.1.2 Visco-inertial Dissipation Losses**

Particle starts to oscillate in forward and backward directions under the action of wave. The reason of this oscillation is the density difference between surrounding fluid and particle. As particle oscillates, shear stress is generated; as a result, the movement of particle is softened by the viscosity of the surrounding fluid. This leads the conversion of some mechanic energy to heat so pressure of the wave decreases. Visco-inertial losses increase as the density difference between particle and fluid get higher. In addition, visco-inertial losses are effected by the sizes of particles in suspensions.

### 5.1.3 Thermal Dissipation Losses

The temperatures of the particles in suspension increases and decreases periodically with respect to surrounding liquid as a result of the propagation of ultrasound. This is due to unlike thermal properties of particles and surrounding liquid. Heat may be generated by intrinsic absorption or visco-inertial loss mechanisms. Difference in thermal properties causes that generated heat to flow by generating temperature gradients. That heat flow is also responsible for the reduction of the ultrasound pressure amplitude by converting some part of the energy in ultrasound to heat. The largeness of thermal dissipation losses are dependent on the difference between the thermal properties (thermal expansion coefficient, specific heat and thermal conductivity) of particles and surrounding liquid. Furthermore, particle size is also influence the thermal dissipation losses.

### 5.1.4 Scattering Losses

Oscillation of particles under the action of wave results in creation of secondary waves. Hence, some of the mechanical energy of ultrasound is consumed to generate these secondary waves that are propagating in different directions. Hence, an increase in attenuation coefficient is perceived in this case. Scattering losses are significantly based on the particle size and wavelength of ultrasound. If their orders of magnitudes are similar, scattering losses are extremely effective. However, for long wavelengths (i.e.  $r \ll \lambda$ ), scattering losses are insignificantly small.

The overall attenuation in particulate dispersions is the summation of all losses discussed above. However, in many cases one or two of the losses are dominant over the other to determine the overall attenuation. At high frequencies, intrinsic absorption and scattering losses are determining the overall attenuation. However, at lower frequencies, visco-inertial and thermal losses are effective on the overall attenuation.

## 5.2 Overview of the Researches Done for Ultrasonic Particle Size Determination

The simple model for determination of particle size distribution by ultrasonic spectrum was derived by R. Urick [82]. In the model, density and compressibility of the suspension was calculated by taking volume fraction average i.e. ideal solution behavior was assumed. Attenuation was calculated by H. Lamb's formula [83]. Thermal losses, acoustic scattering and frequency dependence of sound speed were ignored. Hence, a spectrum, depending on the viscosity of continuous phase, volume fraction of phases and frequency, was obtained. R. Urick and S. Ament [84] developed the second model on size distribution characterization. It was more complicated and realistic than the initial one. Sound speed was dependent on frequency and absorption in continuous phase was neglected in this model. Theoretical results of bromoform/water and mercury/water emulsions were fairly validated by the experimental measurements.

Interaction between particle and ultrasound resembles to that of between particle and light. Hence, models applied in the optic techniques are sometimes applied in ultrasonic techniques. One of such study was done by U. Riebel and co-workers [85]. They analyzed particles between 20 and 1000  $\mu\text{m}$ . They obtained sound attenuation spectra between the frequencies of 1.7 to 81 MHz. Their model depended on the analogous forms of the relations applied in laser diffraction techniques. Integral form of Lambert-Beer equation was adapted to polydisperse suspensions and was used for evaluating attenuation spectra. Particle size analyses of concentrated dispersions up to 10 % by volume were done successfully.

A. Harker and J. Temple [86] treated the sound propagation in suspensions in terms of the hydrodynamics of the system. They used mass and momentum conservation equations in their model, and evaluated the momentum transfer between the phases. By modifying the momentum equation with wave propagation, the model was developed. Several assumptions were done to construct the model. Gravitational field, heat and mass transfer between phases were neglected. Viscous losses in the continuous phase and attenuation in the solid phase were ignored, as well. Based on

the result of the experiments, it was reported that model fails to characterize system in which the acoustic impedance of phases are similar.

An extensive modelling study was done by J. Allegra and S. Hawley [87]. Their model included thermal and visco-inertial losses as well as scattering losses. The derivation of model depended on the simultaneous solution of conservation of mass, momentum and energy equations for wave propagation in particulate systems. According to their experiments, viscous losses were dominant when the wavelengths of the ultrasound and particle size were in the same order since the relative velocity of particle to fluid was highest at this point. At low frequencies both phases followed the wave propagation with small relative motion. In addition, there was very limited motion of both phases under the action of high frequency waves. It was also reported that at low frequencies, temperature between particle and surrounding fluid was identical; however, at higher frequencies different temperatures in the phases existed. Mathematical dependency of thermal and viscous losses followed similar pattern. They depend on  $f^{0.5}$  at high frequencies and depend on  $f^2$  at low frequencies.

The model developed by J. Allegra and S. Hawley [87] was later used in other studies. For example, U. Kaatz et al. [88] measured broadband attenuation spectrum in the frequency range of 0.1 and 2000 MHz for polystyrene latex dispersions. The size of particles were between 60 and 100 nm. The model of J. Allegra and S. Hawley [87] was used to interpret the spectra. In addition, up to certain particle size/wavelength ratio (100 MHz for the corresponding system), spectrum was defined by scattering while viscous losses were important at the intermediate frequencies. In addition, S. MingXu et al. [81] worked on the droplet size of two-phase fat emulsions with both attenuation and velocity spectra by using J. Allegra and S. Hawley's model [87] as in the previous work. Ultrasound attenuation was found to increase with droplet concentration. In addition, concentration did not affect the results of particle size distribution. It was revealed that uncertainties in the estimation of physical properties of particles were one of the fundamental sources of errors estimating particle size distribution. The results obtained from attenuation spectra were moderately larger than those obtained by velocity spectra. Similar

results with velocity spectra and optical technique was acquired. Additionally, ultrasonic measurement gave narrower distribution than that of the optical technique.

In their study J. Tebbutt et al. [90] compared four models developed earlier to investigate sound propagation in colloidal suspensions. The models they handled were; the R. Urick model [82], the R. Urick and S. Ament model [84], the A. Harker and J. Temple model [86] and the J. Allegra and S. Hawley model [87]. Each of the models had different complexity in terms of their mathematical structure. Therefore, the applicability of each model was restricted with their underlying assumptions. To compare their results with each other, simulations were done for three different suspensions. Results of the simulations revealed that the J. Allegra and S. Hawley model was the most applicable model for each suspension studied. This was also the most complicated model in terms of physical properties required in the model. It was also observed as more physical properties included in the models, the accuracy of the models increased. The simpler models gave more accurate results when the thermophysical properties of the phases were close to each other. On the other hand, simpler models are useful when the available physical data about the phases is limited.

S. MingXu et al. [89] developed a mathematical model to evaluate the echoes from broadband ultrasonic attenuation spectrum for characterization of particle size distribution. The frequency range was in between 1 MHz and 20 MHz. Their model was based on the evaluation and superposition of viscous and scattering losses of ultrasound. Viscous losses were taken into account by momentum conservation equation, and scattering losses were calculated by the relation developed by U. Riebel et al. [91]. By inverting the spectra, particle size distribution was obtained. Attenuation coefficients of some sizes were close to each other in narrow frequency band. Use of broadband spectrum eliminated this complication. Size distributions of different types of sand sediments with different concentrations were analyzed prosperously by this technique. Therefore, broadband spectrum was also reported to be more accurate in the case of concentrated systems.

D. McClements et al. [80] reported some points in order to generalize the applicability of ultrasonic particle size determination. They suggested that although use of multiple scattering theory in calculations gave accurate results, the extent of the theory should be enlarged to evaluate more concentrated dispersions. Flocculation of particles should also be taken into account. In addition, several physical and thermal properties of particle and fluid should be known to interpret the spectra. Hence, a database was reported to be required for the thermophysical properties of common materials found in dispersions. Presence of bubbles was one of the major drawback of ultrasonic techniques due to their strong capability of scattering ultrasound. Methodologies to avoid these effects of bubbles should be developed.

S. Dukhin et al. [79] modified the theory developed by R. Gibson and M. Toksoz [92] to include effects of particle-particle interactions. The interactions between particles were taken into account in the calculation of drag coefficient. A well agreement between experimentally obtained spectra and theoretical spectra was acquired up to concentrations of 30 % by volume. It was also possible to analyze systems having bimodal size distribution by the modified theory. It was noted that to characterize aggregated dispersion successfully, an aggregation degree should be incorporated in the model.

### **5.3 Mathematical Modeling of Ultrasound Propagation in Particulate Dispersions**

In this study we consider particles smaller than 1 mm. Hence, below that size no scattering effect is observed ( $r \ll \lambda$ ). Therefore, a model depending on the visco-inertial losses is derived in this study. At time “ $t_1$ ” ultrasound propagation starts and continues until “ $t_1+n$ ” (Figure 5.1). During this interval both particles and fluid oscillates. When wave propagation stops, these oscillations decelerate and eventually stop. Unlike other previously developed models, this model is based on the particle size characterization by evaluating the experimental data in this period. For this

purpose, physics of the problem for both periods are analyzed separately. Then their results are combined to simulate the ultrasound propagation in such media.

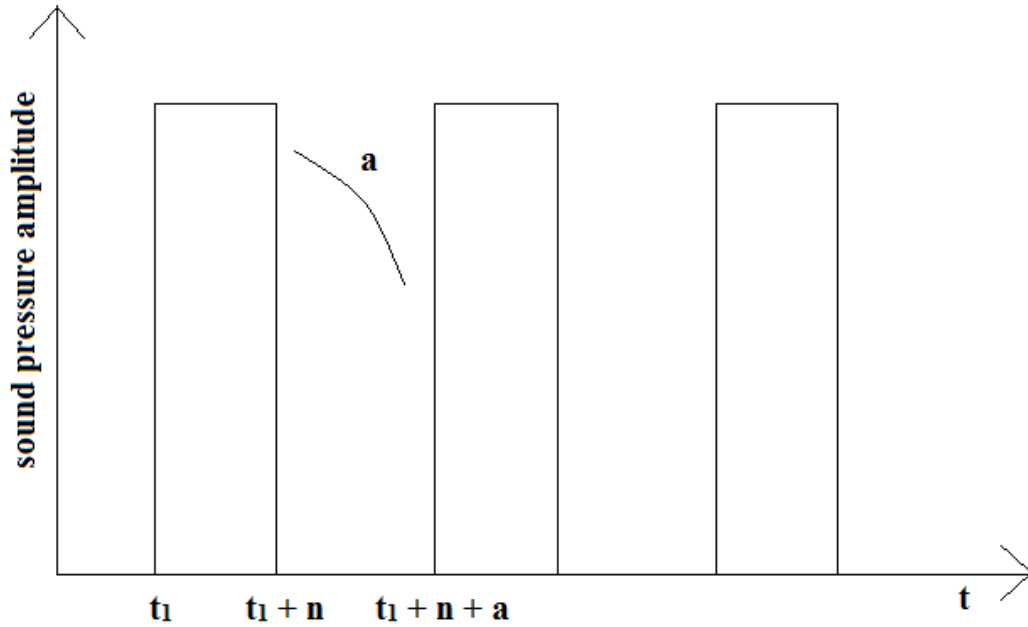


*Figure 5.1 Illustration of Modulated Ultrasound Propagation in Particulate Dispersions*

### 5.3.1 Obtaining the Governing Differential Equations for the Wave Propagations in Particulate Dispersions

To investigate the modulated ultrasound propagation in particulate dispersions, conservation of mass and momentum equations should be solved. The model is first developed for continuous wave propagation then it will be extended for modulated wave. Equation of continuity for each phase can be written as;

$$\frac{\partial}{\partial t}(\varphi\rho_s) + \frac{\partial}{\partial z}(\varphi\rho_s v_s) = 0 \quad \text{eqn. 5.1}$$

$$\frac{\partial}{\partial t}((1-\varphi)\rho_f) + \frac{\partial}{\partial z}((1-\varphi)\rho_f v_f) = 0 \quad \text{eqn. 5.2}$$

Note that eqn. 5.1 represents solid phase while eqn. 5.2 is for fluid phase. Fluid dynamics of the system should be clearly understood for proper modeling. Summation of the forces acting on a particle will give the rate of change of momentum such that;

$$\begin{aligned} \frac{4}{3} \pi r^3 \rho_s \frac{\partial v_s}{\partial t} = & 6\pi\eta r v_r - \frac{4}{3} \pi r^3 \frac{\partial P}{\partial z} + \frac{1}{2} \frac{4}{3} \pi r^3 \rho_f \frac{1+2\phi}{1-\phi} \frac{\partial v_r}{\partial t} \\ & + 6r^2 \sqrt{\pi\rho_f\eta} \int_0^t \left( \frac{d}{d\tau} v_r(\tau) \right) (t-\tau)^{-1/2} d\tau - \frac{4}{3} \pi r^3 (\rho_s - \rho_f) g \end{aligned} \quad \text{eqn. 5.3}$$

Where  $\phi$  is the volume fraction of particles and  $v_r$  is relative velocity of fluid with respect to solid ( $v_r = v_f - v_s$ ).

The force balance is constructed based on the study of C. Tchen [93] (modification of the B. Basset's work [94]). The identification of each term is provided below;

$6\pi\eta r v_r =$  Stoke's drag force

$\frac{4}{3} \pi r^3 \frac{\partial P}{\partial z} =$  pressure gradient due to acceleration of fluid

$\frac{1}{2} \frac{4}{3} \pi r^3 \rho_f \frac{1+2\phi}{1-\phi} \frac{\partial v_r}{\partial t} =$  inertia of virtual mass attached to the particle

$6r^2 \sqrt{\pi\rho_f\eta} \int_0^t \left( \frac{d}{d\tau} v_r(\tau) \right) (t-\tau)^{-1/2} d\tau =$  diffusion of vorticity past the particle

(Basset's history term)

$\frac{4}{3} \pi r^3 (\rho_s - \rho_f) g =$  gravity

Basset's term can be omitted since viscous damping in the fluid is small compared to drag force. Similarly, gravity can also be omitted. The derivation of inertia of virtual mass attached to the particle (added-mass) is given below;

### Added-mass term

$$-\frac{\partial P}{\partial z} = \rho_f \frac{\partial v_s}{\partial t} \quad \text{eqn. 5.4}$$

The particle will experience lift force of  $F_L$  ;

$$F_L = -V \frac{\partial P}{\partial z} = -V \rho_f \frac{\partial v_s}{\partial t} \quad \text{eqn. 5.5}$$

In addition, acceleration of particles with respect to fluid generates drag force of  $F_D$ ;

$$F_D = \rho_f V^* \left( \frac{\partial v_s}{\partial t} - \frac{\partial v_f}{\partial t} \right) \quad \text{eqn. 5.6}$$

$F_D$  is damped by  $F_L$  ;

$$\rho_f V \frac{\partial v_s}{\partial t} = \rho_s V \frac{\partial v_f}{\partial t} - \rho_f V^* \left( \frac{\partial v_s}{\partial t} - \frac{\partial v_f}{\partial t} \right) \quad \text{eqn. 5.7}$$

and

$$\frac{\partial v_s}{\partial t} = \frac{\partial v_f}{\partial t} \frac{V^* + V}{V^* + V(\rho_s / \rho_f)} \quad \text{eqn. 5.8}$$

For a single sphere, induced mass of  $\rho_f V^*$  is calculated as  $\frac{1}{2} \rho_f V$  by H. Lamb et al [83]. To calculate the induced mass for the existence of many sphere, it is assumed that particle of radius “ $r$ ” affects the fluid with a volume of “ $r^*$ ” . Hence, volume fraction of particles is  $\phi = (r / r^*)^3$  . If same procedure is applied, then it is obtained that;

$$V^* = \frac{1}{2} V \frac{1+2\phi}{1-\phi} \quad \text{eqn. 5.9}$$

It is more useful to use the waveform of momentum equation due to the sinusoidal character of the motion. The waveform transformation of the equation was developed by G. Stokes [95];

$$\begin{aligned} \frac{4}{3} \pi r^3 \rho_s \frac{\partial v_s}{\partial t} &= \frac{4}{3} \pi r^3 \rho_f \left( \frac{1}{2} \frac{1+2\varphi}{1-\varphi} + \frac{9}{4r} \sqrt{\frac{2\eta}{w\rho_f}} \right) \frac{\partial v_r}{\partial t} \\ &+ 3\pi \rho_f r^3 w \left( \frac{1}{r} \sqrt{\frac{2\eta}{w\rho_f}} + \frac{2\eta}{wr^2 \rho_f} \right) v_r - \frac{4}{3} \pi r^3 \frac{\partial P}{\partial z} \end{aligned} \quad \text{eqn. 5.10}$$

Momentum equation can be expressed for both phase such that;

$$\frac{\partial}{\partial t} (\varphi \rho_s v_s) + v_s \frac{\partial}{\partial z} (\varphi \rho_s v_s) = \varphi \rho_f \left( \frac{1}{2} \frac{1+2\varphi}{1-\varphi} + \frac{9}{4} \frac{\delta}{r} \right) \frac{\partial v_r}{\partial t} + \frac{9}{4} \rho_f w \varphi \left( \frac{\delta}{r} + \frac{\delta^2}{r^2} \right) v_r - \varphi \frac{\partial P}{\partial z} \quad \text{eqn. 5.11}$$

$$\begin{aligned} \frac{\partial}{\partial t} [(1-\varphi) \rho_f v_f] + v_f \frac{\partial}{\partial z} [(1-\varphi) \rho_f v_f] &= -\varphi \rho_f \left( \frac{1}{2} \frac{1+2\varphi}{1-\varphi} + \frac{9}{4} \frac{\delta}{r} \right) \frac{\partial v_r}{\partial t} \\ &- \frac{9}{4} \rho_f w \varphi \left( \frac{\delta}{r} + \frac{\delta^2}{r^2} \right) v_r + (\varphi - 1) \frac{\partial P}{\partial z} \end{aligned} \quad \text{eqn. 5.12}$$

where

$$\delta = \sqrt{\frac{2\eta}{w\rho_f}} \quad . \quad \text{eqn. 5.13}$$

Eqns. 5.11 and 5.12 can be revised for polydisperse systems as shown in Appendix A7.

Compressibility of the solution and density variations of fluid and particle with respect to pressure can be written as;

$$\beta = (1-\varphi^0) \beta_f + \varphi^0 \beta_s \quad \text{eqn. 5.14}$$

$$\rho_f = \rho_f^0 + \rho_f^0 \beta_f P \quad \text{eqn. 5.15}$$

$$\rho_s = \rho_s^0 + \rho_s^0 \beta_s P \quad \text{eqn. 5.16}$$

Wave solutions can be written as;

$$v_s = v_{s0k} \exp[i(\sigma x - \omega t)] \quad \text{eqn. 5.17}$$

$$v_f = v_{f0k} \exp[i(\sigma x - \omega t)] \quad \text{eqn. 5.18}$$

$$\rho_s = \rho_s^0 + \rho_{s0k} \exp[i(\sigma x - \omega t)] \quad \text{eqn. 5.19}$$

$$\rho_f = \rho_f^0 + \rho_{f0k} \exp[i(\sigma x - \omega t)] \quad \text{eqn. 5.20}$$

$$P = P_{0k} \exp[i(\sigma x - \omega t)] \quad \text{eqn. 5.21}$$

$$\varphi = \varphi^0 + \varphi_{0k} \exp[i(\sigma x - \omega t)] \quad \text{eqn. 5.22}$$

Inserting the wave solutions into the governing equations;

$$\rho_{f0k} = \rho_f^0 \beta_f P_{0k} \quad \text{eqn. 5.23}$$

$$\rho_{s0k} = \rho_s^0 \beta_s P_{0k} \quad \text{eqn. 5.24}$$

$$-i\omega(\rho_s^0 \varphi_{0k} + \varphi^0 \rho_{s0k}) + i\sigma \rho_s^0 u_{s0k} = 0 \quad \text{eqn. 5.25}$$

$$-i\omega(-\rho_f^0 \varphi_{0k} + (1 - \varphi^0) \rho_{f0k}) + i\sigma(1 - \varphi^0) \rho_f^0 = 0 \quad \text{eqn. 5.26}$$

$$-i\omega \varphi^0 \rho_s^0 u_{s0k} = \varphi^0 \rho_f^0 \left[ \frac{1}{2} \left( \frac{1 + 2\varphi^0}{1 - \varphi^0} \right) + \frac{9}{4} \frac{\delta}{r} \right] (u_{f0k} - u_{s0k}) (-i\omega) + \frac{9}{4} \rho_f^0 \omega \varphi^0 \left[ \frac{\delta}{r} + \frac{\delta^2}{r^2} \right] (u_{f0k} - u_{s0k}) - P_{0k} i\sigma \quad \text{eqn.5.27}$$

$$-i\omega(1 - \varphi^0) \rho_f^0 u_{f0k} = -\varphi^0 \rho_f^0 \left[ \frac{1}{2} \left( \frac{1 + 2\varphi^0}{1 - \varphi^0} \right) + \frac{9}{4} \frac{\delta}{r} \right] (u_{f0k} - u_{s0k}) (-i\omega) - \frac{9}{4} \rho_f^0 \omega \varphi^0 \left[ \frac{\delta}{r} + \frac{\delta^2}{r^2} \right] (u_{f0k} - u_{s0k}) - (1 - \varphi^0) P_{0k} i\sigma \quad \text{eqn.5.28}$$

For simplicity

$$Q = \frac{1}{2} \left( \frac{1 + 2\varphi^0}{1 - \varphi^0} \right) + \frac{9}{4} \frac{\delta}{r} \quad \text{eqn. 5.29}$$

$$R = \frac{9}{4} \left[ \frac{\delta}{r} + \frac{\delta^2}{r^2} \right] \quad \text{eqn. 5.30}$$

$$S = Q + iR \quad \text{eqn. 5.31}$$

For non-trivial solution following determinant should be zero.

$$\begin{pmatrix} 0 & 0 & 0 & 1 & -\rho_f^0 \beta_f & 0 \\ 0 & 0 & 1 & 0 & -\rho_s^0 \beta_s & 0 \\ i\sigma \rho_s^0 & 0 & -i\omega \varphi^0 & 0 & 0 & -i\omega \rho_s^0 \\ 0 & i\sigma(1-\varphi)\rho_f^0 & 0 & -i\omega(1-\varphi^0) & 0 & -i\omega \rho_f^0 \\ -i\omega \varphi^0 (\rho_s^0 + \rho_f^0 S) & i\omega \varphi^0 \rho_f^0 S & 0 & 0 & i\sigma \varphi^0 & 0 \\ i\omega \varphi^0 \rho_f^0 S & -i\omega \rho_f^0 (1-\varphi^0 + \varphi^0 S) & 0 & 0 & i\sigma(1-\varphi^0) & 0 \end{pmatrix} \begin{pmatrix} u_{s0k} \\ u_{f0k} \\ \rho_{s0k} \\ \rho_{f0k} \\ P_{0k} \\ \varphi_{0k} \end{pmatrix} = 0$$

eqn. 5.32

Solving for  $\sigma$  yields;

$$\sigma^2 = \omega^2 \left[ (1-\varphi)\beta_f + \varphi\beta_s \right] \frac{\rho_f \left[ \rho_s (1-\varphi + \varphi S) + \rho_f S(1-\varphi) \right]}{\rho_s (1-\varphi)^2 + \rho_f [S + \varphi(1-\varphi)]}$$

eqn. 5.33

By substituting the calculated value of “ $\sigma$ ” into the wave solutions, propagation of sound in polydispersed solution can be simulated. However, this simulation is valid for continuous wave propagation. The model should be extended to capture the modulated wave propagation. This can be achieved by separately analyzing the behavior of the system when the wave is stopped.

### 5.3.2 Investigation of the Behavior of the Particles and Fluid when Wave is Stopped

Recalling the equation of continuity for solid and liquid phases;

$$\begin{aligned} \frac{\partial}{\partial t} (\varphi \rho_s v_s) + v_s \frac{\partial}{\partial z} (\varphi \rho_s v_s) &= \frac{1}{2} \varphi \rho_f \left( \frac{1+2\varphi}{1-\varphi} \right) \left( \frac{\partial v_f}{\partial t} - \frac{\partial v_s}{\partial t} \right) + \frac{9}{2} \frac{\eta}{r^2} \varphi (v_f - v_s) - \varphi \frac{\partial P}{\partial z} \\ + \frac{9r}{2\pi} \varphi \sqrt{\pi \rho_f \eta} \int_0^t \left( \frac{d}{d\tau} (v_f - v_s) \right) (t-\tau)^{-1/2} d\tau \end{aligned}$$

eqn. 5.34

$$\begin{aligned} \frac{\partial}{\partial t} ((1-\varphi)\rho_f v_f) + v_f \frac{\partial}{\partial z} ((1-\varphi)\rho_f v_f) &= -\frac{1}{2} \varphi \rho_f \left( \frac{1+2\varphi}{1-\varphi} \right) \left( \frac{\partial v_f}{\partial t} - \frac{\partial v_s}{\partial t} \right) - \frac{9}{2} \frac{\eta}{r^2} \varphi (v_f - v_s) \\ + (\varphi-1) \frac{\partial P}{\partial z} - \frac{9r}{2\pi} \varphi \sqrt{\pi \rho_f \eta} \int_0^t \left( \frac{d}{d\tau} (v_f - v_s) \right) (t-\tau)^{-1/2} d\tau \end{aligned}$$

eqn. 5.35

Basset's term can not be omitted for this case since viscous damping is important for fluid motion. Equation of continuity dictates that the terms  $\frac{\partial}{\partial Z}(\varphi\rho_s v_s)$  and  $\frac{\partial}{\partial Z}((1-\varphi)\rho_f v_f)$  are zero since there is no compression due to the wave propagation such that;

$$\frac{\partial}{\partial t}(\varphi\rho_s) + \frac{\partial}{\partial Z}(\varphi\rho_s v_s) = 0 \quad \text{eqn. 5.36}$$

$$\frac{\partial}{\partial t}((1-\varphi)\rho_f) + \frac{\partial}{\partial Z}((1-\varphi)\rho_f v_f) = 0 \quad \text{eqn. 5.37}$$

Since time derivatives of density and volume fractions are zero then those terms go to zero.

Following conversion can also be done;

$$-\frac{\partial P}{\partial Z} = \rho_f \frac{\partial v_f}{\partial t} \quad \text{eqn. 5.38}$$

By rearranging the governing differential equations;

$$\left[ \varphi\rho_s + \frac{1}{2}\varphi\rho_f \left( \frac{1+2\varphi}{1-\varphi} \right) \right] \frac{\partial v_s}{\partial t} + \frac{9}{2} \frac{\eta}{r^2} \varphi v_s = \left[ \varphi\rho_f + \frac{1}{2}\varphi\rho_f \left( \frac{1+2\varphi}{1-\varphi} \right) \right] \frac{\partial v_f}{\partial t} + \frac{9}{2} \frac{\eta}{r^2} \varphi v_f \quad \text{eqn. 5.39}$$

$$+ \frac{9r}{2\pi} \varphi \sqrt{\pi\rho_f \eta} \int_0^t \left( \frac{d}{d\tau} (v_f - v_s) \right) (t-\tau)^{-1/2} d\tau$$

$$\frac{1}{2} \varphi\rho_f \left( \frac{1+2\varphi}{1-\varphi} \right) \frac{\partial v_s}{\partial t} + \frac{9}{2} \frac{\eta}{r^2} \varphi v_s - \frac{9r}{2\pi} \varphi \sqrt{\pi\rho_f \eta} \int_0^t \left( \frac{d}{d\tau} (v_f - v_s) \right) (t-\tau)^{-1/2} d\tau$$

$$= \frac{1}{2} \varphi\rho_f \left( \frac{1+2\varphi}{1-\varphi} \right) \frac{\partial v_f}{\partial t} + \frac{9}{2} \frac{\eta}{r^2} \varphi v_f \quad \text{eqn. 5.40}$$

Subtracting eqn. 5.40 from eqn. 5.39;

$$\varphi\rho_s \frac{\partial v_s}{\partial t} = \varphi\rho_f \frac{\partial v_f}{\partial t} \quad \text{eqn. 5.41}$$

or

$$\frac{\partial v_s}{\partial t} = \frac{\rho_s}{\rho_f} \frac{\partial v_f}{\partial t}$$

eqn. 5.42

Inserting eqn. 5.42 into eqn. 5.40;

$$\begin{aligned} & \frac{1}{2} \varphi \rho_f \left( \frac{1+2\varphi}{1-\varphi} \right) \frac{\rho_s}{\rho_f} \frac{dv_f}{dt} + \frac{9}{2} \frac{\eta}{r^2} \varphi v_s - \frac{9r}{2\pi} \varphi \sqrt{\pi \rho_f \eta} \int_0^t \left( \frac{dv_f}{d\tau} \left( 1 - \frac{\rho_s}{\rho_f} \right) \right) (t-\tau)^{-1/2} d\tau \\ & = \frac{1}{2} \varphi \rho_f \left( \frac{1+2\varphi}{1-\varphi} \right) \frac{dv_f}{dt} + \frac{9}{2} \frac{\eta}{r^2} \varphi v_f \end{aligned} \quad \text{eqn. 5.43}$$

Rearranging;

$$v_s = \frac{\frac{1}{2} \varphi \left( \frac{1+2\varphi}{1-\varphi} \right) (\rho_f - \rho_s) \frac{dv_f}{dt} + \frac{9\eta}{2r^2} \varphi v_f + \frac{9r}{2\pi} \varphi \sqrt{\pi \rho_f \eta} \int_0^t \frac{dv_f}{d\tau} \left( 1 - \frac{\rho_s}{\rho_f} \right) (t-\tau)^{-1/2} d\tau}{\frac{9\eta}{2r^2} \varphi} \quad \text{eqn. 5.44}$$

Inserting  $v_s$  into the eqn. 5.44 into eqn. 5.39, the resulting integro-differential equation can be solved for  $v_f$  by the method proposed by J. Day [96]. Hence, response of the medium after the cessation of wave can be analyzed once  $v_f$  is determined.

## 5.4 Simulations of Ultrasound Propagating in Particulate Suspensions

Based on the model developed for the propagation of modulated ultrasound in particulate dispersions, simulations are done with various particle sizes. Results of the simulations show that the method is applicable in the particle size interval range between 25  $\mu\text{m}$  and 300  $\mu\text{m}$ . For particle sizes less than 25  $\mu\text{m}$ , particles immediately stop their motion when wave propagation stops. Since, drag force per unit surface area is higher for smaller particles. Hence, devices are not sensitive enough to catch such quick stoppage. For those larger than 300  $\mu\text{m}$ , sound pressure amplitude is not sufficient to drive particles. Thus, they do not have any affect on propagation.

Simulations for mono-sized particles are done for particle sizes of 10  $\mu\text{m}$ , 100  $\mu\text{m}$  and 1000  $\mu\text{m}$ . They are depicted in Figures 5.2, 5.3 and 5.4.

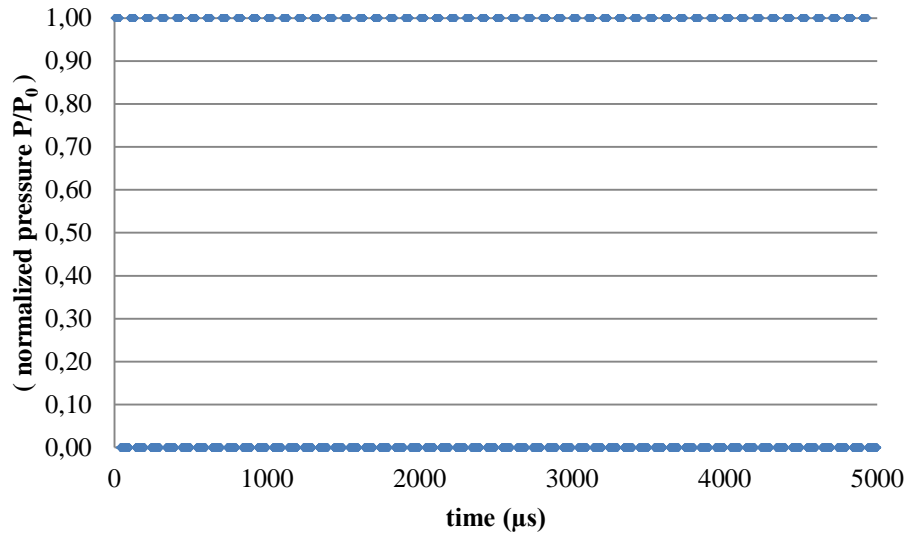


*Figure 5.2 Modulated Ultrasound Propagation for Particle Size of 10  $\mu\text{m}$*

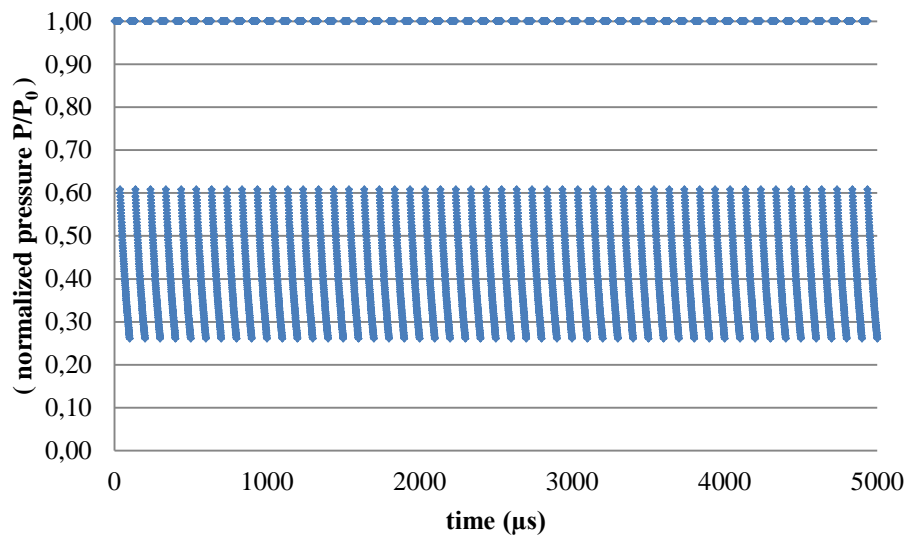


*Figure 5.3 Modulated Ultrasound Propagation for Particle Size of 100  $\mu\text{m}$*

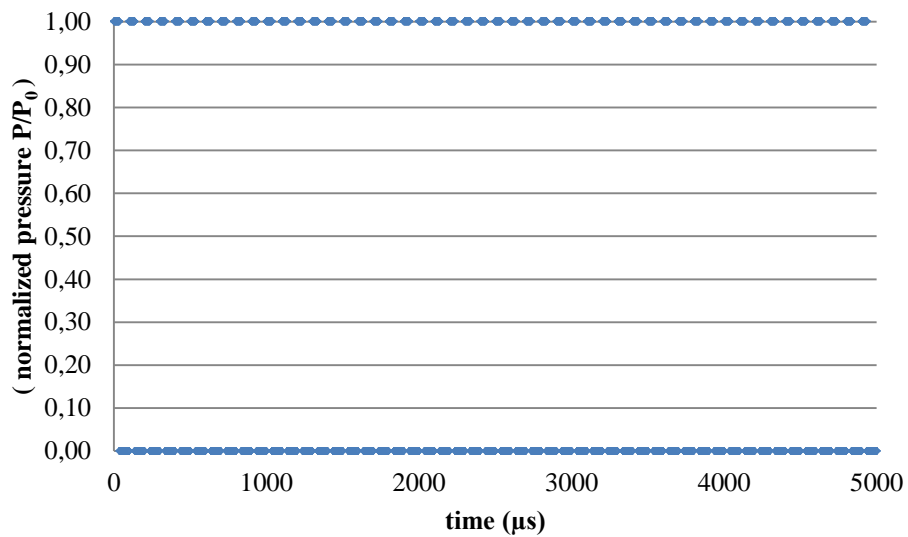


**Figure 5.4** *Modulated Ultrasound Propagation for Particle Size of 1000  $\mu\text{m}$*

For the simulation for size of 10  $\mu\text{m}$ , particles immediately stop their motions. Hence, their stoppage behavior are not clearly perceived. For size of 100  $\mu\text{m}$ , this stoppage behavior is apparent. Thus, it makes it possible to do particle size characterization in this interval. Furthermore, for larger particles (i.e. 1000  $\mu\text{m}$ ) ultrasound is not able to move these particles. Hence, no data is provided for particle size characterization. To figure out the limits of the method, further simulations are done with 25  $\mu\text{m}$ , 50  $\mu\text{m}$ , 150  $\mu\text{m}$  and 300  $\mu\text{m}$ . The results are provided in Figures 5.5, 5.6, 5.7 and 5.8. Results of the simulations reveal that the method is applicable in the particle size range between 25  $\mu\text{m}$  and 300  $\mu\text{m}$ . Out of these limits, the method fails to characterize particle size.

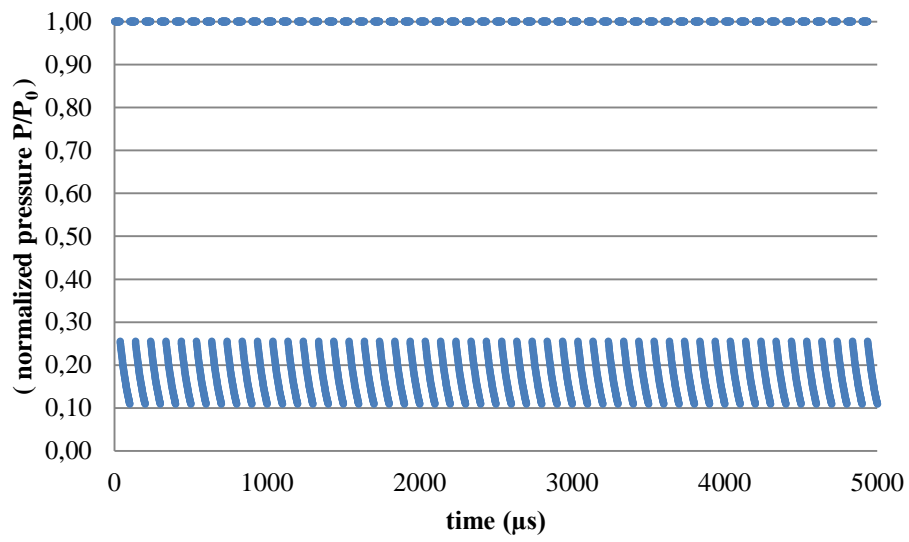


*Figure 5.5 Modulated Ultrasound Propagation for Particle Size of 50  $\mu m$*

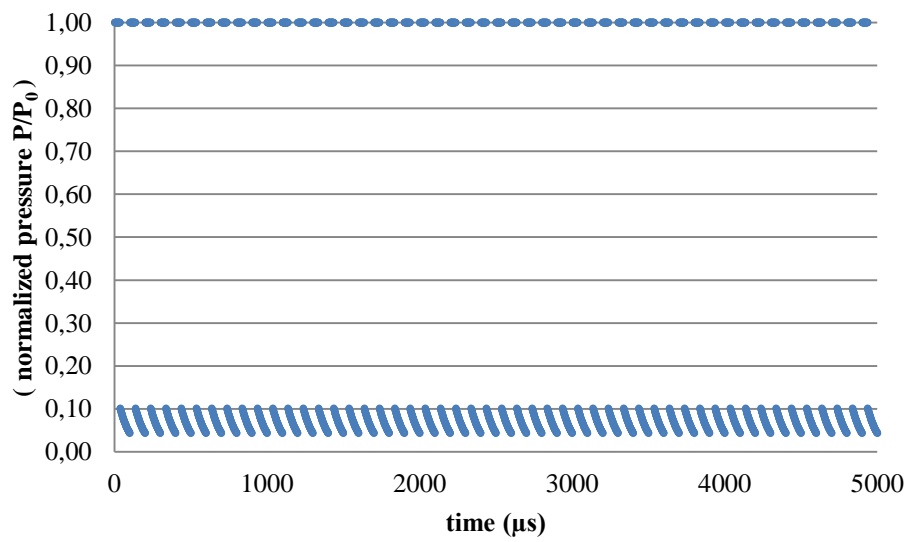


*Figure 5.6 Modulated Ultrasound Propagation for Particle Size of 25  $\mu m$*

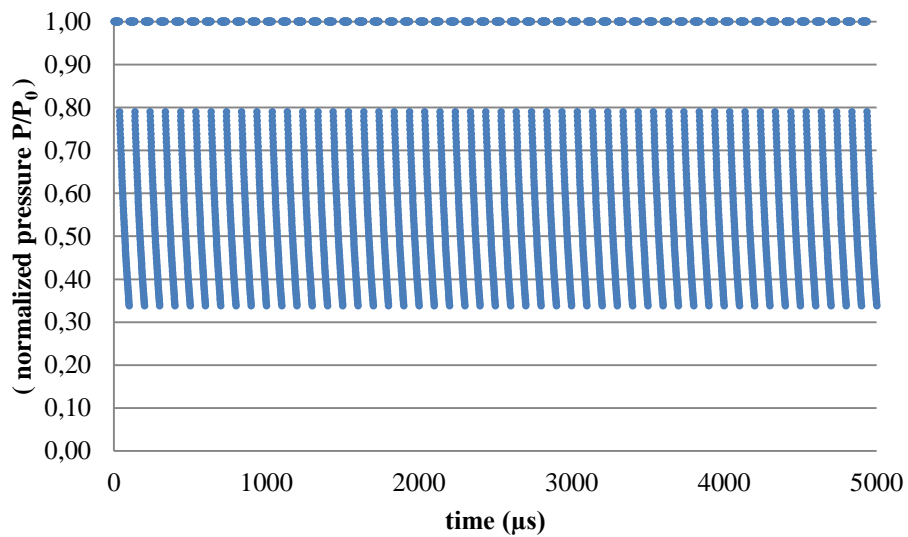


**Figure 5.7** *Modulated Ultrasound Propagation for Particle Size of 150  $\mu\text{m}$*

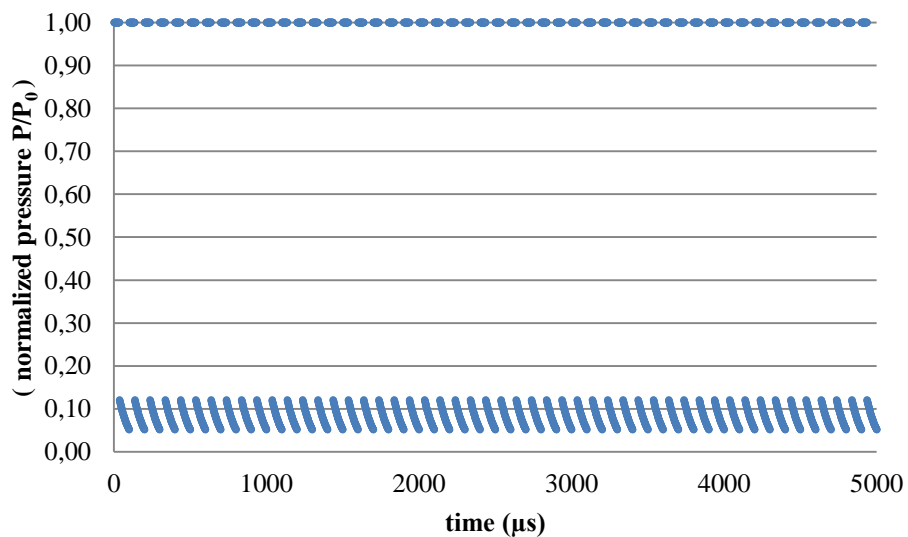


**Figure 5.8** *Modulated Ultrasound Propagation for Particle Size of 300  $\mu\text{m}$*

In addition, to evaluate the effect of volume fractions of particles, ultrasound propagation simulations are also done with volume fractions of 0.2 and 0.3 for 100  $\mu\text{m}$  particles. The results are shown in Figures 5.9 and 5.10. Results of the simulations indicate that as volume fractions of particles increases, sound pressure levels decreases since sound absorption level increases with volume fraction.

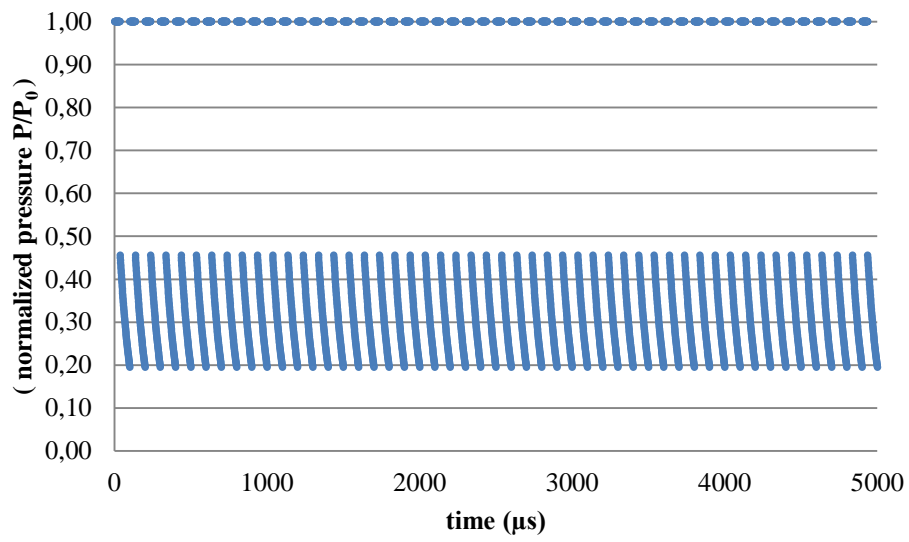


*Figure 5.9 Modulated Ultrasound Propagation for Volume Fraction of 0.2*

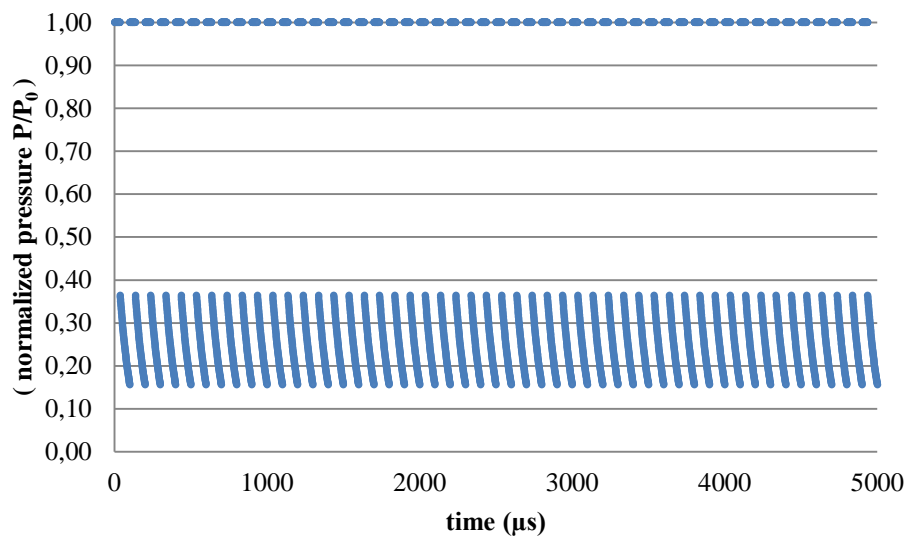


*Figure 5.10 Modulated Ultrasound Propagation for Volume Fraction of 0.3*

## 5.5 Experimental Procedure

In particle size measurement experiments, colemanite/ water suspensions are used. Deionized water obtained from Innovation Pure Water System is used to prepare suspensions.

Colemanite particle used in particle size characterization part are taken from Eti Mine Woks General Management. Its specification is provided in Appendix A13. Particle size of the colemanite samples are 10  $\mu\text{m}$ , 75  $\mu\text{m}$ , 100  $\mu\text{m}$ , 150  $\mu\text{m}$  and 1000  $\mu\text{m}$ . Dispersions are prepared with 0.05, 0.10, 0.15, 0.20, 0.25 and 0.30 colemanite volume fractions.

Room temperature is kept at 25°C during the experiments by the help of air conditioner. The piezzo ceramic transducer (SUHNER Switzerland RG 174/U 50 ohm) is immersed into 1 liter sample solution for measurements. The deepness of the transducer tip is adjusted to be 2 cm away from the surface of the dispersion. Uniformity of the suspension is maintained by a stirrer. Echo-history data with respect to position are acquired and they are used to determine the particle size by the help of models developed. In the experiments, pulse repetition frequencies are kept as 8000  $\mu\text{s}$ . In addition, base frequency of ultrasound is 2 MHz.

Furthermore, particle sizes of the samples are also determined by a conventional particle sizer “Mastersizer 2000 equipment” (Figure 5.11).



*Figure 5.11 Mastersizer 2000 equipment*

Specifications of the Mastersizer 2000 is given in Appendix 11.

## **5.6 Ultrasonic Particle Size Measurements**

To evaluate the mathematical model derived for particle size measurement, ultrasonic measurements are done with Ultrasound Doppler Velocimeter (DOP 2000). In addition, to check the performance of ultrasonic experiments, particle sizes are also done with “Mastersizer 2000 equipment”.

In experiments, dispersions of colemanite/water are prepared for various colemanite particle sizes (10  $\mu\text{m}$ , 75  $\mu\text{m}$ , 100  $\mu\text{m}$ , 150  $\mu\text{m}$  and 1000  $\mu\text{m}$ ) and colemanite volume fractions (0.05, 0.10, 0.15, 0.20, 0.25 and 0.30).

Results of the experimental measurements are listed in Table 5.1. In the table the first column includes the results of the conventional particle size measurement device, Mastersizer 2000. The other figures are ultrasound results at different particle loadings. Algorithm for the calculation of a particle size from the ultrasound

measurements is provided in Appendix A8. In addition, particle size measurements with Mastersizer are also depicted in Appendix A9.

**Table 5.1 Particle Size Measurements of Colemanite/Water Dispersions**

particle size ( $\mu\text{m}$ )	volume fraction					
	0.05	0.10	0.15	0.20	0.25	0.30
10	-	-	-	-	-	-
75	63	64	70	71	70	70
100	91	93	94	95	95	95
150	139	141	141	142	142	141
1000	-	-	-	-	-	-

In 10 $\mu\text{m}$  colemanite dispersions, ultrasonic measurements are not applicable. The reason of this is that particle motion stops when the wave is stopped. Therefore, ultrasonic device can not detect the stoppage behavior of particles. Thus, the method is not appropriate in that particle size range. For, 75  $\mu\text{m}$ , 100  $\mu\text{m}$  and 150  $\mu\text{m}$  particle size range the results of ultrasonic technique are in good agreement with those of the conventional method. Optimum volume fraction for measurements is 0.20. In this fraction, maximum deviation of particle size measured by ultrasound is 5%. On the other hand, for 1000  $\mu\text{m}$  particle size the method can not work. Ultrasound pressure can not vibrate the particles hence no motion is observed.



## CHAPTER 6

### CONCLUSIONS & RECOMMENDATIONS

In this study, suitable mathematical models are developed to perform ultrasonic characterization of material. The theoretical results are compared with those experimentally obtained. The study is divided into the following three parts: Characterization of non-linear viscoelastic properties, concentration measurement and characterization of particle size. The main conclusions and recommendations of this study are listed below.

- By using the model developed simulations of ultrasound propagation in Oldroyd-B fluid are done with different viscoelastic parameters to investigate the effects of Oldroyd-B parameters on ultrasound propagation. From the simulations it is noticed that as relaxation time increases, the increments in loading periods get more apparent. At low relaxation times the pressures reaches their equilibrium values immediately. Solvent viscosity is mainly responsible for the magnitude of the sound pressure level. Higher solvent viscosities give higher pressures. The effects of retardation times are observed in recovery periods. If it is small, the pressure immediately becomes zero during recovery period. When it gets higher, the recovery period is observed clearer.
- The order of magnitude of duration time in loading periods and recovery periods (“n” and “a”) should be same with those of relaxation and retardation times. Otherwise, they cannot be characterized.
- Oldroyd-B parameters of CMC/water solutions of 2,3 and 4 wt. % are obtained by ultrasonic measurements. Results of the ultrasonic experiments show that as concentration of CMC in the solution increases the value of

relaxation time and retardation time increases. This shows that elastic character of the solutions increases with CMC addition.

- Any viscoelastic model can be applied in the method developed. Provided that time constant in the materials have the same order of magnitude with the pulse repetition frequency, their values can be determined with the technique developed.
- In concentration measurement part, a model based on Peng-Robinson Equation of State is derived. Sound speeds in ethanol/water, methanol/methyl acetate, ethanol/methyl acetate and ethyl acetate/ethanol systems are measured and sound speeds in those solutions are calculated by the model developed based on Peng-Robinson Equation of State. On the other hand, considerable deviation arises between experimental measurements and the model due to the poor estimation of saturated liquid densities by Peng-Robinson Equation of State.
- By the use of volume translated Peng-Robinson Equation of State, results of concentration estimation by the ultrasound based model are in well agreement with experimental measurements.
- Measurements also show that use of speed of sound is a promising tool to understand the intermolecular interactions in mixtures. Deviation of sound speed from ideality helps to interpret the framework of the final structure and interactions between unlike molecules such as hydrogen bondings and dipole-dipole interactions. Hence, use of speed of sound can be benefited in thermodynamical and physicochemical researches.
- For some sound speed values there are two possible solution concentrations. If operator has the idea about which concentration is more possible one, the correct concentration can be estimated for that type of situations.
- The technique is limited with to estimate the concentration of binary mixtures. If attenuation can be related with concentration, then the method is extended for ternary mixtures.
- Moreover, provided that attenuation is related with the concentration properly, carrying out experiment with different frequencies make it possible

estimate concentration for multicomponent mixtures since attenuation is strongly dependent on frequency.

- Estimation of concentration from sound speed can also be applied in kinetic studies. Since measurements are fast, rate of change of any component in reacting systems can be instantaneously determined.
- As ultrasound has high penetration capacity, speed of sound can also be used in medical diagnosis and imaging. Deviation of the sound speed in tissues can be a sign of defect.
- In particle size measurement part a mathematical model based on pulse repetition frequency of ultrasound is developed. By the use of the model, numerical simulations are done and it is concluded that the technique is suitable to characterize the particle size between 25  $\mu\text{m}$  and 300  $\mu\text{m}$ .
- The ultrasound method is suited best for the particle size range between 25  $\mu\text{m}$  and 300  $\mu\text{m}$ .
- Experimental measurements were done with 10  $\mu\text{m}$ , 75  $\mu\text{m}$ , 100  $\mu\text{m}$ , 150  $\mu\text{m}$  and 1000  $\mu\text{m}$  colemanite/water dispersions for volume fractions of 0.05, 0.10, 0.15, 0.20, 0.25 and 0.30. These results compared well with those of ultrasonic method in the case of 75  $\mu\text{m}$ , 100  $\mu\text{m}$ , 150  $\mu\text{m}$  particle dispersions. For 10  $\mu\text{m}$  and 1000  $\mu\text{m}$  particles, however, ultrasonic technique did not work.
- Due to their high surface energy, some particles like metal oxides can easily agglomerate. Laser based techniques fail to measure particle sizes in such situations. Nevertheless, the developed technique is suitable for this types of measurements.
- Ultrasonic particle size measurement technique can also be applied in kinetic studies. For example, particle growth rate can be instantaneously determined.



## REFERENCES

- [1] “Ultrasonics: A Technique of Material Characterization”, D. K. Pandey, S. Pandey, Acoustic Waves (2010)
- [2] “Characterization of Material Properties by Ultrasonics”, P. P. Nanekar, B. K. Shah , BARC Newsletter, issue 249 (2003)
- [3] “Non-Destructive Characterization of Polymers During Injection Molding with Ultrasonic Attenuation Measurement”, P. Zhao, J. Z. Fu, S. B. Cui, Materials Research Innovations, vol. 15 (2011)
- [4] “Ultrasonic Characterization of the Crystallization Behavior of Poly(ethylene terephthalate)” , L. Zhao, Z. Sun, J. Tatibouet, S. Guo, Journal of Applied Polymer Science, vol.114 issue 5, pp. 2731- 2739 (2009)
- [5] “Acoustic Methods of Investigating Polymers”, I. Perepechko, Mir Publishers, Moscow (1975)
- [6] “Propagation of Ultrasonic Waves in Viscous Fluids”, O. Assia, D. Hakim Faculty Of Physics, University Of Sciences and Technology Houari Boumedienne P.O. 32, El Alia, Bab Ezzouar, Algiers, Algeria (2010)
- [7] ”Acoustics for Engineers: Troy Lectures”, J. Blauert, N. Xiang, (2009)
- [8] “Sound and Light”, Hillesheim, Heather., New York NY : Infobase Learning, Jan. (2012)
- [9] “The Social and Economic Roots of Newton's 'Principia'”, In Science At The Crossroads (Editor: Bernal, J. D.), Hessen, B, Frank Cass & Co. Ltd, U.K., 2nd Edition, pp. 147-212 (1931)
- [10] “Sound Propagation in Liquids”, S. Parthasarathy M. Pancholy, Annalen der Physik, vol. 452 issue 6-8 (1956), pp. 417–422
- [11] “Polymer Science and Technology for Scientists and Engineers”, R. A. Pethrick, Dunbeath : Whittles (2010)

- [12] "Physical Acoustics", W. P. Mason, H. J. Mcskimin, Academic: New York; vol. 1A. (1964)
- [13] "Piezoelectric Crystals and Their Applications to Ultrasound", W. P. Mason, D. Van Nostrand, Princeton (1950)
- [14] "Ultrasonic Testing of Materials", J. Krautkramer, Springer-Verlag: Berlin, Germany (1977)
- [15] "Ultrasonic Characterization of Polymers as Function of Temperature, Pressure and Frequency", L. Pich, F. Massines, G. Lessard, IEEE Ultrasonic Symposium, Denver (1987), pp. 1125-1130
- [16] "Polymer Characterization by Ultrasonic Wave Propagation", Francesca Lionetto, Alfonso Maffezzoli, Department of Innovation Engineering, University Of Salento, 73100 Lecce, Italy (2009)
- [17] "Science and Technology of Ultrasonics", B. Raj, Narosa Publishing House (2004)
- [18] "Glass Transition Characterization of Homogeneous and Heterogeneous Polymers by an Ultrasonic Method" N. T. Nguyen, M. Lethiecq, Journal of Ultrasonics, vol. 33 issue 4 (1995), pp. 323-329
- [19] "Elastic Waves in Solids I", D. Royer E. Dieulesaint, Springer, New York (2000)
- [20] "Acoustic Fields and Waves in Solids "B. A. Auld, Krieger Pub Co, New York (1990)
- [21] "Calculation of Third-Forth Order Elastic Constants of Alkali Halide Crystal ", S. Mori, Y. Hiki, Journal of Physical Society Japan, vol. 45, pp 1449-1456 (1978)
- [22] "Use of Sound Velocity Measurements in Determining the Debye Temperature of Solids", G.A. Alers, Physical Acoustics IIIB, Academic Press (1965)
- [23] "Elements of Acoustics", S. Temkin, John Wiley & Sons Inc, New York (1981)
- [24] "General Relationships Between Ultrasonic Attenuation and Dispersion", M. O'Donnell, E. T. Jaynes, J. G. Miller, Journal of Acoustic Society America, vol. 63 issue 6 (1978), pp. 1935-1937
- [25] "Fundamental Physics of Ultrasound", V. Shutilov, G. Breach, New York (1988)

- [26] “Theoretical Acoustics”, P. Morse, K. Ingard, Princetown University Press, Princetown, NJ (1986)
- [27] ” Acoustic Waves: Devised Imaging and Analog Signal”, G. S. Kino, Prentice Hall, Englewood Cliffs (1987)
- [28] V. A. Grechishkin, L. G. Kazarian, I. Perepechko, *Akust. Zh.*, vol. 16 (1970), pp. 223
- [29] “The Measurement of Molecular Orientation in Fibers by Acoustic Methods”, W. W. Moseley, *Journal of Applied Polymer Science*, vol. 3 issue 9 (1960), pp. 266
- [30] “Mechanical and Sound Adsorption Properties of Cellular Poly (lacticacid) Matrix Composites Reinforced with 3D Ramie Fabrics Woven with Co-wrapped Yarns”, N. Zhou, X. Geng, M. Ye, L. Yao, Z. Shan, Y. Qiu, *Industrial Crops and Products*, vol. 56 (2014), pp. 1-8
- [31] “Investigation of the Crosslinking Behaviour of Ethylene Vinyl Acetate (EVA) for Solar Cell Encapsulation by Rheology and Ultrasound”, W. Stark, M. Jaunich, W. Bohmeyer, K. Lange, *Polymer Testing*, vol. 31 issue 7 (2012), pp. 904-908
- [32] “Determination of Ultrasonic-based Rheological Properties of Dough during Fermentation”, L. J. Pyrak-Nolte, S.G Lee, O. Campanella, *Journal of Texture Studies*, vol. 35 issue 1 (2004), pp. 33–51
- [33] “Shear Wave Propagation in Silica Aerogels at Ultrasonic Frequencies”, G. Álvarez-Arenas , *Forum Acusticum*, Sevilla, 2002
- [34] “An Ultrasound Imaging Method for in Vivo Tracheal Bulk and Young’s Moduli of Elasticity”, T. L. Miller, A. R. Altman, T. Tsud, T. H. Shaffer, *Journal of Biomechanics*, vol. 40 issue 7 (2007), pp. 1615-1621
- [35] “Fundamental Principles of Polymeric Materials 2nd Ed”, S. L. Rosen, Wiley (1993)
- [36] “Characterization of Blood Clot Viscoelasticity by Dynamic ultrasound Elastography and Modeling of the Rheological Behavior”, C. Schmitt, A. H. Henni, GuyCloutier, *Journal of Biomechanics*, vol. 44 issue 4 (2011), pp. 622-629

- [37] “Harmonic wave propagation through viscoelastic heterogeneous media exhibiting mild stochasticity I. Fundamental solutions”, G. D. Manolis, R. P. Shaw, *Soil Dynamics and Earthquake Engineering*, vol. 15 issue 2 (1996), pp. 119-127
- [38] “Monitoring the rheological properties and solid content of selected food materials contained in cylindrical cans using audio frequency sound waves”, B. Mert, Osvaldo H. Campanella, *Journal of Food Engineering*, vol. 79 issue 2 (2007), pp. 546-552
- [39] “The Wave Equation with Viscoelastic Attenuation and Its Application in Problems of Shallow Sea Acoustics”, P. S. Petrov, A. D. Zakharenko, M.Y. Trofimov, *Acoustical Physics*, vol. 58 issue 6 (2012), pp. 700-707
- [40] “Dynamics of Bubble Oscillation and Wave Propagation in Viscoelastic Liquids”, M. Ichihara, H. Ohkunitani, Y. Ida, M. Kameda, *Journal of Volcanology and Geothermal Research*, vol. 129 issue 1-3 (2004), pp. 37-60
- [41] “Collapse of Spherical Cavities in Viscoelastic Fluids”, H. S. Fogler, J. D. Goddard, *Physics of Fluids*, vol. 13 issue 5 (1970), pp. 1135-1141
- [42] “Propagation of Acoustic Waves in a Viscoelastic Two-phase System: Influence of Gas Bubble Concentration”, E. Marchetti, M. Ichihar, M. Ripepe, *Journal of Volcanology and Geothermal Research*, vol. 137 issue 1-3 (2004), pp. 93-108
- [43] “Theory of Viscoelasticity An Introduction”, R.M. Christensen, Academic Press Inc. (1982)
- [44] “Influence of Viscoelastic Properties on The Propagation of Small Amplitude Sound Waves”, O. C. Sotolongo, A.V. Vázquez, J. M. Antuna, *Brazilian Journal of Physics*, vol. 27 issue 3 (1997), pp. 379-383
- [45] “Theoretical and Experimental Investigation of Fluid Rheology Effects on Modulated Ultrasound Propagation”, O. Özkök, Y. Uludağ, *Journal of Ultrasonics*, vol. 54 issue 7 (2014), pp. 2034-2041
- [46] “Polymer Engineering Science and Viscoelasticity: An Introduction”, H. F. Brinson, L. C. Brinson, Springer (2008)
- [47] “Viscoelastic Properties of Polymers, 3rd Ed.”, J. D. Ferry, John Wiley & Sons (1980)

- [48] “Creep and Relaxation of Nonlinear Viscoelastic Materials with an Introduction to Linear Viscoelasticity”, W.N. Findley, J. S. Lai, K. Onaran, Dover Publications (1989)
- [49] “Transport Phenomena, Second Edition”, R.B. Bird, W.E. Stewart, E.N. Lightfoot, John Wiley & Sons (2002)
- [50] “Introduction to Polymer Viscoelasticity, 3rd Ed.”, M. T. Shaw, W. J. Macknight, John Wiley & Sons (2005)
- [51] “Unit Operations of Chemical Engineering, Seventh Edition”, W. L. McCabe, J. C. Smith, P. Harriott, McGraw Hill (2005)
- [52] “Dynamics of Polymeric Liquids Volume 1: Fluid Mechanics, 2nd Ed.”, R. B. Bird, R. C. Armstrong, O. Hassager, John Wiley& Sons (1987)
- [53] “Excess Molar Volume and Isentropic Compressibility for Binary or Ternary Ionic Liquid Systems”, Durban University of Technology, 2008, MS Thesis
- [54] “Simultaneously Measuring Thickness, Density, Velocity and Attenuation of Thin Layers Using  $V(z, t)$  Data From Time-resolved Acoustic Microscopy”, C. Jian, B. Xiaolong, Y. Keji, J. Bing-Feng, Journal of Ultrasonics, vol. 56 (2015), pp. 505-511
- [55] “Ultrasound for Defect Detection and Grading in Wood and Lumber”, M. E. Schafer, 2000 IEEE Ultrasonics Symposium Proceedings, vol. 1-2 (2000), pp.771-778
- [56] “Ultrasonic Characterization of Phase Morphology of High Density Polyethylene/Polyamide 6 Blend Melts”, S. Wang, C. Lin, H. Sun, F. Chen, J. Li, S. Guo, Polymer Engineering and Science, vol. 52 issue 2 (2012), pp. 338-345
- [57] “Liquid Propellant Handling, Transfer, and Storage”, P. M. Terlizzi, H. Streim, Industrial and Engineering Chemistry, vol. 48 issue 4 (1956), pp. 774-777
- [58] “Velocity of Sound as a Bond Property”, R. T. Langeman, J. E. Correy, Journal of Chemical Physics, vol.10 issue 12 (1942), pp. 759
- [59] “Dispersion of Sound Velocity in Some Alcohols”, G.R. Rendall, Indian Academy of Science, vol. 16 (1942), pp. 369-378
- [60] “A Theory of Liquid Structure”, H. Eyring, J. O. Hirschfelder, Journal of Chemical Physics, vol.5 (1937), pp. 896

- [61] “Compressibility of Liquid Mixtures Assuming Incompressible Cores”, P. Resa, L. Elvira, *Chemical Physics Letters*, vol. 481 issue 4-6 (2009), pp. 198-203
- [62] “Volumetric and Thermodynamic Studies of Molecular Interactions in Binary Liquid Mixtures of n-alkanes with Heptan-2-ol at 298.15 K: Comparison with Prigogin Flory-Patterson Theory”, A. R. Mahajan, S. R. Mirgane, *Chemical Engineering Communications*, vol. 200 issue 12 (2013), pp. 1666-1682
- [63] “Thermodynamic Study of Binary Liquid Mixture of Water and DMSO at T = 308.15 K”, H. Kumar, *International Journal of Chemical Science and Technology*, vol. 2 issue 1 (2012), pp. 1-8
- [64] “Theoretical Prediction of Speeds of Sound for Binary Mixtures of 2-methyl-1-propanol with n-alkanes at 298.15 K”, G. P. Dubey, M. Sharma, *International Journal of Science, Environment and Technology*, vol. 2 (2013), pp. 502-509
- [65] “Experimental and Theoretical Values of Sound Speeds and Viscosities for the Binary Systems of MTBE with Hydrocarbons”, K. V. N. S. Reddy, P. S. Rao, A. Krishnaiah, *Journal of Molecular Liquids*, vol. 135 issue 1-3 (2007), pp. 14-20
- [66] “Densities, Excess Molar Volumes, Ultrasonic Speeds, and Isentropic Compressibilities of Hexan-1-ol with 1,2-Dichloroethane, 1,2-Dibromoethane, and 1,1,2,2-Tetrachloroethane at (293.15 and 298.15) K”, S. C. Bhatia, R. Bhatia, G. P. Dubey, *International Journal of Thermodynamics*, vol. 31 issue 11 (2010), pp. 2119-2146
- [67] “Densities, Speeds of Sound and <sup>1</sup>H NMR Spectroscopic Studies for Binary Mixtures of 1-hexyl-3-methylimidazolium Based Ionic Liquids with Ethylene Glycol Monomethyl Ether at Temperature from T = (288.15–318.15) K”, A. Pal, B. Kumar, *Fluid Phase Equilibria*, vol. 334 (2012), pp. 157-165
- [68] “Theoretical Study of Ultrasonic Velocity in Binary Liquid Mixtures at 300 °C” B. Jacobson, *Acta Chem. Scand.* vol. 6 (1952), pp. 1485-1498
- [69] “Study of Molecular Interaction in Ternary Mixtures through Ultrasonic Speed Measurements”, W. Schaaffs, *Acoustica*, vol. 33 (1975), pp. 272-276
- [70] “Empirical formula for sound velocity in liquid mixtures”, O. Nomato, *J. Phys. Soc. Jpn.*, vol. 13 (1958), 1528

- [71] "Thermodynamic Properties and Velocity of Sound", W. Van Dael, Butterworth, London, Chap. 5 (1975)
- [72] "Theories of Ultrasonic Velocities and Their Application in Binary Liquid Mixtures of o-chlorophenol with Some Aliphatic Esters at Different Temperatures", G. R. Satyanarayana, K. B. Krishna, Der Pharma Chemica, vol.6 issue 5 (2014), pp. 158-165
- [73] "Thermodynamic Models for Industrial Applications From Classical and Advanced Mixing Rules to Association Theories", G. M. Kontogeorgis, G. K. Folas, Wiley (2010)
- [74] "The Thermodynamics of Phase and Reaction Equilibria", İ. Tosun, Elsevier (2002)
- [75] "A Consistent Correction for Redlich-Kwong-Soave Volumes", A. Peneloux, E. Rauzy, R. Freze, Fluid Phase Equilibria, vol. 8 issue 1 (1982), pp. 7-23
- [76] "Study of Densities, Viscosities, and Speeds of Sound of Binary Liquid Mixtures of butan-1-ol with n-alkanes (C6, C8 and C10) at T = (298.15, 303.15 and 308.15) K", G.P. Dubey, M. Sharma, N. Dubey, Journal of Chemical Thermodynamics, vol. 40 issue 2 (2008), pp. 309-320
- [77] "Excess Volumes for n-alkanols + n-alkanes II. Binary Mixtures of n-pentanol, n-hexanol, n-octanol, and n-decanol + n-heptane", A. J. Treszczanowicz, G. C. Benson, Journal of Chemical Thermodynamics, vol. 10 issue 10 (1978), pp. 967-974
- [78] "Ultrasonic Speeds and Isentropic Compressibilities of n-alkanol + n-heptane Mixture at 298.15 K", O. Kiyohara, G. C. Benson, Journal of Chemical Thermodynamics, vol. 11 issue 9 (1979), pp. 861-873
- [79] "Acoustic Spectroscopy for Concentrated Polydisperse Colloids with High Density Contrast", A. S. Dukhin, P. J. Goetz, Langmuir, vol. 12 issue 21 (1996), pp. 4987-4997
- [80] "Principles of Ultrasonic Droplet Size Determination in Emulsions", D. J. McClements, Langmuir, vol. 12 issue 14 (1996), pp. 3454-3461
- [81] "Particle Sizing in Dense Two-phase Droplet Systems by Ultrasonic Attenuation and Velocity Spectra", S. MingXu, M. Xue, Science in China, vol. 52 issue 6 (2009), pp. 1502-1510
- [82] "A Sound Velocity Method for Determining the Compressibility of Finely Divided Substances", R.J. Urick, Journal of Applied Physisc, vol. 18 issue 11 (1947), pp. 983

- [83] “Hydrodynamics, 6th edition”, H. Lamb, sections 361-363, Dover Publications, New York, (1945)
- [84] “Sound Propagation in Composite Media” R.J. Urick, W.S. Ament, Journal of Acoustical Society of America, vol. 21 issue 2 (1949), pp. 115-119
- [85] “The Fundamentals of Particle Size Analysis by Means of Ultrasonic Spectrometry”, U. Riebel, F. Uffler, Journal of Particle & Particle Systems Characterization, vol. 6 issue 1-4 (1989), pp. 135-143
- [86] “Velocity and Attenuation of Ultrasound in Suspensions of Particles in Fluids”, A. H. Harker, J. A. G. Temple, Journal of Physics, vol. 21 issue 11 (1987), pp. 1576-1588
- [87] “Attenuation of Sound in Suspensions and Emulsions: Theory and Experiments”, J. R. Allegra, S. A. Hawley, Journal of Acoustical Society of America, vol. 51 issue 5 (1972), pp. 1545-1564
- [88] “Broadband Study of the Scattering of Ultrasound by Polystyrene-latex-in-Water Suspensions” U. Kaatze, C. Tiachimow, R. Pottel, M. Brai, Annalen der Physik, vol. 5 (1996), pp. 13-33
- [89] “Particle Size Characterization by Ultrasonic Attenuation Spectra”, S. MingXu, M. Xue, X. Cai, Z. Shang, F. Xu, Particuology, vol. 6 issue 4 (2008), pp. 276-281
- [90] “Ultrasonic Wave Propagation in Colloidal Suspensions and Emulsions: A Comparison of Four Models”, J.S. Tebbutt, R.E. Challis, Ultrasonics, vol. 34 issue 2-5 (1996), pp. 363-368
- [91] “The Fundamentals of Particle Size Analysis by Means of Ultrasonic Spectrometry”, U. Riebel, F. Löffler, Particle & Particle System Characterization, vol. 6 issue 1-4 (1989), pp. 135-143.
- [92] “Viscous Attenuation of Acoustic Waves in Suspensions”, R. L. Gibson, M. N. Toksoz, Journal of Acoustical Society of America, vol. 85 issue 5 (1989), pp. 1925-1934.
- [93] “Mean Value and Correlation Problems connected with the Motion of Small Particles Suspended in a Turbulent Fluid”, C. Tchen, PhD Thesis, University of Delft (1947)
- [94] “A Treatise on Hydrodynamics with Numerous Examples”, A. B. Basset, Dover Publications, New York (1988)

- [95] “On the Discontinuity of Arbitrary Constants which Appear in Divergent Developments”, G.G. Stokes, Transactions Cambridge Philosophical Society, 1851, pp. 105-129
- [96] “Note on the Numerical Solutions of Integro-differential Equations” , J. T. Day, The Computer Journal, Wisconsin (1967)
- [97] “Investigation of Fluid Rheology Effects on Ultrasound Propagation”, O. Özkök, METU, 2012, M.Sc. Thesis
- [98] “The Theory of Elasticity”, L. D. Landau, E. M. Lifshits, Pergamon Press, Moscow (1965)
- [99] DOP2000 Model 2125/2032 User’s Manual, Signal Processing S.A. Switzerland
- [100] ARES G2 Rheometer User’s Manual, TA Instruments
- [101] Mastersizer 2000, User’s Manual, Malvern



## APPENDIX

### A1. Linear Viscoelastic Models

#### Maxwell Model

Maxwell model is one of the most straightforward viscoelastic constitutive models. It contains serially joined spring and dashpot elements (Figure A1.1) [35].

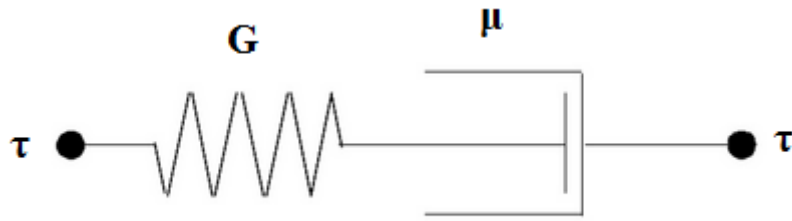


*Figure A1.0.1 Spring-dashpot Representation of Maxwell Model*

In Maxwell Model, the spring and dashpot undergo the same stress;

$$\tau = \tau_{\text{spring}} = \tau_{\text{dashpot}} \quad \text{eqn. A1.1}$$

Moreover, the total strain is obtained by adding the strains on the spring and dashpot;

$$\gamma = \gamma_{\text{spring}} + \gamma_{\text{dashpot}} \quad \text{eqn. A1.2}$$

Taking the derivative with respect to time;

$$\dot{\gamma} = \dot{\gamma}_{\text{spring}} + \dot{\gamma}_{\text{dashpot}} \quad \text{eqn. A1.3}$$

Note that,  $\dot{\gamma}_{\text{dashpot}} = \tau_{yx} / \mu$  and  $\dot{\gamma}_{\text{spring}} = \tau_{yx} / G$ , inserting them in to eqn. A1.3 gives the

Maxwell model as;

$$\tau_{yx} + \frac{\mu}{G} \frac{\partial \tau_{yx}}{\partial t} = -\mu \dot{\gamma}_{yx} \quad \text{eqn. A1.4}$$

In addition, the ratio  $\mu / G$  in eqn. A1.4 gives stress relaxation time and can be designated as  $\tau_0$  and changing  $\mu$  with  $\eta_0$ , the eqn. A1.4 will become;

$$\tau_{yx} + \lambda \frac{\partial \tau_{yx}}{\partial t} = -\eta_0 \dot{\gamma}_{yx} \quad \text{eqn. A1.5}$$

To analyze the stress relaxation behavior, differential eqn. A1.5 can be solved for constant strain,  $\gamma_0$ . Hence, eqn. A1.1 becomes;

$$\tau_{yx}(t) = \tau_0 e^{-t/\lambda} = \gamma_0 G e^{-t/\lambda} = \gamma_0 G(t) \quad \text{eqn. A1.6}$$

### **Voigt-Kelvin Model**

In Voigt-Kelvin Model, spring and dashpot are adopted as in parallel (Figure A1.2). Hence, the strain endured by the dashpot and the spring are same [35];

$$\gamma = \gamma_{\text{spring}} = \gamma_{\text{dashpot}} \quad \text{eqn. A1.7}$$

So, the total stress on the material is the addition of the stress on the spring with the stress on the dashpot.

$$\tau = \tau_{\text{spring}} + \tau_{\text{dashpot}} \quad \text{eqn. A1.8}$$

Combining eqn. A1.7 and A1.8 gives the governing differential equation for Voigt-Kelvin model.

$$\tau_{yx} = \eta_0 \frac{\partial \gamma_{yx}}{\partial t} + G \gamma_{yx} \quad \text{eqn. A1.9}$$

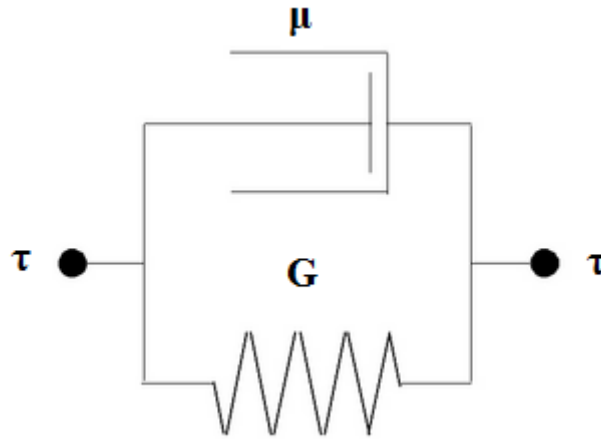


**Figure A1.0.2** Spring-dashpot Representation of Voigt-Kelvin Model

Creep behavior can be investigated by solving differential eqn. A1.9 with constant shear stress,  $\tau_0$ . Then, it is obtained that [35];

$$\gamma_{yx}(t) = \frac{\tau_0}{G}(1 - e^{-t/\lambda}) = \tau_0 J(t) \quad \text{eqn. A1.10}$$

To analyze creep recovery, stress is removed. Hence, strain decreases with time according to the following relation;

$$\gamma_{yx}(t) = \frac{\tau_0}{G} e^{-t/\lambda} \quad \text{eqn. A1.11}$$

### The Jeffreys Model

Maxwell model can be extended by adding time derivative of rate of strain to obtain a more accurate model. By this way Jeffreys model is obtained such that;

$$\tau + \lambda_1 \frac{\partial}{\partial t} \tau = -\eta_0 \left( \dot{\gamma} + \lambda_2 \frac{\partial}{\partial t} \dot{\gamma} \right) \quad \text{eqn. A1.12}$$

Here,  $\lambda_1$  indicates the relaxation time and  $\lambda_2$  is the retardation time. It should also be noted that addition of higher time derivatives of stress and rate of strain by suitable constants as multipliers more precise models can be obtained.

## Generalized Models and Spectra

The rheological behavior of viscoelastic materials may not only be governed by a single kinetic element. There may be many contributions of different kinetic elements due to the complexity of the structure of the material. To illustrate, branches of polymer and different chain lengths may exhibit different relaxation behavior. Hence, each kinetic element presents its relaxation behavior separately. To include all the rheological behaviors generalized models can be used. Suppose that rheological behavior of a viscoelastic material is governed by “n” kinetic elements. Each of them has different characteristic times [5]. This situation can be expressed by Generalized Maxwell Model by adding “n” Maxwell elements in parallel such that;

$$\tau_{yx}(t) = \sum_{i=1}^n \tau_{yx,i}(t) = \gamma_0 \sum_{i=1}^n G_i e^{-t/\lambda_i} \quad \text{eqn. A1.13}$$

If “n” Voigt-Kelvin elements are serially connected, Generalized Voigt-Kelvin Model is obtained;

$$\gamma_{yx}(t) = \sum_{i=1}^n \frac{\tau_0}{G_i} (1 - e^{-t/\lambda_i}) \quad \text{eqn. A1.14}$$

If the numbers of characteristic times are increased to infinity in generalized models, a continuous distribution of characteristic times with respect to modulus is obtained. These distributions are known as the relaxation or retardation spectra. A detailed work on obtaining spectra by ultrasonic methods is done in our previous study [97].

## A2. Derivation of Loss and Storage Modulus in Terms of Acoustic Parameters

The governing differential equation for the longitudinal sound wave propagation in elastic medium can be written as;

$$\rho \frac{\partial^2 \mathbf{u}}{\partial t^2} = \left[ \mathbf{K} + \frac{4}{3} \mathbf{G} \right] \frac{\partial^2 \mathbf{u}}{\partial x^2} \quad \text{eqn. A2.1}$$

Assuming that “u” is proportional with  $\exp\{i\omega t - \alpha x\}$ , and inserting this into the eqn. A2.1;

$$V^2 = \frac{\mathbf{K} + \frac{4}{3} \mathbf{G}}{\rho} \quad \text{eqn. A2.2}$$

where V is the longitudinal sound wave velocity in eqn. A2.2. Complex modulus has already been defined in eqn. 1.5 as;

$$M^* = M' + iM'' \quad \text{eqn. 1.5}$$

Assuming “u” is proportional with  $\exp\{i\omega t - (\alpha + i\omega/V)x\}$ , the relation between M', M'' and  $\alpha$ , V can be obtained.

Separating the imaginary and real parts of the M, it is found that;

$$M' = \frac{\rho c^2 \left[ 1 - \left( \frac{\alpha \lambda}{2\pi} \right)^2 \right]}{\left[ 1 + \left( \frac{\alpha \lambda}{2\pi} \right)^2 \right]^2} \quad \text{eqn. A2.3}$$

$$M'' = \frac{2\rho c^2 \frac{\alpha \lambda}{2\pi}}{\left[ 1 + \left( \frac{\alpha \lambda}{2\pi} \right)^2 \right]^2} \quad \text{eqn. A2.4}$$

In addition the value of “ $\frac{\alpha\lambda}{2\pi}$ ” is usually very low with respect to 1. Hence, further simplifications on the eqns. A2.3 and A2.4 give that;

$$M' = \rho V^2 \quad \text{eqn. A2.5}$$

$$M'' = \frac{2\rho V^3 \alpha}{w} \quad \text{eqn. A2.6}$$

### A3. Obtaining the Governing Differential Equations Used in the Characterization of Viscoelasticity

Considering the longitudinal sound wave propagation in isotropic heat conducting viscoelastic medium; conservation of mass, momentum and energy equations reduces to;

$$\frac{\partial \rho}{\partial t} + \rho \frac{\partial v_x}{\partial x} = 0 \quad \text{eqn. A3.1}$$

$$\rho \frac{\partial^2 \mathbf{u}}{\partial t^2} - \frac{\partial \sigma_{xx}}{\partial x} = 0 \quad \text{eqn. A3.2}$$

$$\rho C_v \frac{\partial T}{\partial t} - \frac{T \alpha_v}{\rho} K_T \frac{\partial \rho}{\partial t} = - \frac{\partial q_x}{\partial x} \quad \text{eqn. A3.3}$$

For the velocity of particles of the medium;

$$v = \frac{du}{dt} \quad \text{eqn. A3.4}$$

To solve the systems of differential equations simultaneously, it is essential to express the stress tensor. The stress tensor for an isotropic viscoelastic media can be written as [98];

$$\bar{\sigma}_{ik} = \sigma_{ik} + \sigma_{ik}' \quad \text{eqn. A3.5}$$

where  $\sigma_{ik}$  = stress tensor of elastic solid

and  $\sigma_{ik}'$  = dissipative stress tensor

For bodies under elastic deformation, the stress tensor can be formulated by;

$$\sigma_{ik} = \left( \frac{\partial A}{\partial u_{ik}} \right)_T \quad \text{eqn. A3.6}$$

where A = Helmholtz free energy

$u_{ik}$  = strain tensor

For small deformations strain tensor is determined by;

$$\mathbf{u}_{ik} = \frac{1}{2} \left( \frac{\partial \mathbf{u}_i}{\partial x_k} + \frac{\partial \mathbf{u}_k}{\partial x_i} \right) \quad \text{eqn. A3.7}$$

It can also be written as;

$$\mathbf{u}_{ik} = \left( \mathbf{u}_{ik} - \frac{1}{3} \delta_{ik} \mathbf{u}_{ll} \right) + \frac{1}{3} \delta_{ik} \mathbf{u}_{ll} \quad \text{eqn. A3.8}$$

Helmholtz free energy as a function of temperature can be written as;

$$A(T) = A_0(T) - K_T \alpha_v (T - T_0) \mathbf{u}_{ll} + G \left( \mathbf{u}_{ik} - \frac{1}{3} \delta_{ik} \mathbf{u}_{ll} \right)^2 + \frac{K_T}{2} \mathbf{u}_{ll}^2 \quad \text{eqn. A3.9}$$

Inserting into eqn. A3.6;

$$\sigma_{ik} = -K_T \alpha_v (T - T_0) \delta_{ik} + K_T \mathbf{u}_{ll} \delta_{ik} + 2G \left( \mathbf{u}_{ik} - \frac{1}{3} \delta_{ik} \mathbf{u}_{ll} \right) \quad \text{eqn. A3.10}$$

Hence;

$$\sigma_{xx} = -K_T \alpha_v (T - T_0) + \left( K_T + \frac{4}{3} G \right) \frac{\partial \mathbf{u}_x}{\partial x} \quad \text{eqn. A3.11}$$

The term  $\left( K_T + \frac{4}{3} G \right)$  can also be expressed as longitudinal modulus, L.

#### A4. Interpretation of Experimental Measurements with the Model Developed

Loss and storage components of longitudinal modulus can also be calculated once acoustic parameters are obtained (eqns. 1.13 and 1.14). Hence, it can be written that;

$$\frac{\rho c^2 \left[ 1 - \left( \frac{\alpha \lambda}{2\pi} \right)^2 \right]}{\left[ 1 + \left( \frac{\alpha \lambda}{2\pi} \right)^2 \right]^2} = \frac{\eta_p \lambda_1 w^2}{1 + (\lambda_1 w)^2} \quad \text{eqn. A4.1}$$

and

$$\frac{2\rho c^2 \frac{\alpha \lambda}{2\pi}}{\left[ 1 + \left( \frac{\alpha \lambda}{2\pi} \right)^2 \right]^2} = \eta_s w + \frac{\eta_p w}{1 + (\lambda_1 w)^2} \quad \text{eqn. A4.2}$$

Since, we may not know the density of the material, we can eliminate the density by dividing eqn. A4.2 to eqn. A4.1. It is obtained that;

$$\frac{\frac{\alpha \lambda}{\pi}}{1 - \left( \frac{\alpha \lambda}{2\pi} \right)^2} = \frac{1}{\lambda_1 w} + \frac{\eta_s (1 + (\lambda_1 w)^2)}{\eta_p \lambda_1 w^2} \quad \text{eqn. A4.3}$$

Hence,  $\lambda_1$ ,  $\eta_s$  and  $\eta_p$  can be calculated once the attenuation and sound speed is measured. Mathematical model is instrumental for determination of  $\lambda_2$ . The equation for the sound pressure is already modeled as;

$$P = \sum_{j=0}^m P_{0k} e^{-\sigma x} [e^{i\omega t} H(t - (t_1 + j(n+a))) - e^{i\omega t} H(t - (t_1 + (j+1)n + ja))] + e^{i\omega(t_1 + (j+1)n + ja)} H(t - (t_1 + (j+1)n + ja)) \frac{\exp\left(-\frac{(t - (t_1 + (j+1)n + ja))}{\lambda_2}\right) \frac{1}{(-\lambda_2 P_{0k} + 1)}}{1 + \exp\left(-\frac{(t - (t_1 + (j+1)n + ja))}{\lambda_2}\right) \frac{P_{0k}}{(-\lambda_2 P_{0k} + 1)} \lambda_2} \quad \text{eqn. A4.4}$$

Suppose that the time is  $t = t_1 + mn + ma$  (just before the beginning of the  $m^{\text{th}}$  wave)

Then, the equation takes the form;

$$P = \sum_{j=0}^{m-1} P_{0k} e^{-\sigma x} \left( e^{i\omega(t_1 + (j+1)n + ja)} \mathbf{H}(t - (t_1 + (j+1)n + ja)) \frac{\exp\left(-\frac{(t - (t_1 + (j+1)n + ja))}{\lambda_2}\right) \frac{1}{(-\lambda_2 P_{0k} + 1)}}{1 + \exp\left(-\frac{(t - (t_1 + (j+1)n + ja))}{\lambda_2}\right) \frac{P_{0k}}{(-\lambda_2 P_{0k} + 1)} \lambda_2} \right)$$

eqn.A4.5

To simplify the case, take  $m=3$  and  $t_1=0$ , then;

$$\frac{P}{P_{0k}} = e^{-\sigma x} \left( e^{i\omega n} \frac{\exp\left(-\frac{2n+3a}{\lambda_2}\right) \frac{1}{(-\lambda_2 P_{0k} + 1)}}{1 + \exp\left(-\frac{2n+3a}{\lambda_2}\right) \frac{1}{(-\lambda_2 P_{0k} + 1)} \lambda_2} + e^{i\omega(2n+a)} \frac{\exp\left(-\frac{n+2a}{\lambda_2}\right) \frac{1}{(-\lambda_2 P_{0k} + 1)}}{1 + \exp\left(-\frac{n+2a}{\lambda_2}\right) \frac{1}{(-\lambda_2 P_{0k} + 1)} \lambda_2} + e^{i\omega(3n+2a)} \frac{\exp\left(-\frac{a}{\lambda_2}\right) \frac{1}{(-\lambda_2 P_{0k} + 1)}}{1 + \exp\left(-\frac{a}{\lambda_2}\right) \frac{1}{(-\lambda_2 P_{0k} + 1)} \lambda_2} \right)$$

eqn. A4.6

Let's take  $\exp(-a/\lambda_2)$  to out of parenthesis.

$$\frac{P}{P_{0k}} = e^{-\frac{a}{\lambda_2}} \left( e^{iwn-\sigma x} \frac{\exp\left(-\frac{2n+2a}{\lambda_2}\right) \frac{1}{(-\lambda_2 P_{0k} + 1)}}{1 + \exp\left(-\frac{2n+3a}{\lambda_2}\right) \frac{1}{(-\lambda_2 P_{0k} + 1)} \lambda_2} + e^{iw(2n+a)-\sigma x} \frac{\exp\left(-\frac{n+a}{\lambda_2}\right) \frac{1}{(-\lambda_2 P_{0k} + 1)}}{1 + \exp\left(-\frac{n+2a}{\lambda_2}\right) \frac{1}{(-\lambda_2 P_{0k} + 1)} \lambda_2} + e^{iw(3n+2a)-\sigma x} \frac{\frac{1}{(-\lambda_2 P_{0k} + 1)}}{1 + \exp\left(-\frac{a}{\lambda_2}\right) \frac{1}{(-\lambda_2 P_{0k} + 1)} \lambda_2} \right) \quad \text{eqn. A4.7}$$

Taking the natural logarithm of both sides;

$$\ln\left(\frac{P}{P_{0k}}\right) = -\frac{a}{\lambda_2} + \ln \left( e^{iwn-\sigma x} \frac{\exp\left(-\frac{2n+2a}{\lambda_2}\right) \frac{1}{(-\lambda_2 P_{0k} + 1)}}{1 + \exp\left(-\frac{2n+3a}{\lambda_2}\right) \frac{1}{(-\lambda_2 P_{0k} + 1)} \lambda_2} + e^{iw(2n+a)-\sigma x} \frac{\exp\left(-\frac{n+a}{\lambda_2}\right) \frac{1}{(-\lambda_2 P_{0k} + 1)}}{1 + \exp\left(-\frac{n+2a}{\lambda_2}\right) \frac{1}{(-\lambda_2 P_{0k} + 1)} \lambda_2} + e^{iw(3n+2a)-\sigma x} \frac{\frac{1}{(-\lambda_2 P_{0k} + 1)}}{1 + \exp\left(-\frac{a}{\lambda_2}\right) \frac{1}{(-\lambda_2 P_{0k} + 1)} \lambda_2} \right) \quad \text{eqn. A4.8}$$

or in general form;

$$\ln \frac{P}{P_{0k}} = -\frac{a}{\tau} + \ln \left[ \sum_{j=0}^{m-1} K_j \frac{\exp\left(-\frac{[(m-1)-j](n+a)}{\lambda_2}\right) \frac{1}{(-\lambda_2 P_{0k} + 1)}}{1 + \exp\left(-\frac{[(m-1)-j]n + (m-j)a}{\lambda_2}\right) \frac{1}{(-\lambda_2 P_{0k} + 1)} \lambda_2} \right]$$

eqn. A4.9

where

$$K_j = e^{-\sigma x} e^{iw(t_1 + (j+1)n + ja)} \quad \text{eqn. A4.10}$$

Taking the derivative with respect to “a”;

$$\begin{aligned} \frac{d}{da} \left( \ln \frac{P}{P_{0k}} \right) &= -\frac{1}{\tau_1} + \left[ \sum_{j=0}^{m-1} K_j \frac{\exp\left(-\frac{[(m-1)-j](n+a)}{\lambda_2}\right) \frac{1}{(-\lambda_2 P_{0k} + 1)}}{1 + \exp\left(-\frac{[((m-1)-j)n + (m-j)a]}{\lambda_2}\right) \frac{1}{(-\lambda_2 P_{0k} + 1) \lambda_2}} \right]^{-1} \\ &\left[ \sum_{j=0}^{m-1} K_j \frac{\exp\left(-\frac{[(m-1)-j](n+a)}{\lambda_2}\right) \frac{1}{(-\lambda_2 P_{0k} + 1)}}{1 + \exp\left(-\frac{[((m-1)-j)n + (m-j)a]}{\lambda_2}\right) \frac{1}{(-\lambda_2 P_{0k} + 1) \lambda_2}} \left(-\frac{1}{\lambda_2}\right) \right. \\ &+ \frac{\exp\left(-\frac{[(m-1)-j](n+a)}{\lambda_2}\right) \frac{1}{(-\lambda_2 P_{0k} + 1)}}{\left(1 + \exp\left(-\frac{[((m-1)-j)n + (m-j)a]}{\lambda_2}\right) \frac{1}{(-\lambda_2 P_{0k} + 1) \lambda_2}\right)^2} \exp\left(-\frac{[((m-1)-j)n + (m-j)a]}{\lambda_2}\right) \\ &\left. + jK_j \frac{\exp\left(-\frac{[(m-1)-j](n+a)}{\lambda_2}\right) \frac{1}{(-\lambda_2 P_{0k} + 1)}}{1 + \exp\left(-\frac{[((m-1)-j)n + (m-j)a]}{\lambda_2}\right) \frac{1}{(-\lambda_2 P_{0k} + 1) \lambda_2}} \right] \end{aligned}$$

$$\text{eqn. A4.11}$$

The second term in the right hand side of the equation corresponds to superposition of recovery terms growing in number at the end of each signal. Here, if “n” is taken sufficiently large, all of the recovery terms except the final one become negligibly small, so second term in the equation goes to zero, then the equation reduces to;

$$\frac{d}{da} \left( \ln \frac{P}{P_{0k}} \right) \cong -\frac{1}{\tau_2} \quad \text{eqn. A4.12}$$

Eqn. A4.12 can be used to obtain relaxation time of a viscoelastic solution through modulated ultrasound pulse measurements.

## A5. CMC/water Solutions Rheological Data

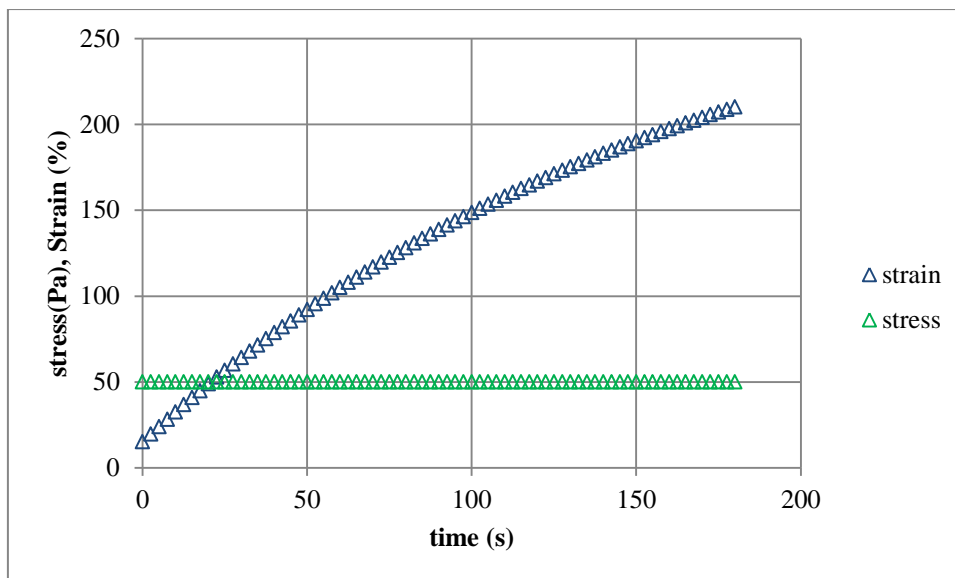


*Figure A5.1 CMC/water Stress/strain Data (2 wt.%)*

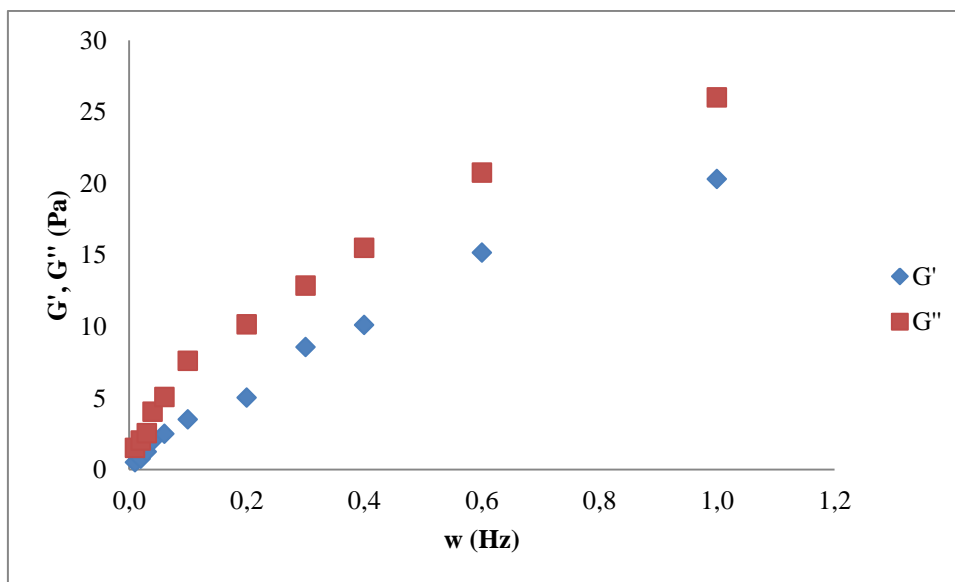


*Figure A5.2 CMC/water Loss/Storage Modulus (2 wt.%)*

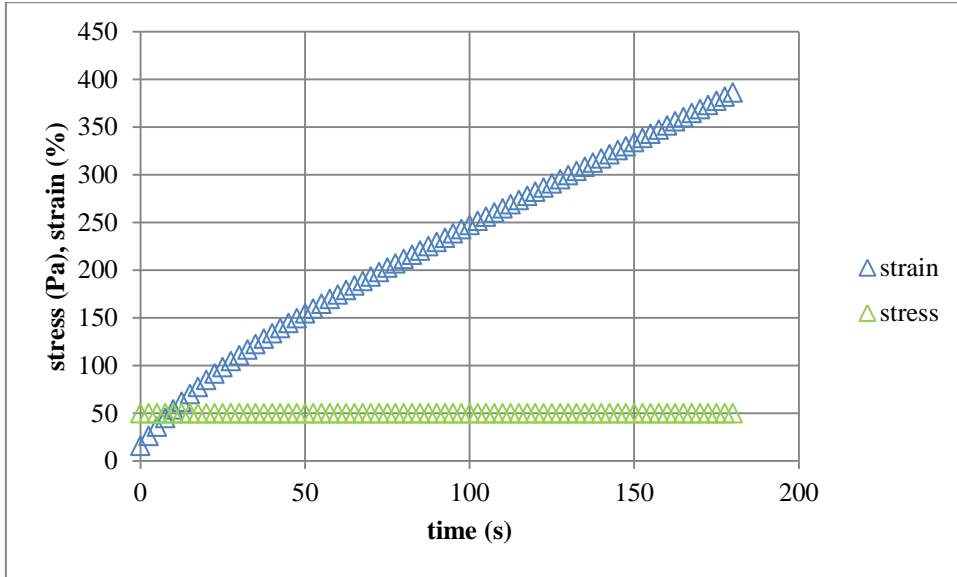


*Figure A5.3 CMC/water Stress/strain Data (3 wt.%)*

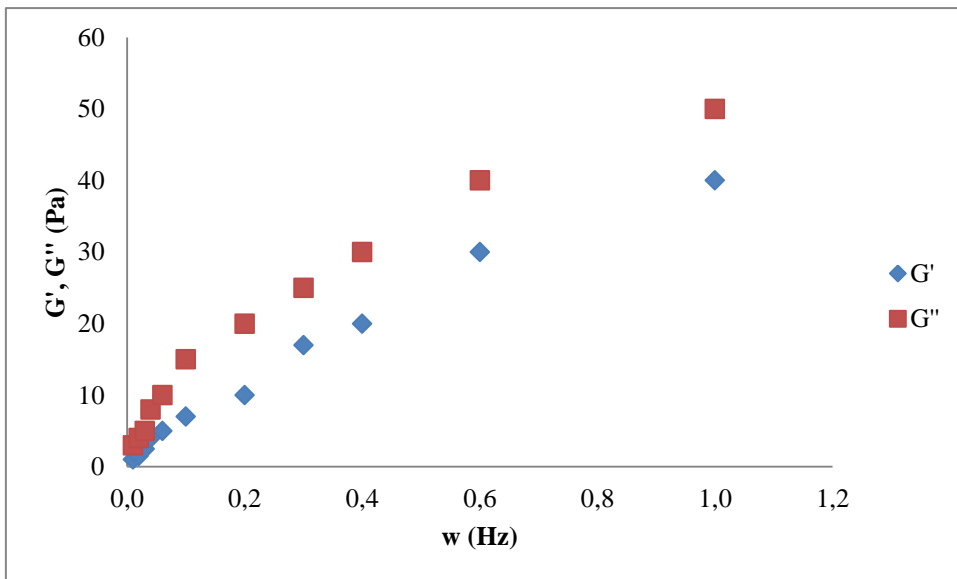


*Figure A5.4 CMC/water Loss/Storage Modulus (3 wt.%)*

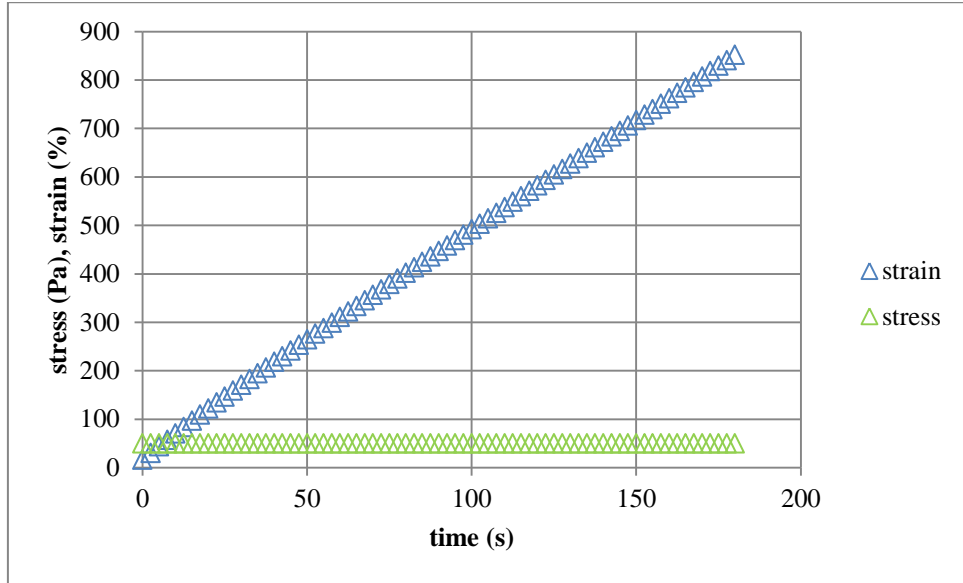


*Figure A5.5 CMC/water Stress/strain Data (4 wt.%)*

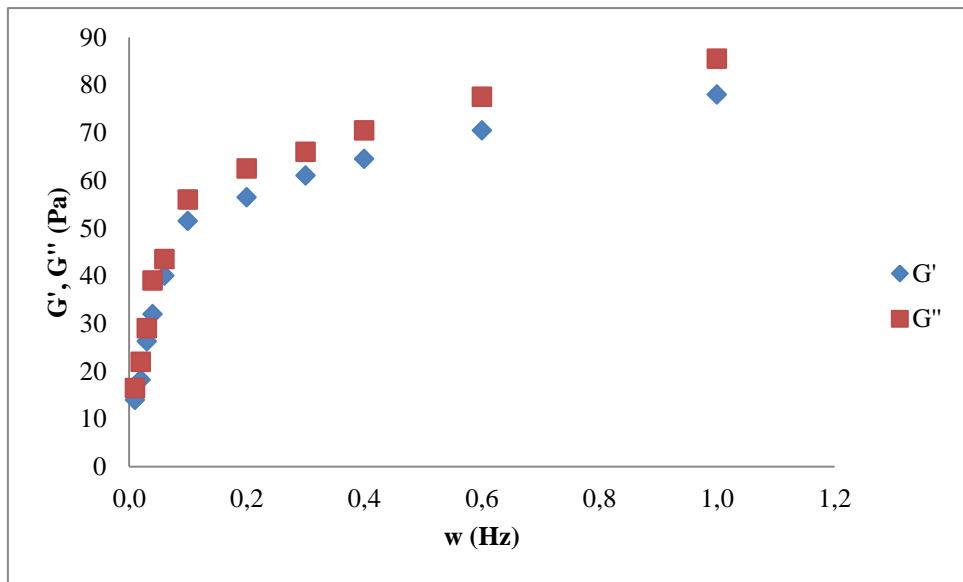


*Figure A5.6 CMC/water Loss/Storage Modulus (4 wt.%)*

## A6. Review of Cubic Equation of States

The pressures are depicted as  $P = P(\tilde{V}, T)$  in cubic equation of states. The most common ones are given in the Table A6.1 [74].

*Table A6.1 Cubic Equation of States*

Equation	P	a	b
Van der Waals	$\frac{RT}{\tilde{V}-b} - \frac{a}{\tilde{V}^2}$	$\frac{27}{64} \left( \frac{R^2 T_c^2}{P_c} \right)$	$\frac{1}{8} \left( \frac{RT_c}{P_c} \right)$
Redlich-Kwong	$\frac{RT}{\tilde{V}-b} - \frac{a}{\tilde{V}(\tilde{V}+b)\sqrt{T}}$	$0.42748 \left( \frac{R^2 T_c^{2.5}}{P_c} \right)$	$0.08664 \left( \frac{RT_c}{P_c} \right)$
Soave-Redlich-Kwong	$\frac{RT}{\tilde{V}-b} - \frac{a}{\tilde{V}(\tilde{V}+b)}$	$0.42748 \left( \frac{R^2 T_c^2}{P_c} \right) \alpha$	$0.08664 \left( \frac{RT_c}{P_c} \right)$
Peng-Robinson	$\frac{RT}{\tilde{V}-b} - \frac{a}{\tilde{V}(\tilde{V}+b) + b(\tilde{V}-b)}$	$0.45724 \left( \frac{R^2 T_c^2}{P_c} \right) \alpha$	$0.07780 \left( \frac{RT_c}{P_c} \right)$

Cubic equations of states are commonly applied in thermodynamics. Since, they can be used in broad temperature and pressure interval. Additionally, they are able to identify materials in both vapor and liquid phases. Soave-Redlich-Kwong and Peng-Robinson are mostly used ones. The name cubic comes from that they are in the third degree in molar volume such that;

$$\tilde{V}^3 + c_1 \tilde{V}^2 + c_2 \tilde{V} + c_3 = 0 \quad \text{eqn. A6.1}$$

In Table A6.1, first terms are same ( $RT/(\tilde{V}-b)$ ) and they describe the repulsive forces between molecules. Second terms are defining the attractive forces between molecules. “a” and “b” are depicting the attractive forces and volume of the molecules, respectively. Parameter “ $\alpha$ ” is temperature dependent equation of state variable and defines as;

$$\alpha = \left[ 1 + (0.480 + 1.574\omega - 0.176\omega^2) (1 - \sqrt{T_r}) \right]^2 \quad \text{(Soave-Redlich-Kwong) eqn. A6.2}$$

$$\alpha = \left[ 1 + (0.37464 + 1.54226\omega - 0.26992\omega^2) (1 - \sqrt{T_r}) \right]^2 \quad (\text{Peng-Robinson}) \quad \text{eqn. A6.3}$$

At a specified T and P, eqn. A6.1 has three roots. When  $T > T_c$ , the root greater than “b” is the only acceptable root and other are complex numbers. For the case when  $T < T_c$ , smallest and largest root are the roots for molar volumes of saturated liquid and vapor, respectively.

Eqn. A6.1 can also be defined in terms of compressibility factors Z such that,

$$Z^3 + pZ^2 + qZ + r = 0 \quad \text{eqn. A6.4}$$

Parameters “p”, “q” and r calculations are shown in Table A6.2;

*Table A6.2 Equations to Calculate “p”, “q” and “r”*

Equation	p	q	r
Van der Waals	-1-B	A	-AB
Redlich-Kwong	-1	A-B-B <sup>2</sup>	-AB
Soave-Redlich-Kwong	-1	A-B-B <sup>2</sup>	-AB
Peng-Robinson	-1+B	A-2B-3B <sup>2</sup>	-AB+B <sup>2</sup> +B <sup>3</sup>

where;

$$B = \frac{bP}{RT}$$

$$A = \frac{aP}{(RT)^2} \quad \text{for van der Waals, Soave-Redlich-Kwong, Peng-Robinson}$$

$$A = \frac{aP}{R^2 T^{2.5}} \quad \text{for Redlich-Kwong}$$

Cubic equation of states can also be used for estimating properties of mixtures. For this purpose, equations in Table A6.1 should be modified with mixture properties such that (Table A6.3);

**Table A6.3 Cubic Equation of States for Mixtures**

Equation	P	a <sub>ii</sub>	b <sub>i</sub>
Van der Waals	$\frac{RT}{\tilde{V}_{mix} - b_{mix}} - \frac{a_{mix}}{\tilde{V}_{mix}^2}$	$\frac{27}{64} \left( \frac{R^2 T_{c_i}^2}{P_{c_i}} \right)$	$\frac{1}{8} \left( \frac{RT_{c_i}}{P_{c_i}} \right)$
Redlich-Kwong	$\frac{RT}{\tilde{V}_{mix} - b_{mix}} - \frac{a_{mix}}{\tilde{V}_{mix} (\tilde{V}_{mix} + b_{mix}) \sqrt{T}}$	$0.42748 \left( \frac{R^2 T_{c_i}^{2.5}}{P_{c_i}} \right)$	$0.08664 \left( \frac{RT_{c_i}}{P_{c_i}} \right)$
Soave-Redlich-Kwong	$\frac{RT}{\tilde{V}_{mix} - b_{mix}} - \frac{a_{mix}}{\tilde{V}_{mix} (\tilde{V}_{mix} + b_{mix})}$	$0.42748 \left( \frac{R^2 T_{c_i}^2}{P_{c_i}} \right) \alpha_i$	$0.08664 \left( \frac{RT_{c_i}}{P_{c_i}} \right)$
Peng-Robinson	$\frac{RT}{\tilde{V}_{mix} - b_{mix}} - \frac{a_{mix}}{\tilde{V}_{mix} (\tilde{V}_{mix} + b_{mix}) + b_{mix} (\tilde{V}_{mix} - b_{mix})}$	$0.45724 \left( \frac{R^2 T_{c_i}^2}{P_{c_i}} \right) \alpha_i$	$0.07780 \left( \frac{RT_{c_i}}{P_{c_i}} \right)$

“a<sub>ii</sub>” and “b<sub>ii</sub>” are the parameters for individual components. Mixture parameters can be calculated by van der Waals mixing rule such that;

$$a_{mix} = \sum_{i=1}^k \sum_{j=1}^k x_i x_j a_{ij} \quad \text{eqn. A6.5}$$

$$b_{mix} = \sum_{i=1}^k \sum_{j=1}^k x_i x_j b_{ij} \quad \text{eqn. A6.6}$$

Unlike parameters a<sub>ij</sub> and b<sub>ij</sub> can be calculated by;

$$a_{ij} = (1 - k_{ij}) \sqrt{a_{ii} a_{jj}} \quad k_{ij} = k_{ji}$$

$$b_{ij} = \frac{b_i + b_j}{2}$$

Where k<sub>ij</sub> is adjustable binary interaction parameter.

Parameters α<sub>i</sub> are also calculated for individual component. Equation for compressibility takes the form of;

$$Z_{\text{mix}}^3 + pZ_{\text{mix}}^2 + qZ_{\text{mix}} + r = 0 \quad \text{eqn. A6.7}$$

The parameters “p”, “q” and “r” are calculated for mixtures properties as in Table A6.3 .  
However,  $A_{\text{mix}}$  and  $B_{\text{mix}}$  should be used instead. They can be found by;

$$B_{\text{mix}} = \frac{b_{\text{mix}} P}{RT}$$

$$A_{\text{mix}} = \frac{a_{\text{mix}} P}{(RT)^2} \text{ for Van der Waals, Soave-Redlich-Kwong, Peng-Robinson}$$

$$A_{\text{mix}} = \frac{a_{\text{mix}} P}{R^2 T^{2.5}} \text{ for Redlich-Kwong}$$

## A7. Polydispersed System Revision

It can be achieved as;

$$\begin{aligned} \frac{\partial}{\partial t}(\varphi_j \rho_s v_{s,j}) + v_{s,j} \frac{\partial}{\partial z}(\varphi_j \rho_s v_{s,j}) &= \varphi_j \rho_f \left( \frac{1}{2} \frac{1+2\varphi_j}{1-\varphi_j} + \frac{9}{4} \frac{\delta}{r_j} \right) \left( \frac{\partial v_f}{\partial t} - \frac{\partial v_{s,j}}{\partial t} \right) \\ + \frac{9}{4} \rho_f w \varphi_j \left( \frac{\delta}{r_j} + \frac{\delta^2}{r_j^2} \right) (v_f - v_{s,j}) &- \left( \frac{\partial P}{\partial z} \right) \varphi_j \end{aligned} \quad \text{eqn. A7.1}$$

$$\begin{aligned} \frac{\partial}{\partial t}[(1-\varphi) \rho_f v_f] + v_f \frac{\partial}{\partial z}[(1-\varphi) \rho_f v_f] &= - \sum_{j=1}^n \left[ \varphi_j \rho_f \left( \frac{1}{2} \frac{1+2\varphi_j}{1-\varphi_j} + \frac{9}{4} \frac{\delta}{r_j} \right) \left( \frac{\partial v_f}{\partial t} - \frac{\partial v_{s,j}}{\partial t} \right) \right] \\ - \sum_{j=1}^n \left[ \frac{9}{4} \rho_f w \varphi_j \left( \frac{\delta}{r_j} + \frac{\delta^2}{r_j^2} \right) (v_f - v_{s,j}) \right] &+ (\varphi - 1) \frac{\partial P}{\partial z} \end{aligned} \quad \text{eqn. A7.2}$$

Not that  $\varphi_j$  is the volume fraction of particles with radius of  $r_j$ . In addition, we have “n”

different particle sizes. Also,  $\sum_{j=1}^n \varphi_j = \varphi$  (total volume fraction of solids)

Hence, following set of momentum equations is obtained for each particle size;

For  $j=1$

$$\begin{aligned} \frac{\partial}{\partial t}(\varphi_1 \rho_s v_{s,1}) + v_{s,1} \frac{\partial}{\partial z}(\varphi_1 \rho_s v_{s,1}) &= \varphi_1 \rho_f \left( \frac{1}{2} \frac{1+2\varphi_1}{1-\varphi_1} + \frac{9}{4} \frac{\delta}{r_1} \right) \left( \frac{\partial v_f}{\partial t} - \frac{\partial v_{s,1}}{\partial t} \right) \\ + \frac{9}{4} \rho_f w \varphi_1 \left( \frac{\delta}{r_1} + \frac{\delta^2}{r_1^2} \right) (v_f - v_{s,1}) &- \left( \frac{\partial P}{\partial z} \right) \varphi_1 \end{aligned} \quad \text{eqn. A7.3}$$

For  $j=2$

$$\begin{aligned} \frac{\partial}{\partial t}(\varphi_2 \rho_s v_{s,2}) + v_{s,2} \frac{\partial}{\partial z}(\varphi_2 \rho_s v_{s,2}) &= \varphi_2 \rho_f \left( \frac{1}{2} \frac{1+2\varphi_2}{1-\varphi_2} + \frac{9}{4} \frac{\delta}{r_2} \right) \left( \frac{\partial v_f}{\partial t} - \frac{\partial v_{s,2}}{\partial t} \right) \\ + \frac{9}{4} \rho_f w \varphi_2 \left( \frac{\delta}{r_2} + \frac{\delta^2}{r_2^2} \right) (v_f - v_{s,2}) &- \left( \frac{\partial P}{\partial z} \right) \varphi_2 \end{aligned} \quad \text{eqn. A7.4}$$

For  $j=n$

$$\begin{aligned} \frac{\partial}{\partial t}(\varphi_n \rho_s v_{s,n}) + v_{s,n} \frac{\partial}{\partial z}(\varphi_n \rho_s v_{s,n}) &= \varphi_n \rho_f \left( \frac{1}{2} \frac{1+2\varphi_n}{1-\varphi_n} + \frac{9}{4} \frac{\delta}{r_n} \right) \left( \frac{\partial v_f}{\partial t} - \frac{\partial v_{s,n}}{\partial t} \right) \\ + \frac{9}{4} \rho_f \omega \varphi_n \left( \frac{\delta}{r_n} + \frac{\delta^2}{r_n^2} \right) (v_f - v_{s,n}) &- \left( \frac{\partial P}{\partial z} \right) \varphi_n \quad (j=n) \end{aligned} \quad \text{eqn. A7.5}$$

Suppose that density of the phases change according to pressure such that;

$$\rho_f = \rho_f^0 + \rho_f^0 \beta_f P \quad \text{eqn. A7.6}$$

$$\rho_{s,j} = \rho_{s,j}^0 + \rho_{s,j}^0 \beta_s P \quad \text{eqn. A7.7}$$

Since each particle experiences the same pressure, pressure variation for each particle will be same.

Furthermore, equation of continuity can also be converted to the following form for solid particles;

$$\frac{\partial}{\partial t}(\varphi_j \rho_s) + \frac{\partial}{\partial z}(\varphi_j \rho_s v_{s,j}) = 0 \quad \text{eqn. A7.8}$$

For j=1

$$\frac{\partial}{\partial t}(\varphi_1 \rho_s) + \frac{\partial}{\partial z}(\varphi_1 \rho_s v_{s,1}) = 0 \quad \text{eqn. A7.9}$$

For j=2

$$\frac{\partial}{\partial t}(\varphi_2 \rho_s) + \frac{\partial}{\partial z}(\varphi_2 \rho_s v_{s,2}) = 0 \quad \text{eqn. A7.10}$$

For j=n

$$\frac{\partial}{\partial t}(\varphi_n \rho_s) + \frac{\partial}{\partial z}(\varphi_n \rho_s v_{s,n}) = 0 \quad \text{eqn. A7.11}$$

For fluid phase

$$\frac{\partial}{\partial t}((1-\varphi)\rho_f) + \frac{\partial}{\partial z}((1-\varphi)\rho_f v_f) = 0 \quad \text{eqn. A7.12}$$

Hence, governing differential equations are obtained. Next step is simultaneous solution of these equations. For this purpose wave solutions of the parameters should be inserted into the governing differential equations.

Wave solutions of each parameter can be defined as;

$$v_{s,j} = v_{s0k,j} \exp[i(\sigma x - \omega t)] \quad \text{eqn. A7.13}$$

$$v_f = v_{f0k} \exp[i(\sigma x - \omega t)] \quad \text{eqn. A7.14}$$

$$\rho_s = \rho_s^0 + \rho_{s0k} \exp[i(\sigma x - \omega t)] \quad \text{eqn. A7.15}$$

$$\rho_f = \rho_f^0 + \rho_{f0k} \exp[i(\sigma x - \omega t)] \quad \text{eqn. A7.16}$$

$$P = P_{0k} \exp[i(\sigma x - \omega t)] \quad \text{eqn. A7.17}$$

$$\varphi_j = \varphi_j^0 + \varphi_{0k,j} \exp[i(\sigma x - \omega t)] \quad \text{eqn. A7.18}$$

Inserting the proposed solutions into the governing differential equations and rearranging;

Eqns. A6.6 and A6.7 is converted to;

$$\rho_{f0k} = \rho_f^0 \beta_f P_{0k} \quad \text{eqn. A7.19}$$

$$\rho_{s0k} = \rho_s^0 \beta_s P_{0k} \quad \text{eqn. A7.20}$$

**Mass conservation equations ( n equation for solid phases and 1 equation for fluid);**

$$-i\omega \rho_s^0 \varphi_{0k,1} - i\omega \varphi_1^0 \rho_{s0k} + i\sigma \varphi_1 v_{s0k,1} = 0 \quad \text{eqn. A7.21}$$

$$-i\omega \rho_s^0 \varphi_{0k,2} - i\omega \varphi_2^0 \rho_{s0k} + i\sigma \varphi_2 v_{s0k,2} = 0 \quad \text{eqn. A7.22}$$

$$-i\omega \rho_s^0 \varphi_{0k,n} - i\omega \varphi_n^0 \rho_{s0k} + i\sigma \varphi_n v_{s0k,n} = 0 \quad \text{eqn. A7.23}$$

$$i\omega \rho_f^0 \varphi_{0k} - i\omega (1 - \varphi^0) \rho_{f0k} + i\sigma (1 - \varphi) \rho_f^0 v_{f0k} = 0 \quad \text{eqn. A7.24}$$

**Momentum conservation( n equation for solid phases and 1 equation for fluid);**

$$\left[ -i\omega \varphi_1^0 \rho_f^0 \left[ \frac{1}{2} \left( \frac{1+2\varphi_1}{1-\varphi_1} \right) + \frac{9}{4} \frac{\delta}{r_1} \right] + \frac{9}{4} \rho_f^0 \omega \varphi_1^0 \left( \frac{\delta}{r_1} + \frac{\delta^2}{r_1^2} \right) \right] v_{f0k} + \left[ i\omega \varphi_1^0 \rho_f^0 \left[ \frac{1}{2} \left( \frac{1+2\varphi_1}{1-\varphi_1} \right) + \frac{9}{4} \frac{\delta}{r_1} \right] - \frac{9}{4} \rho_f^0 \omega \varphi_1^0 \left( \frac{\delta}{r_1} + \frac{\delta^2}{r_1^2} \right) + i\omega \varphi_1^0 \rho_s^0 \right] v_{s0k,1} - P_{0k} i\sigma = 0 \quad \text{eqn. A7.25}$$



#### **A8. Algorithm for Particle Size Determination from the Model Developed**

From ultrasound experiments, sound pressure amplitude versus time data is obtained. Matlab code is written for evaluation of the model for particle size characterization from the experimental data. Following algorithm is used in the program developed;

- As an input of the code, estimated size of the particle is entered.
- For the given size, program simulates the pressure change with time in the dispersion.
- If the deviations of simulation results from the experimental measurements are greater than 1%, then another trial for particle size is done. Otherwise, particle size is accepted.

### A9. Particle Size Measurements by Mastersizer 2000

Particle sizes of colemanite/water dispersion used in ultrasonic measurements are figurized in Figures A9.1, A9.2, A9.3, A9.4 and A9.5.

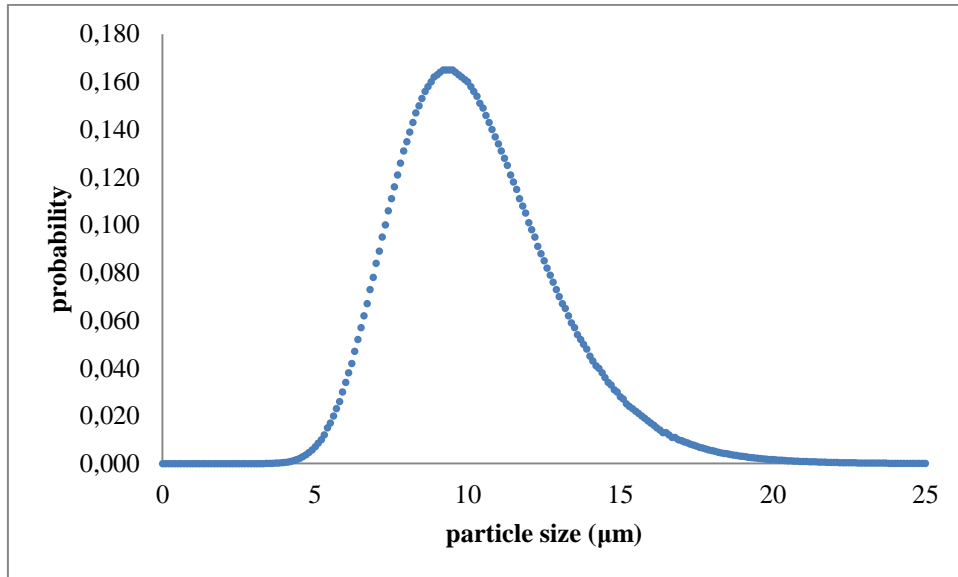


*Figure A9.1 Particle Size Measurement of 10 µm Particle*

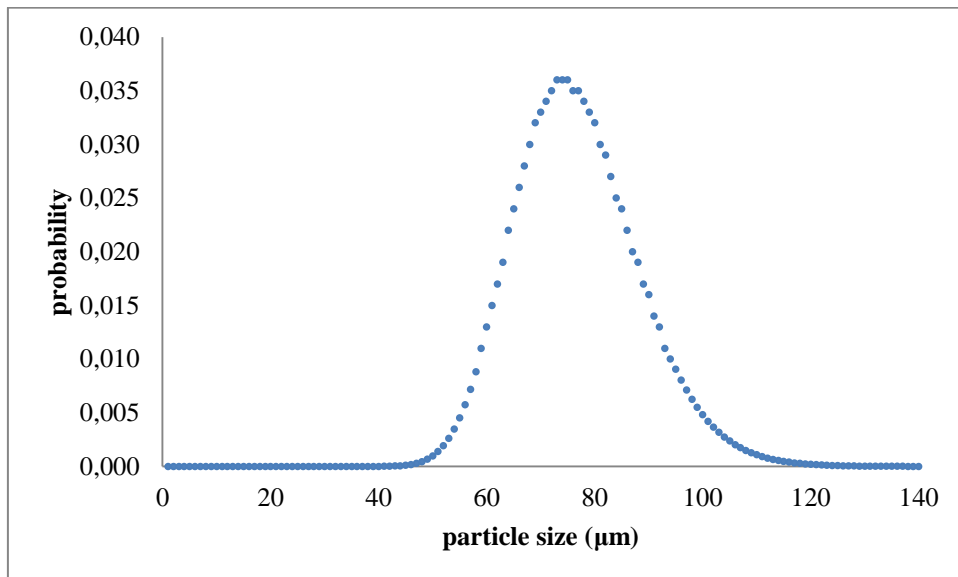


*Figure A9.2 Particle Size Measurement of 75 µm Particle*

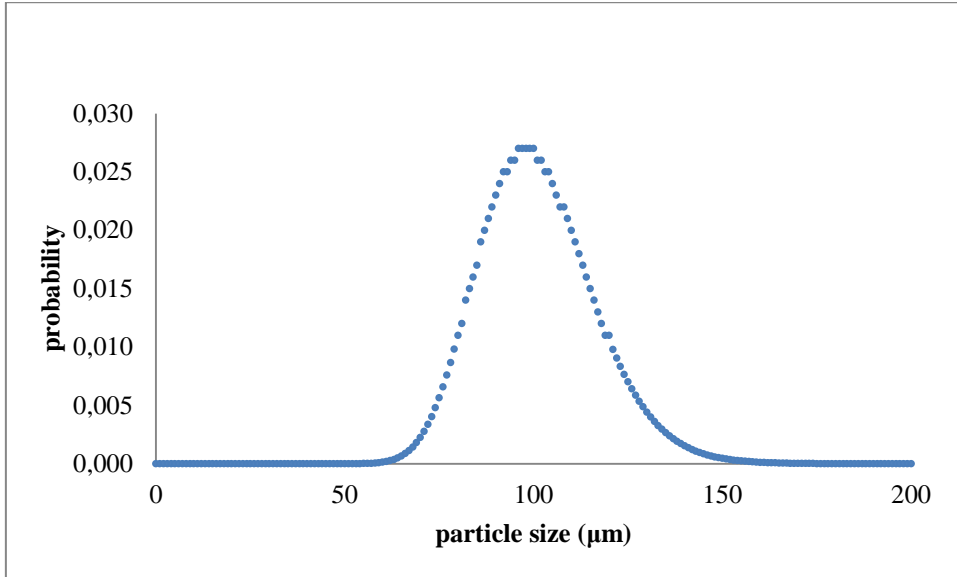


*Figure A9.3 Particle Size Measurement of 100 μm Particle*

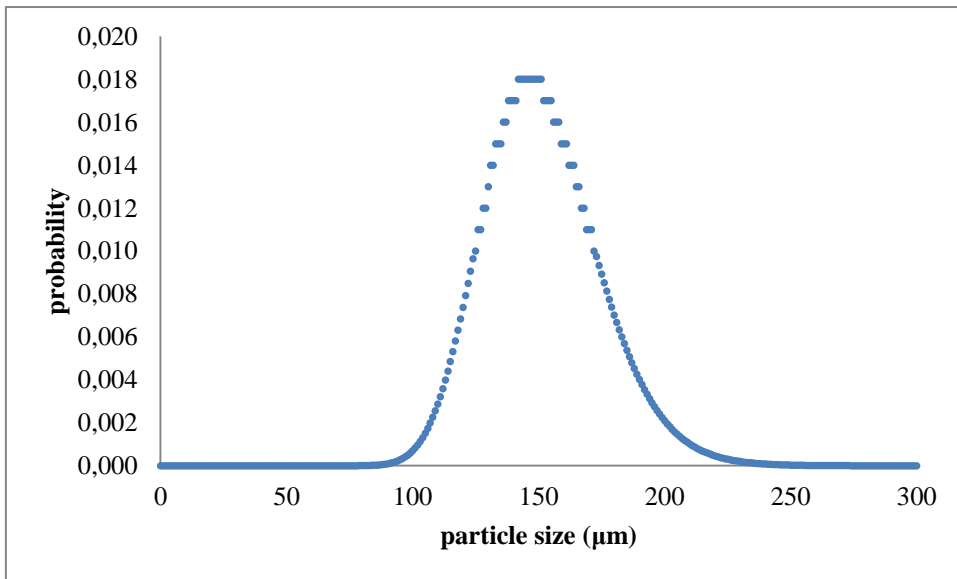


*Figure A9.4 Particle Size Measurement of 150 μm Particle*

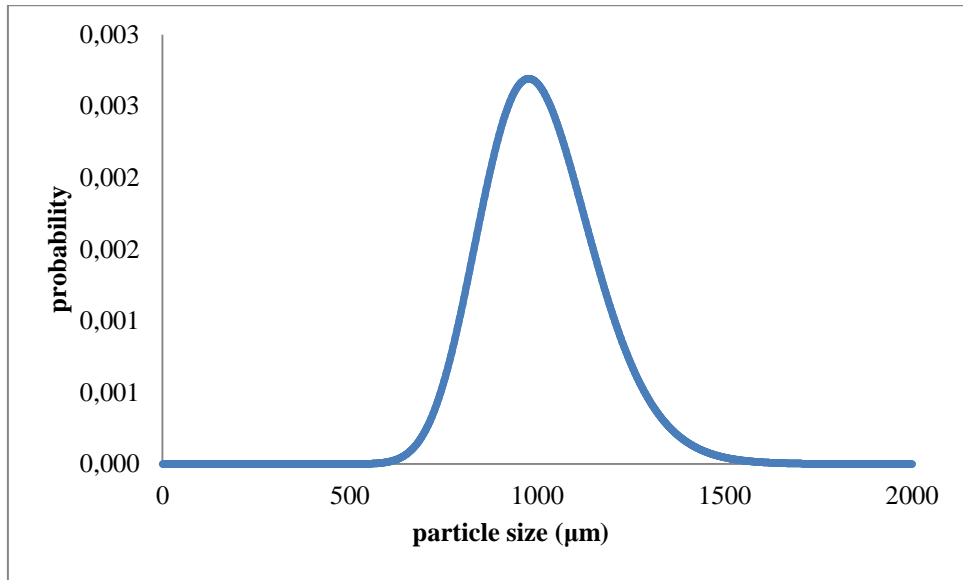


*Figure A9.5 Particle Size Measurement of 1000 µm Particle*

## A10. Technical Specifications of DOP2000

### Technical Specifications [99]

#### Emission

Emitting Frequency

Model 2032

5 different frequencies : 0.5, 1 , 2, 4 and 8

MHz

Emitting Power

3 levels. Instantaneous maximum power for setting (approx. ) :

low = 0.5 W, medium = 5 W, high = 35 W

Number of emitted cycles

2, 4 or 8 cycles

Pulse Repetition Frequency selectable values between 10000  $\mu$ s and

64  $\mu$ s, step of 1  $\mu$ s

#### Reception

Number of Gates

variables between 1000 and 3, step of 1 gate

Position of the First Channel movable by step of 250 ns

Amplification (TGC)

Uniform, Slope, Custom

Slope mode

Exponential amplification between two defined depth values.

Value at both depths variable between -40 dB and +40 dB

Custom mode

User's defined values between -40 dB and + 40 dB

In cells.

Variable number, size and position of the cells.

Sensitivity	> -100 dBm
Resolution	
Sampling Volume: lateral size	resolution defined by the acoustical characteristics of the transducer
Sampling Volume: longitudinal size	Model 2032 Minimum value of 1.2 $\mu$ s or 0.9 mm Depends on busrt length Maximum value of 16 $\mu$ s or 12 mm (c = 1500 m/s, approximate value, defined at 50 % of the received)
Display Resolution	distance between the center of each sample Volume selectable between 0.25 $\mu$ s or 0.187 mm and 20 $\mu$ s or 15 mm, step of 0.25 $\mu$ s (c =1500 m/s)
Velocity Resolution	1 LSB, doppler frequency given in a signed Byte format Maximum = 0.0091 mm/s; minimum = 91.5 mm/s (c=1500 m/s)
Ultrasonic Processor	
Doppler Frequency	computation based on a correlation algorithm
Bandwidth of Demodulated Signals	Model 2032 Bandwidth 220 kHz
Wall Filter	Stationary echoes removed by IIR high-pass Filter 2 <sup>nd</sup> order
Number of Emissions per Profile	between 1024 and 8, any values

Detection Level	5 levels of the received Doppler energy may disable the computation
Acquisition Time per Profile	minimum: about 2-3 ms
Filters on profiles	moving average: Based on 2 to 32000 profiles Zero values included or rejected Median, based on 3 to 32 profiles
Maximum Velocity	11.72 m/s for bi-directional flow (at 0.5 MHz, $c = 1500$ m/s) variable positive and negative velocity range.
Acquisition	
Compute and Display	velocity Doppler energy Echo modulus Velocity profile with echo modulus or Doppler energy Velocity profile with velocity versus time of One selected gate Velocity profile with flow rate versus time (circular section assumed) Velocity profile with real time histogram Echo modulus with real time histogram Doppler energy with real time histogram Power spectrum of one selected gated
Cursor	displays the velocity and depth value, tracking

	Mode ( follow the displayed curve).
	Statistical values available.
Statistics	Mean, standard deviation, minimum, maximum
Trigger	by external signal, change in the logic state (TTL/CMOS level)  by keyboard action  Selectable repeated acquisition procedure  Of bloc of profiles  Automatic record capability
Trigger Delay	from a 1 ms to 1s, step of 1 ms
Utilities	freeze/run mode
Velocity Component	automatic computation of the projected velocity component
Replay Mode	replays a recorded measure from the disk
Memory/Files	
Internal Memory	variable size, memorization from 2 to 32000
	Profiles
Configuration	10 saved configurations
Data File	Binary  (include: ASCII short into blocks, 476 bytes  Of ASCII comments, all parameters, all data  Profiles) ASCII (statistical information available)

## **A11. Technical Specification of ARES Rheometer (TA Instruments, Spain) [100]**

### **Force/Torque Rebalance Transducers**

Transducer Type	Force/Torque Rebalance
Transducer Torque Motor	Brushless DC
Transducer Normal/Axial Motor	Brushless DC
Minimum Transducer Torque in Oscillation	0.05 $\mu\text{N}\cdot\text{m}$
Minimum Transducer Torque in Steady Shear	0.1 $\mu\text{N}\cdot\text{m}$
Maximum Transducer Torque	200 $\text{mN}\cdot\text{m}$
Transducer Torque Resolution	1 $\text{nN}\cdot\text{m}$
Transducer Normal/Axial Force Range	0.001 to 20 N
Transducer Bearing	Groove Compensated Air

### **Drive Motor**

Maximum Motor Torque	800 $\text{mN}\cdot\text{m}$
Motor Design	Brushless DC
Motor Bearing	Jeweled Air, Sapphire
Displacement Control/Sensing	Optical Encoder
Strain Resolution	0.04 $\mu\text{rad}$
Min. Angular Displacement in Oscillation	1 $\mu\text{rad}$
Max. Angular Displacement in Steady Shear	Unlimited
Angular Velocity Range	1 x 10 <sup>-6</sup> rad/s to 300 rad/s
Angular Frequency Range	1 x 10 <sup>-7</sup> rad/s to 628 rad/s
Step Change in Velocity	5 ms
Step Change in Strain	10 ms

### **Orthogonal Superposition and DMA modes**

Minimum Transducer Force in Oscillation	0.001 N
Maximum Transducer Force	20 N
Minimum Displacement in Oscillation	0.5 $\mu\text{m}$
Maximum Displacement in Oscillation	50 $\mu\text{m}$
Displacement Resolution	10 nm
Axial Frequency range	1 x 10 <sup>-5</sup> Hz to 16 Hz

### **Stepper Motor**

Movement/Positioning	Micro-stepping Motor/Precision Lead Screw
Position Measurement	Linear Optical Encoder
Positioning Accuracy	0.1 micron

### **Temperature Systems**

Smart Swap	Standard
Forced Convection Oven, FCO	-150 °C to 600 °C
FCO Camera Viewer	Optional
Advanced Peltier System, APS	-10 °C to 150 °C
Peltier Plate	-40 °C to 180 °C
Sealed Bath	-10 °C to 150 °C

## **A12. Technical Specification of Mastersizer2000 [101]**

### **General**

Particle size:	Suspensions, emulsions, dry powders
Principle:	Laser light scattering
Analysis:	Mie and Fraunhofer scattering
Data acquisition rate:	10 kHz
Typical measurement time:	<10 sec
Dimensions (W, D, H):	690mm x 300mm x 450mm
Weight:	30 kg

### **Optics**

Red light source:	Max. 4mW He-Ne, 632.8nm
Blue light source:	Max. 10mW LED, 470nm
Lens arrangement:	Reverse Fourier (convergent beam)
Effective focal length:	300mm

### **Detector**

Arrangement:	Log-spaced array
Angular range:	0.015 - 144 degrees
Alignment:	Automatic

### **Size**

Particle size:	0.01 - 3500 $\mu\text{m}$
Number of size classes:	100 (user adjustable)
Accuracy:	Better than 0.6%
Precision / Repeatability:	Better than 0.5% variation
Reproducibility:	Better than 1% variation

### A13. Colemanite Specification

Formula:  $2\text{CaO} \cdot 3\text{B}_2\text{O}_3 \cdot 5\text{H}_2\text{O}$  (Di-Calcium Hexaborate Pentahydrate)

CAS No: 12291-65-5

*Table A13.1 Chemical Specification of Colemanite*

<b>Component</b>	<b>Content</b>
B <sub>2</sub> O <sub>3</sub>	40.00 ±0.50 %
CaO	27.00 ±1.00 %
SiO <sub>2</sub>	4.00-6.50%
SO <sub>4</sub>	0.60% max.
As	35 ppm max.
Fe <sub>2</sub> O <sub>3</sub>	0.08% max.
Al <sub>2</sub> O <sub>3</sub>	0.40% max.
MgO	3.00% max.
SrO	1.50% max.
Na <sub>2</sub> O	0.50% max.
L.O.I.	25.00% max.
Moisture	1.00% max.
Bulk Density	1.00 ton/m <sup>3</sup> max



## CURRICULUM VITAE

**Surname, Name** Özkök, Okan  
**Nationality** Turkish  
**Date of Birth** 10/04/1987  
**Place of Birth** Ankara  
**e-mail** ozkok@metu.edu.tr

## EDUCATION

**2012-2017** Middle East Technical University, Ankara /Turkey  
PhD in Department of Chemical Engineering  
**2010-2012** Middle East Technical University, Ankara /Turkey  
M.Sc. in Department of Chemical Engineering  
**2005-2010** Middle East Technical University, Ankara /Turkey  
B.Sc. in Department of Chemical Engineering

## EXPERIENCES

**09/2014-Present** Market Research Executive, Eti Mine Works  
General Management  
**08/2011-09/2014** Research Assistant, Department of Chemical  
Engineering, Middle East Technical University

## **PUBLICATIONS**

- Investigation of Fluid Rheology Effects on Ultrasound Propagation, Okan Özkök, METU, 2012, M.Sc. Thesis
- Theoretical and Experimental Investigation of Fluid Rheology Effects on Modulated Ultrasound Propagation, Okan Özkök, Yusuf Uludağ, Ultrasonics, Volume 54, Issue 7, September 2014, Pages 2034-2041